1-1-2012

Mixing Characteristics of External Loop Airlift Bioreactor using Electrical Resistance Tomography

Mian Hamood-Ur-Rehman
Ryerson University

MIXING CHARACTERISTICS OF EXTERNAL LOOP AIRLIFT BIOREACTOR USING ELECTRICAL RESISTANCE TOMOGRAPHY

by

MIAN HAMOOD-UR-REHMAN

B.Sc., Bhauddin Zakariya University, Multan, Pakistan, 2004

A thesis

presented to Ryerson University

in partial fulfillment of the requirements for the degree of

Master of Applied Science

in the program of

Chemical Engineering

Toronto, Ontario, Canada, 2012

Author's Declaration

I hereby declare that I am the sole author of this thesis. This is a true copy of the thesis, including any required final revisions, as accepted by my examiners.

I authorize Ryerson University to lend this thesis to other institutions or individuals for the purpose of scholarly research.

I further authorize Ryerson University to reproduce this thesis by photocopying or by other means, in total or in part, at the request of other institutions or individuals for the purpose of scholarly research.

I understand that my thesis may be made electronically available to the public.

ABSTRACT

Mixing Characteristics of External Loop Airlift Bioreactor Using Electrical Resistance Tomography (ERT)

Mian Hamood-ur-Rehman

Master of Applied Science, Chemical Engineering, Ryerson University

Toronto, Canada, 2012

In the present work, a novel packed bed external loop pneumatically agitated airlift bioreactor with an internal gas distributor (perforated plate) between two rolls of packing in the riser was designed and built. This novel approach combines advantages of packed bed and external loop airlift bioreactors. The main objective of this research work was to characterize the hydrodynamic performance of this novel reactor through a non-intrusive flow visualization technique called electrical resistance tomography (ERT). The tomography images, which were generated using a linear back projection algorithm, were employed to explore the effects of different design parameters and operating conditions. These include the effect of the two packing in the riser and the internal gas distributor (perforated plate) installed between the two packing. Other parameters investigated include the effect of sparger configuration, gas flow rate, and liquid height in the bioreactor on the different hydrodynamic parameters such as gas holdup, mixing time, and liquid circulation velocity. Results showed that the gas holdup and mixing time increased in the presence of the gas distributor, while the riser superficial liquid velocity was decreased. Furthermore, gas holdup and mixing time increased, superficial liquid velocity decreased when decreasing liquid height in the reactor, and when using packing or gas distributor between two packings in the riser. These results can be used to improve mixing characteristics in external loop airlift bioreactors for wider range of applications.

ACKNOWLEDGEMENTS

I would like to express my sincere gratitude to my supervisors, Dr. Yaser Dahman and Dr. Farhad Ein-Mozaffari for their invaluable supervision, useful comments, ideas and suggestions throughout the research to accomplish this thesis.

I would like to show my deep appreciation to technologists; Ali Hemmati and Daniel Boothe and the faculty members in Chemical Engineering Department of Ryerson University for the facilities and assistance provided during my stay at the university.

The financial support of Natural Sciences and Engineering Research Council of Canada (NSERC) is gratefully acknowledged.

TABLE OF CONTENTS

List of Tables

List of Figures

CHAPTER 1

INDTRODUCTION

Bioreactors are being used in bioprocess industries for the manufacturing of many useful daily life products. This includes commercial manufacture of pharmaceuticals, enzymes, fragrances, dyes and antibiotics (Sarkar et al., 2008; Zhang et al., 2005; Al-Qodah and Lafi, 2001). There are different types of bioreactors used in industries. These bioreactors include stirred tank bioreactors, packed bed bioreactors, fluidized bed bioreactors, bubble column bioreactors, and airlift bioreactors. A stirred tank bioreactor is more commonly used for the microbial fermentations. This type of bioreactors consists of a vessel that contains baffles and an impeller connected to an external motor at the top or at the bottom of the bioreactor. This impeller drives the stirrer system, which causes an intense mixing in the bioreactor. The function of baffles is to promote mixing and mass transfer by increasing turbulence, preventing vortex formation, and eliminating dead spaces (Garcia-Ochoa and Gomez, 2004). Providing a sparger at the bottom of the bioreactor, stirred tank bioreactors are called sparged stirred tank bioreactors. One of the important types includes packed bed bioreactor with a sparger located at the bottom of this bioreactor. In packed bed bioreactors, packing is used as a support for immobilized microorganisms or enzymes (Horiuchi et al., 2000). These bioreactors are widely used in several processes including waste water treatment. Another type of bioreactors is fluidized bed bioreactor. This bioreactor consists of a vessel containing a high biomass concentration attached on an inert support material and the processing liquid with a sparger located at the bottom (Fuentes et al., 2009; Tavares et al., 1995). Bubble column bioreactors are tall column bioreactors that are sparged with air using a sparger usually located at the bottom of the

bioreactor. The air bubbles provide oxygen needed by the aerobic microorganisms in these bioreactors (Vial et al. 2005; Merchuk et al., 1994).

A very famous and important type of bioreactors is airlift bioreactors. Airlift bioreactors are encountered in the fields of aerobic fermentations, waste water treatment, and other operations, where low shear stress is required (Mohanty et al., 2008; Loh and Ranganath, 2005; Klein et al., 2005). There are two main types of airlift bioreactors, namely the internal loop airlift bioreactors and the external loop airlift bioreactors. The main difference between these two types is that the internal loop airlift bioreactors consist of two concentric columns, while the external loop airlift bioreactors consist of two separate columns connected near the top and at the bottom by two horizontal sections. This design gives a separate gas disengagement section to external loop airlift bioreactors, which helps in maximum deaeration (Kilonzo et al., 2010; Gumery et al., 2009; Mohanty et al., 2008; Klein et al., 2005; Han et al., 2000; Gavrilescu and Tudose, 1997; Tang and Fan, 1987). External loop airlift reactors are frequently used in chemical and biochemical industries due to their simple construction, good heat and mass transfer, and good mixing characteristics as the gas phase in the reactor performs the dual functions of aeration and agitation. The applications of these bioreactors have been increasing and making them as one of the most important bioreactor configurations. Many investigators have studied external loop bioreactors experimentally and theoretically (Yazdian et al., 2009; Sarkar et al., 2008; Mohanty et al., 2007; Zhang et al., 2005; Shimizu et al., 2001).

In this study a novel external loop airlift bioreactor, with an internal gas distributor (perforated plate) installed between two rolls of packing in the riser, was designed and investigated. The advantages of packed bed bioreactors and external loop airlift bioreactors were combined in this bioreactor. Different configurations of bioreactor were used in order to investigate the hydrodynamic parameters. These configurations included installing a perforated plate (without

any packing) in the riser, installing one bed of packing in the riser and installing an internal gas distributor between two beds of packing in the riser.

Gas holdup, liquid circulation velocity, and mixing time are the most important parameters characterizing hydrodynamics in airlift bioreactors. These parameters are very important in order to design and scale-up the external loop airlift bioreactors. Different investigators have measured gas holdup, liquid circulation velocity and mixing time by a variety of techniques in a variety of different bioreactor geometries (Yazdian et al., 2009; Essadki et al., 2008; Loh and Liu, 2001; Han et al., 2000; Bello et al., 1984; Bello, 1981).

The applications of electrical resistance tomography (ERT) is increasing for being employed as a reliable non-intrusive tool for direct analysis of the hydrodynamics of multiphase flows in recent years (Gumery et al., 2011; Jin et al., 2007; Jin et al., 2006). This non-intrusive technique can be used for flow visualization. It can clearly show the presence of second phase in a two-phase flow system (Ishkintana and Bennington, 2010; Hosseini et al., 2010). This technology manipulates data obtained from sensors located on the periphery of the vessel in order to get the precise quantitative information from locations where it is hard to reach. This technology collects the information on the flow regime and concentration distribution in process vessels (Williams and Beck, 1995). An ERT system consists of electrodes located on the periphery of the vessel, data acquisition system and a host computer. In the present study eight planes, each consisting of 16 electrodes, were installed on riser and downcomer of the bioreactor. Plane 1, plane 2, plane 3 and plane 4 were located on the downcomer from top to bottom and plane 5, plane 6, plane 7 and plane 8 were located on the riser from bottom to top.

In this work, gas holdup, mixing time and liquid circulation velocity were measured using electrical resistance tomography system for the external recirculated airlift bioreactor. These

hydrodynamic parameters can be determined by first finding the change in fluid conductivity in the bioreactor. The experimental results demonstrated that the gas flow rate, liquid height, sparger configuration and the bioreactor configuration had a very significant effect on these hydrodynamic parameters.

The objective of this research work is to investigate the feasibility of ERT system in order to evaluate the effect of the gas flow rate, bioreactor liquid height, sparger configuration on hydrodynamic parameters in a novel external loop airlift bioreactor. Chapter 2 is based on a brief literature review in order to understand the types of bioreactors and the performance of external loop airlift bioreactors. Gas holdup, liquid circulation velocity and mixing time were also discussed in chapter 2. Chapter 3 gives the experimental setup and procedure used to perform all the experimental work successfully. Chapter 4 provides the experimental and ERT results found in this research work as well as the discussion. Finally, chapter 5 summarizes the conclusions obtained in this research and the recommendations for future work.

CHAPTER 2

LITERATURE REVIEW

2.1. Introduction

Biotechnology research has been advanced both on laboratory and on industrial scale. A large variety of microorganisms are being genetically engineered for possible use in production processes. Many cell cultures require oxygen for the survival and growth of their cells. For these cells, continuous supply of oxygen is necessary as the solubility of oxygen in this medium is very low (Yuguo et al., 1999). There are different methods to aerate cultures in bioreactors that include surface aeration, membrane aeration, and sparged aeration. Membrane aeration system is relatively complex and not scalable for commercial applications. Sparging aeration is simple, efficient, and easy to scale up and is widely used for oxygenation at large scales. Aeration is also used to remove carbon dioxide from culture medium that is a major by-product when animal cells consume oxygen. When the sparging aeration system is used in the bioreactors, the dissolved carbon dioxide can transfer from liquid medium to rising bubbles and then leave the culture system through exit gas. In sparged stirred tank bioreactors, the air enters the bioreactors through a sparger at the bottom and forms bubbles into the culture fluid, this leads to a dramatic increase in the oxygen transfer area, while the agitation is used to break up bubbles and thus further increase the volumetric oxygen transfer coefficient.

Sparging without mechanical agitation can also be used for aeration and agitation. Two classes of bubble driven bioreactors are bubble column fermentors and airlift (or gaslift) fermentors. Bubble driven bioreactors are commonly used in the culture of shear sensitive organisms such as moulds and plant cells. An airlift fermentor differs from bubble column bioreactor because of its

fluid flow characteristics by the introduction of a draft tube which improves circulation and hence provides better mass and heat transfer efficiencies and more uniform shear conditions. Airlift bioreactors have been extensively used in biotechnology industries in recent years in a variety of arrangements and applications. This includes commercial manufacture of pharmaceuticals, enzymes, fragrances, dyes and antibiotics (Sarkar et al., 2008; Zhang et al., 2005; Al-Qodah and Lafi, 2001). The main advantages of this type of reactor are simple construction and operation, low investment and operational cost, absence of regions of high shear, very fine gas dispersion, high mixing and mass transfer performance and relatively low power requirements (Benyahia and Jones, 1997). The concept of airlift depends upon the hydrostatic pressure difference due to gas injection into a section of the reactor. Airlift bioreactors are characterized by the bulk circulation of fluid, in a defined pattern, through specifically designed channels. This flow pattern gives rise to hydrodynamic conditions that are unique to airlifts.

In airlift bioreactors, the gas phase is introduced from the sparger at the bottom of the up-flow channel (i.e., riser). The gas phase carries the liquid/slurry phase upward in the riser and is disengaged from the liquid/slurry phase at the top of the column. The liquid/slurry phase then flows in the down-flow channel (i.e., downcomer) and circulates back to the bottom of the riser. At higher velocity, some small bubbles may be entrained into the downcomer with the circulating liquid. Depending on the gas liquid/slurry separation efficiency, the gas holdup in the downcomer is much lower than in the riser. The generated density and pressure difference between the riser and downcomer drives the liquid/slurry phase circulation between the riser and the downcomer. The commonly used designs of airlift bioreactors are internal loop airlift bioreactor and external loop airlift bioreactor. Analyses and description of the behaviour of airlift bioreactors usually involve the use of parameters such as gas holdup, liquid velocity, mass

transfer, and mixing. There is a large degree of interaction between these parameters and thus, description of airlift behaviour is a complex task (Chisti et al., 1988; Xu et al., 2008).

Gas holdup and liquid circulation velocity are key parameters affecting product formation. Non-Newtonian flow behaviours effect the mixing in airlift bioreactors. The gas holdup determines the residence time of the gas in the liquid and in combination with the bubble size influences the gas-liquid interfacial area available for mass transfer. The gas holdups control the liquid velocity and the liquid velocity in turn affects these gas holdups by either enhancing or reducing the velocity of bubble rise. The liquid velocity affects turbulence, the gas-liquid mass transfer, and the shear forces (Mohanty et al., 2007; Zhang et al., 2005; Hwang and Cheng, 1997).

2.2. Different Types of Bioreactors

2.2.1. Stirred Tank Bioreactors

A stirred tank bioreactor is more commonly used for the microbial fermentations. It consists of a vessel that contains baffles and an impeller connected to an external motor at the top or at the bottom of the bioreactor, which drives the stirrer system. The agitation system causes an intense mixing while the baffles promote mixing and mass transfer by increasing turbulence, preventing vortex formation, and eliminating ‘dead spaces’. In the sparged stirred tank bioreactor, a sparger is introduced usually at the bottom of the bioreactor through which a gas or a mixture of gases is distributed in the liquid in the form of bubbles. Figure 2.1 shows a schematic diagram of this simple type of bioreactors.

In this type of bioreactors, the efficiency of gas-liquid contacting in the stirred tank bioreactor is basically measured by the fractional gas holdup. The gas holdup, the energy dissipated by

turbulence, size of the bubbles or their distribution within the fluid effect the mass transfer between the gas-liquid phases (Garcia-Ochoa and Gomez, 2004). These reactors have important advantages for industrial production: easy control of the gas dispersion and medium mixing by stirrer speed, efficient gas dispersion by stirrers, and use in highly viscous media. There are several possibilities in which a conventional stirred tank reactor has to be used because bubble columns may not be suitable. The two most common situations arise when we use viscous broths (filamentous mycelium, viscosity increasing substrates or products) or when extremely high oxygen transfer rates are required. A rather high specific power input is required in stirred tank bioreactor for a sufficient oxygen transfer rate, which is independent of the size of the reactor. Furthermore, at low stirrer speeds, the gas dispersion and mixing efficiency of stirrers are extremely low. Therefore, it is technically and economically inappropriate to use stirred tank reactors for low performance processes (for example biological wastewater treatment) which are carried out in large reactors at low specific power input. The chances of getting contamination are higher in stirred tank bioreactor that is a major drawback in the production of microorganisms. Especially in pharmaceutical industry, it is very crucial that a sterile environment is used since contamination reduces product quality and generates wastes and in order to restore the whole process more time and money are spent. The costs are higher and shear forces are rather high due to the mechanical stirring. Therefore stirred tank bioreactor is less suitable for cells that are shear-sensitive (Gumery et al., 2009; Yuguo et al., 1999; Merchuk et al., 1994).

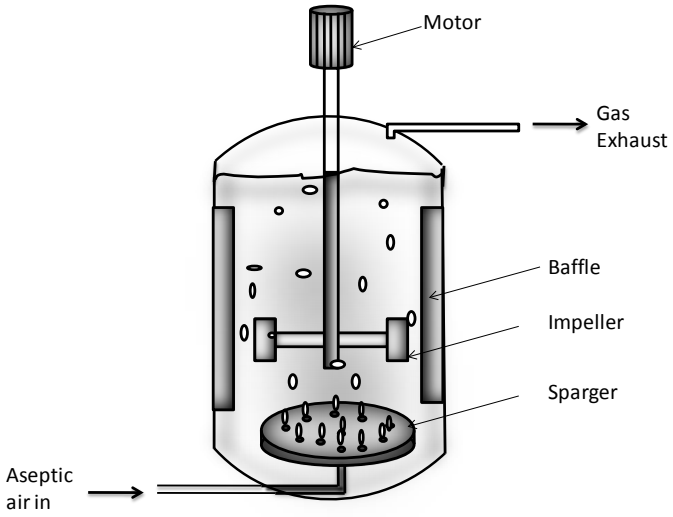

Figure 2.1 Sparged stirred tank bioreactor.

2.2.2. Packed Bed Bioreactors

Packed bed bioreactors have been abundantly used in several industries. In packed bed biological reactors, packing is used as a support for immobilized microorganisms or enzymes. The biocatalyst is immobilized on the packed support in the column and fed with nutrients either from top or from bottom of the bioreactor as shown in Figure 2.2. It is very important to understand the hydrodynamic characteristics of the packed bed bioreactors in order to get the best results for mass transfer and reaction conversions. Microbial cells can also be immobilized on the surface of the packing material as a biofilm. These bioreactors can be used commercially with enzymatic catalysts and with slowly or non-growing cells. Other advantages include rapid start-up, no cell washout, a high cell concentration, and low sensitivity to inlet disturbances (Horiuchi et al., 2000). The characteristic of the flow is changed due to the alterations in the bed porosity during operation. Packed bed reactors often suffer from problems caused by poor mass transfer rates and clogging.

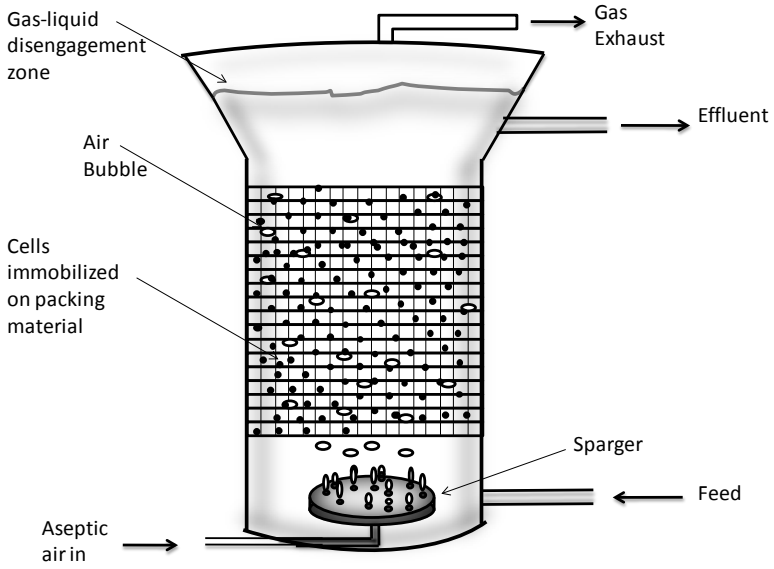

Figure 2.2 Packed bed bioreactor.

2.2.3. Fluidized Bed Bioreactors

Fluidized bed bioreactors are widely used in several bioprocesses. This type of bioreactors consists of a vessel containing high attached biomass concentration on an inert support material and the processing liquid. The air is sparged usually at the bottom of the reactor using a sparger as shown in Figure 2.3. Due to smaller size of support material, these bioreactors offer smaller pressure drop and no bed-clogging problems (Fuentes et al., 2009). These bioreactors are very attractive for wastewater treatment as they offer lower hydraulic retention time, improved chemical oxygen demand (COD) removal efficiency, lower sludge production and less space requirements (Tavares et al., 1995). Enhanced heat and mass transfer properties can be obtained in fluidized bed bioreactors. Insoluble and high viscosity solutions can be used. The immobilization of cells onto or into the solid particles offers very high biomass concentration. The partial replacement of fluidized bed can be achieved because of the use of supporting particles without interrupting the operation in order to maintain high microbial activity.

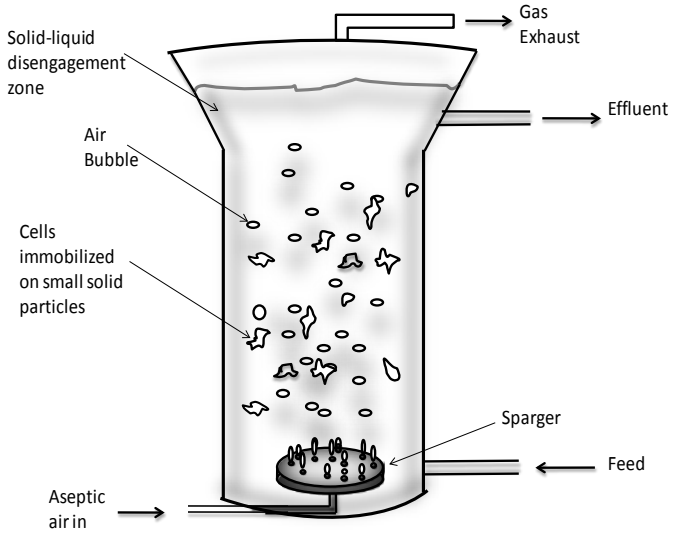

Figure 2.3 Fluidized bed bioreactor.

Intimate contact between the liquid phase and solid phase is achieved in this type of bioreactor. High energy input is required to fluidize the solid particles. Immobilized sensitive cells cannot be used in fluidized bed with high gas flow rate. Solid particles must be non-reactive with the liquid and the gas used.

2.2.4. Bubble Column Bioreactors

Bubble column bioreactors are widely used in the bioprocess industry. This reactor consists of a tall column that is sparged with air using a sparger usually located at the bottom of the reactor which provides the oxygen needed by the aerobic microorganisms. As shown in Figure 2.4, these bioreactors are of very simple design. The energy consumption is lower in these bioreactors than in conventional stirred tank bioreactors. Utilizing these bioreactors reduces the maintenance costs since the absence of moving parts avoids mechanical breakages. The risk of contamination is also low in these bioreactors. Shearing is also much lower than in conventional stirred tank reactor. The tall design leads to high gas holdups and long bubble residence times that provide

better mass transfer. Shearing is not homogeneous in these bioreactors. The tall bubble column bioreactors give spatial inhomogeneities in dissolved oxygen concentration, under steady-state operations. These inhomogeneities are found mostly in the axial direction and affect the local and the overall productivity of bubble column bioreactors (Vial et al. 2005; Merchuk et al., 1994). Rubio et al. (1999) described the importance of axial concentration profile of dissolved oxygen through varying the steady-state concentration of dissolved oxygen axially in the bubble column. The shape of the axial concentration profile changes by changing the overall gas holdup, the overall volumetric gas-liquid mass transfer coefficient, and the axial dispersion coefficient since all these parameters depends on the gas flow rate. The concentration profile is also affected by the static height of liquid in the column. Perez et al. (2006) showed in a derived correlation that the average shear rate depends on the superficial aeration velocity and the rheological properties of the fluid.

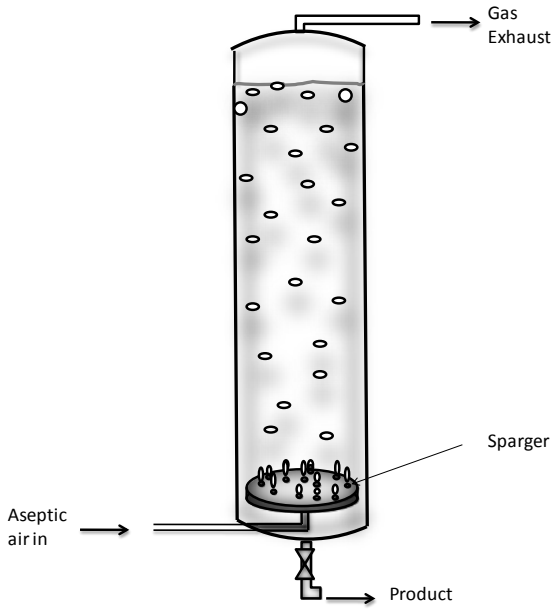

Figure 2.4 Bubble column bioreactor.

2.2.5. Airlift Bioreactors

Airlift (or gaslift) bioreactors are widely used in chemical and biochemical industries. Airlift bioreactors can be divided in two different classes: the internal and external loop bioreactors. The internal loop airlift bioreactor is an important type of airlift bioreactors. These bioreactors consist of a riser, a downcomer, a gas-liquid separator and a base. The sparger is usually provided at the bottom of the riser in the reactor in order to introduce air bubbles into the processing fluid. The internal loop and the inverse internal loop airlift bioreactors are shown in Figures 2.5 (a and b), respectively. The different volumes of air bubbles in the riser and the downcomer create pressure difference between the riser and downcomer which in return drives the liquid/slurry phase circulation between the riser and the downcomer. This liquid/slurry phase flows upward in the riser and the gas is disengaged from the liquid/slurry phase at the top of the column called the gas-liquid disengagement zone.

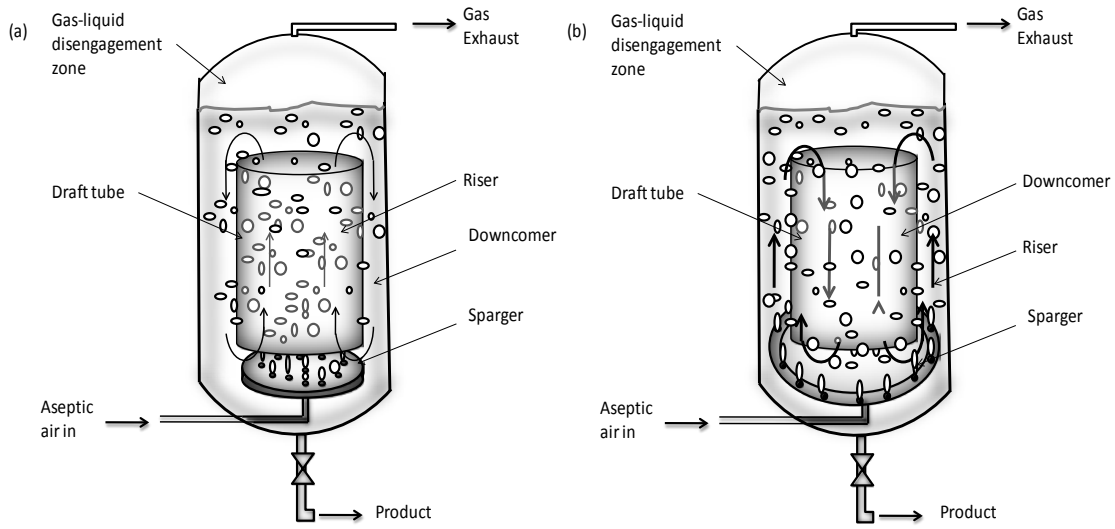

Figure 2.5 Configurations of internal loop airlift bioreactors (a) Internal loop airlift bioreactor, (b) Inverse internal loop airlift bioreactor.

The liquid/slurry phase then flows downward in the downcomer and circulates back to the bottom of the riser. Some small bubbles may be entrained into the downcomer with the circulating liquid at higher velocities (Kilonzo et al., 2007; Klein et al,. 2005; Dhaouadi et al., 2001; Kawase, 1990).

The gas holdup in the downcomer is usually much lower than that in the riser. It is very important to have a thorough knowledge of mixing behaviour for the design, modelling and operation of an airlift bioreactor. These bioreactors are less costly than stirred tank bioreactor and easy to scale-up. There are no serious restrictions with respect to the size of these bioreactors, thus bioreactors, larger than 300 m^3 are nearly exclusively constructed as airlift bioreactors. The design avoids the heat generation by mechanical agitation and reduces the chances of contamination because of impellers. In internal loop airlift bioreactors, the draft tube is used to improve liquid circulation that results in better mixing with high mass transfer rate. The shearing is low due to the absence of mechanical mixers. The power requirement is low. These bioreactors involve bubble coalescence, which can reduce mass transfer rate. Higher initial capital investment is required due to the large scale processes. Furthermore, they require greater air throughput and higher pressures, particularly for large-scale operations. When foaming occurs, the gas/liquid separation becomes inefficient. Another important type of airlift bioreactors called external loop airlift bioreactor is shown in Figure 2.6. The main difference in the design of external loop airlift bioreactors that sets it apart from the internal loop airlift bioreactors is that the riser and the downcomer are connected by a pipe at the bottom and a pipe or a tank at the top (Farouza et al., 2009; Benyahia and Jones, 1997; Bello et al., 1984). The external loop airlift bioreactors will be handled in more details in the following section.

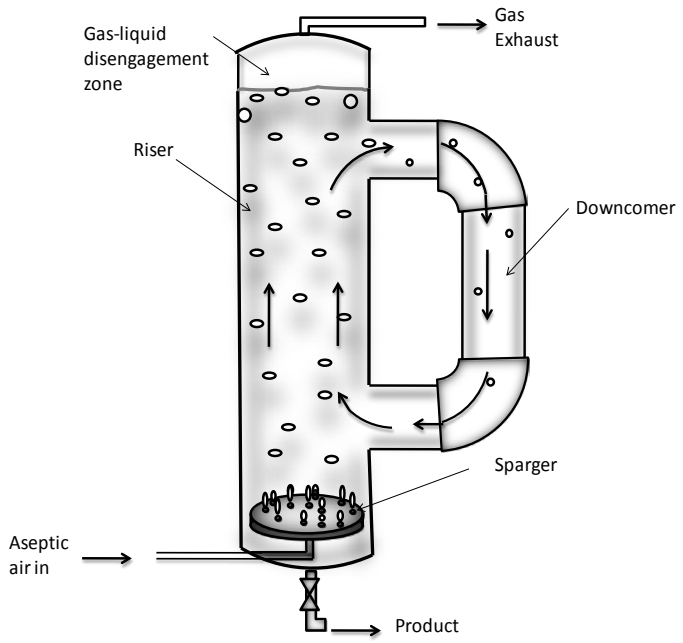

Figure 2.6 External loop airlift bioreactor.

2.3. External Loop Airlift Bioreactors

2.3.1. Description

External loop airlift bioreactors have been the subject of increasing interest in recent years. All external loop airlift bioreactors consist of four distinct sections each with its unique flow characteristics i.e., with variable local hydrodynamics (gas holdup, liquid velocity, and mass transfer rates):

- **The riser**: In this section, the gas is usually sparged at the bottom and the gas-liquid dispersion travels upwards. This section has a higher gas holdup and most of the gas-liquid contact takes place in this section.

- **The downcomer**: This section is adjacent to the riser and is characterized by the dispersion recirculation in a downward direction. The liquid recirculates as a result of density difference due to partial or total disengagement of gas at the top.
- **The base**: The riser and the downcomer are connected at the bottom by a simple horizontal connection and the geometry of this section has an impact on gas holdup, liquid velocity, and solid flow (for three phase flow).
- **The gas-disengager (disengagement zone)**: This section connects the riser to the downcomer at the top of the reactor and allows gas disengagement and liquid recirculation. The geometry of this section has an impact on the gas holdup and liquid velocity.

Figure 2.7 shows external loop airlift bioreactor. In this type of bioreactors, air is sparged in the riser and the fluid re-circulates in the downcomer, while the gas is separated in the disengagement zone or gas separator. The difference in gas holdup in the sparged and un-sparged sections results in a difference in bulk densities between the fluids and because of this bulk densities difference the fluid circulates in the reactor by a gas lift action. The name airlift came up with the fact that when the gas is sparged into the reactor the liquid pool is “airlifted”. The modifications in these bioreactors can be made depending on the requirements of different fermentation processes. The modification is usually made in the gas-disengagement section where the riser and the downcomer are horizontally connected. The design of the gas-disengagement section may affect the performance of the reactor.

Figure 2.8 shows the configurations of external loop airlift reactors according to two types of gas-disengagers. According to Figure 2.8 the external loop airlift bioreactors can be classified into two types according to the design of gas-disengager:

1. Closed Channel Type in which the riser and the downcomer are connected by a horizontal tube gas-disengager. This closed Channel type gas-liquid separator can be used where the cells in the bioreactor are not very sensitive because it lets more bubbles in the downcomer. These bubbles re-enter the riser after passing through the bottom connecting section and allow more turbulence to harm the sensitive cells. It causes more oxygen transfer because of recycling of gas bubbles.
2. Open Channel Type in which the riser and the downcomer are connected by a rectangular tank placed at the top. The open Channel type gas-liquid separator can be used where the cells in the bioreactors are very sensitive because it allows only few bubbles in the downcomer. This type involves less oxygen transfer because most of the gas bubbles are separated from the liquid at the top.

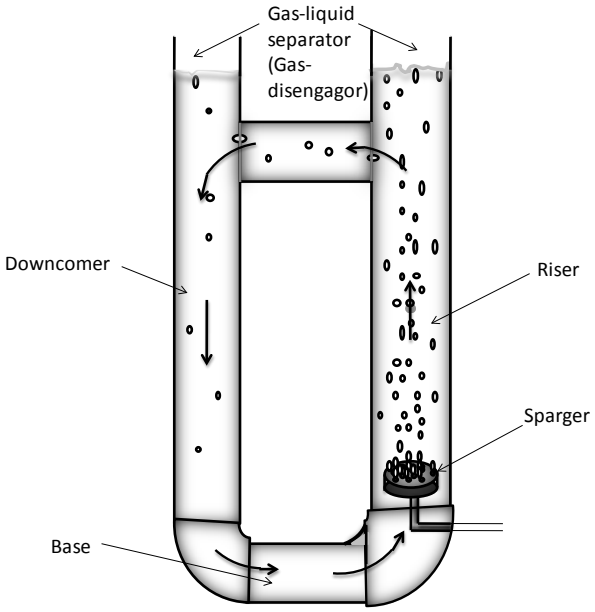

Figure 2.7 External loop airlift bioreactor.

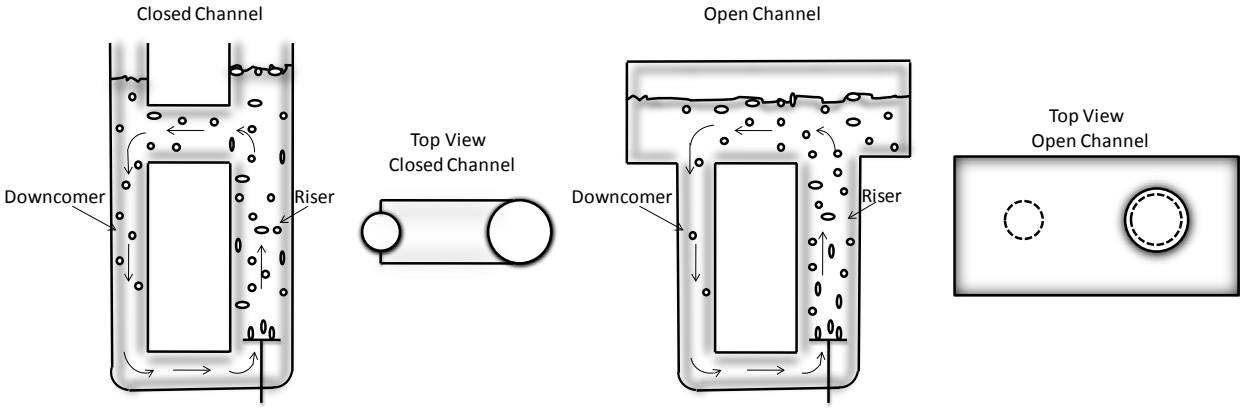

Figure 2.8 Configurations of external loop airlift bioreactors.

2.3.2. External versus Internal Loop Airlift Bioreactors

The external loop airlift bioreactors offer effective heat transfer and efficient temperature control. These bioreactors have low friction in riser and downcomer. Independent control of the gas input-rate and liquid velocity can be achieved by using a throttling device on bottom connecting tube between riser and downcomer of the external loop bioreactor. These bioreactors offer a better opportunity for measurement and control in the riser and the downcomer. The external-loop usually reaches nearly total gas disengagement at the top section (due to the presence of separate gas-disengagement section) giving rise to a higher difference in density or hydrostatic pressure which results in higher circulation velocity as compared to the internal loop airlift bioreactor and consequently improves mixing and heat transfer in the reactor. On the other hand, the external loop offers lower gas recirculation as compared to internal loop airlift, which results in lower mass transfer. Due to their tall design, these bioreactors take a lot of vertical space in the laboratory (Dhaouadi et al., 2006; Zhang et al., 2005; Benyahia and Jones, 1997; kemblowski et al., 1993; Bello et al., 1984).

2.3.3. Gas Holdup in External Loop Airlift Bioreactor

Gas holdup is an important parameter for the designing of airlift reactors. The gas holdup determines the residence time of the gas in the liquid and in combination with the bubble size influences the gas-liquid interfacial area per unit volume, the mass transfer efficiency from gas to liquid and the circulation liquid velocity in airlift reactors. The gas holdup impacts upon the bioreactor design because the total design volume of the bioreactor for any range of operating conditions depend on the maximum gas holdup that must be accommodated. The greater the gas holdup is the greater is the area for mass transfer rate. This also depends on the amount of oxygen present in the bubble as the continuous recirculation of gas decreases the amount of oxygen in the bubble. Overall gas holdup (ε_g) is the gas fraction within the total reactor volume and can be written by the following formula:

$$\varepsilon_g = V_g/ (V_l+V_g+V_s)..... (2.1)$$

where, V_l, V_g and V_s are the volumes of liquid, gas and solid phases, respectively.

Overall ε_g can be calculated by measuring the height of the liquid before the gas is supplied and the height of the liquid after the gas is supplied. The following formula can be used:

$$\varepsilon_g = (H_D – H_L) / H_D..... (2.2)$$

where H_D is the height of the liquid after the gas is supplied (dispersion height) and H_L is the height of the liquid before the gas is supplied (bubble free liquid height).

Several models were presented for gas holdup related to superficial gas velocity and superficial liquid velocity by many investigators (e.g. Al-Masry et al. 1999; Kemblowski et al. 1993; Popovic et al. 2004; Renzo et al. 2005). Yazdian et al. (2009) investigated the effect of gas properties on the gas holdup in an external loop airlift bioreactor. They used oxygen and methane

as sparged gases and found that as the kinematic viscosity of gas was increased (i.e., from oxygen to methane) the gas holdup was decreased. They also noticed that decrease in riser-to-downcomer cross-sectional area ratio (A_r/A_d) ratio led to see an increase in gas holdup which was the result of the reduced liquid circulation due to the increasing resistance of the liquid circulation path as shown in Table 2.1.

Table 2.1 Effects of superficial gas velocity, physical property of gas and riser-to-downcomer cross-sectional area ratio (A_r/A_d) on gas holdup.

Superficial gas velocity (m/s)	Gas holdup					
	Oxygen[1]			Methane[2]		
	$A_r/A_d = 1$	$A_r/A_d = 4$	$A_r/A_d = 9$	$A_r/A_d = 1$	$A_r/A_d = 4$	$A_r/A_d = 9$
0.020	0.020	0.012	0.002	0.018	0.010	0.001
0.040	0.047	0.036	0.023	0.045	0.033	0.021
0.060	0.050	0.037	0.025	0.047	0.035	0.022

[1] $\upsilon_g = 19.04 \times 10^{-6}$ Pa.s
[2] $\upsilon_g = 27.54 \times 10^{-6}$ Pa.s

Liu et al. (2008) studied liquid dispersion in external loop airlift bioreactors. They observed that the gas holdup decreased monotonically with the liquid level in gas-liquid separator, but the liquid circulation velocity and liquid dispersion coefficient increased with the liquid level. The reason was that, with increasing the liquid level in the gas-liquid separator, the flowing resistance at the top section decreased, which in turn increased the liquid circulation velocity and liquid dispersion coefficient and because of the increased liquid circulation velocity, the gas hold up decreased. Table 2.2 shows the decrease of gas hold up with the increase of liquid level in the gas liquid separator. It can also be seen in Table 2.2 that the gas holdup increases with increasing superficial gas velocity.

Table 2.2 Gas holdup for different liquid level in the gas–liquid separator.

Superficial gas velocity (m/s)	Gas holdup for different liquid level in gas-liquid separator (mm)		
	20	100	200
0.093	0.077	0.070	0.060
0.192	0.140	0.125	0.113
0.300	0.180	0.170	0.156

Mohanty et al. (2006) investigated the hydrodynamics in novel multi-stage external loop airlift reactor operating in three stages with hydro-dynamically induced continuous bubble generation, breakup through rupture and regeneration. They used contraction-expansion disks in the riser for better mass transfer. The authors observed that the gas holdup was increased with increasing superficial gas velocity, at a constant superficial liquid velocity as shown in Table 2.3.

Table 2.3 Gas holdup for different superficial gas velocities.

Superficial gas velocity (m/s)	Gas holdup for different superficial liquid velocity (m/s)			
	0.00436	0.00876	0.013	0.0175
0.015	0.473	0.510	0.560	0.580
0.022	0.520	0.560	0.593	0.627
0.035	0.585	0.630	0.662	0.673

They also observed that the gas holdup was increased relatively sharply with the increase in gas velocity in the region of lower gas velocities. The reason was that an increase in gas velocity gave rise to the formation of a large number of bubbles without appreciably increasing the bubble diameters and therefore the gas holdup was increased sharply at low values of gas velocity. While at higher values of gas velocity, the rate of increase in gas holdup with gas velocity was decreased due to the formation of larger bubbles and bubble coalescence. The gas

holdup was observed to be increased with liquid circulation velocity at a constant superficial gas velocity in the riser. The increase in liquid circulation velocity gave the finer dispersion of gas, which increased the gas holdup. The liquid circulation velocity was controlled by the valves between the riser and the downcomer. It was also noticed that by increasing the superficial gas velocity, the liquid circulation velocity was increased which in turn increased the gas holdup. They also reported that the gas holdup for the reactor fitted with the contraction-expansion disks, at the same superficial gas and liquid velocity, was about 45% higher than the reactor without contraction-expansion disks as shown in Table 2.4 and this was possibly due to the finer dispersion achieved in the reactor fitted with the contraction-expansion disks.

Han et al. (2000) investigated the hydrodynamics behaviour in a new gas-liquid-solid inverse fluidized airlift bioreactor. They used the inverted U-type manometers connected to pressure taps located at different positions axially to determine the gas holdup. The following equation was used after measuring the level difference in the inverse U-type manometer (ΔH) and the distance between two measured points (H_0):

$$\varepsilon_g = \frac{\Delta H}{H_0} \text{.....(2.3)}$$

Table 2.4 Gas holdup for different superficial gas velocity with and without contraction-expansion disks.

Superficial gas velocity (m/s)	Gas holdup	
	With contraction-expansion disks	Without contraction-expansion disks
0.015	0.510	0.262
0.022	0.627	0.290
0.035	0.650	0.390

Han and co-workers observed that for any particle loading, the gas holdup was increased with the increase in superficial gas velocity as shown in Table 2.5. They also observed that for a given particle loading, the gas holdup was sharply increased at low gas velocity and at high gas velocity the rate of increase of gas hold up was decreased which was due to the coalescence experienced by the bubbles at high superficial gas velocity. At a fixed superficial gas velocity the gas holdup in the riser was increased with the increase of particle loading.

Table 2.5 Effects of superficial gas velocity and particle loading on gas holdup in the riser.

Superficial gas velocity (m/s)	Gas holdup with particle loading height (m)			
	0	0.20	0.30	0.40
0.015	0.023	0.035	0.040	0.040
0.020	0.028	0.043	0.053	0.053
0.035	0.039	0.055	0.070	0.082

The results for gas holdup in the riser with particle loading in the downcomer were compared with the gas holdup in the riser with no particle loading in the downcomer and it was shown that the gas holdup was greater with the particle loading than that with no particle loading. That means external loop airlift bioreactor with the particle loading provides better gas liquid contact and more mass transfer. The correlations used by Yazdian et al. (2009), Liu et al. (2008), Mohanty et al. (2006), Renzo (2005), Loh and Liu (2001), Freitas et al. (2000) and Kemblowski et al. (1993) for gas holdup calculations are shown in Table 2.6.

Table 2.6 Models for gas holdup in external loop airlift bioreactors.

Reference	Media	Conditions	Equation
Yazdian et al., 2009	Oxygen, methane, Methylomonas spp., methane salt broth	U_{gr}= 0.02 – 0.06 m/s A_r/A_d= 1, 4, 9 H= 2.4m D_r= 0.01 – 0.09m D_d= 0.03m	$\varepsilon_{gr} = 13.19 U_{gr}^{1.43} \left(1+\frac{A_d}{A_r}\right)^{-0.62} (1+s)^{-0.58} \left(\frac{\upsilon_g}{\upsilon_{N_2}}\right)^{-.52}$
Liu et al., 2008	Air, water, FCC catalyst	A_d/A_r= 1 H= 3.2m D_r= 0.1m D_d= 0.1m	$\varepsilon_g = \frac{P_b Ug \ln(1 + (\rho_h gH/P_t))}{\rho_h gH(UL + 0.4(1 + 20\varepsilon_s))}$
Mohanty et al., 2006	Air, water	H= 1.82m D_r= 0.2199m	$\varepsilon_g = 0.187[Fr_G]^{0.184}[Re]^{0.101}[\frac{H}{D_r}]^{0.095}$
Renzo, 2005	Air Water	N/A	$\varepsilon_g = \frac{Q_g/A_r}{0.25 + 1.1(Q_g/A_r + Q_l/A_r)}$
Loh and Liu, 2001	Air, water and expanded polysterene beads(EPS)	A_d/A_r= 1 H= 0.786m D_r= 0.03m D_d= 0.03m	$\varepsilon_g = 0.066\Theta^{-0.164} U_{gr}^{0.013\sigma + 0.545}$
Freitas et al., 2000	Air, water and Ca-alginate beads	U_{gr}= 0.03 – 0.113m/s A_d/A_r= 0.1 H= 2.07m D_r= 0.158m D_d= 0.05m	$\varepsilon_g = \frac{U_{gr}}{C\left[U_{gr} + U_{lr}(1+\frac{\varepsilon_{sr}}{1-\varepsilon_{gr}-\varepsilon_{sr}}) - \varepsilon_{sr}U_{st}\right] + U_{bt}}$
Kemblowski et al., 1993	Air Water Glycol Syrup CMC	A_d/A_r= 0.11 – 1 U_{gr} = 0.001-0.5m/s. H/D_r = 10.2 - 228	$\varepsilon_{gr} = 0.203 \frac{F_r^{0.31}}{M_o^{0.012}} \left(\frac{U_{gr}A_r}{U_{lr}A_d}\right)^{0.74}$

2.3.4. Liquid Circulation Velocity in External Loop Airlift Bioreactor

The liquid circulation in the airlift bioreactors is produced due to the difference in bulk densities of the fluids in the riser and the downcomer. It is a key design parameter for the reactors, which affects the residence time of gas, mass transfer coefficient, turbulence, heat transfer coefficient, shear forces to which the microorganisms are exposed and the mixing time. The cross sectional

area ratio of downcomer to riser is a physical parameter, which strongly affects the liquid circulation velocity.

Popovic et al. (1988) studied liquid circulation velocity in highly viscous non-Newtonian liquids in an external loop airlift bioreactor with an ultrasonic device to measure the liquid velocity in the downcomer. The authors first calibrate the instrument by using a feed tank and a pump. A continuous liquid feed at constant rate was supplied to the bottom of the riser and at the same time the gas was sparged. The calibration liquid containing gas bubbles was collected for the volumetric flow rate measurement after flowing down the downcomer and out of the bottom drain. The following formula was used to calculate the superficial liquid velocity in the downcomer (U_{ld}):

$$U_{ld} = 4Q_L / \pi D_d^2 \text{..... (2.4)}$$

where Q_L is the liquid flow rate and D_d is the diameter of the downcomer. The ultrasonic flow meter recorded the apparent liquid velocity concurrently with the above process. The apparent superficial liquid velocity in the downcomer ($U_{ld,\ apparent}$) was then obtained by:

$$U_{ld,\ apparent} = \text{ultrasonic reading } (1 - \varepsilon_{gd}) \text{..... (2.5)}$$

where, ε_{gd} is the gas holdup in the downcomer section. They used the following continuity relationship to find superficial liquid velocity in the riser (U_{lr}) from the superficial liquid velocity in the downcomer:

$$U_{lr} = U_{ld} (A_d / A_r) \text{..... (2.6)}$$

where, U_{ld} is the superficial liquid velocity in the downcomer, A_d is the cross-sectional area of the downcomer and A_r is the cross-sectional area of the riser. They found that U_{lr} was increased with superficial gas velocity because of the increase in the hydrostatic pressure difference

between the riser and the downcomer as shown in Table 2.7. They also found that, with the increase in apparent viscosity, the superficial liquid velocity in the riser was decreased which was because of the increased total circulation path flow resistance. They observed that the ratio A_d/A_r had a greater effect on the superficial liquid velocity in the riser as shown in Table 2.7. They noticed that for the same operating conditions and rheological behaviour, the U_{lr} in the external loop airlift bioreactor with A_d/A_r= 0.444 was four times greater than the one found for A_d/A_r= 0.111.

Mohanty et al. (2006) investigated the hydrodynamics in novel multi-stage external loop airlift reactor operating in three stages with hydro-dynamically induced continuous bubble generation, breakup through rupture and regeneration. The authors used the neutral buoyancy flow follower technique to determine the liquid circulation velocity. A small piece of plastic tube (outer diameter, 0.009 m; length, 0.02 m; specific gravity, 1.02) was used as a flow follower. This plastic tube started travelling with the liquid a vertical distance in the downcomer and the time was noted for a known vertical distance (0.6m) to calculate the liquid circulation velocity from an average of 10 measurements. They also used the color tracer technique to compare the results obtained by the flow follower technique as multiple factors such as turbulence, small bubbles sticking to the solid follower can affect the accuracy of the flow follower technique. The colour tracer (5 ml of methyl orange solution) was injected at the top of downcomer and the traveling time of color tracer for a known vertical distance (0.6 m) was measured for the calculation of liquid circulation velocity. They found in their experiments that the liquid circulation velocity was strongly dependent on the gas holdup. The following equation had been obtained relating liquid circulation velocity (U_{lc}) with the system fractional gas holdup (ε_g):

$$U_{lc} = 0.248\ \varepsilon_g{}^{1.91} \text{..... (2.7)}$$

Table 2.7 Effect of superficial gas velocity and downcomer-to-riser cross-sectional area ratio (A_d/A_r) on superficial liquid velocity.

Superficial gas velocity (m/s)	Liquid velocity for different A_d/A_r (m/s)		
	0.444	0.25	0.111
0.112	0.125	0.046	0.032
0.125	0.130	0.048	0.036
0.165	0.150	0.060	0.040

Han et al. (2000) studied the hydrodynamics behaviour in a new gas-liquid-solid inverse fluidization airlift bioreactor. They used an external loop bioreactor with solid particles in the downcomer and a screen in the downcomer near top of the downcomer so that the solid particles would not go up to the gas-liquid separator. Tap water and air were used as the liquid and gas phases, whereas perfectly spherical and hollow polyethylene particles with a diameter of 10mm and density 388kg/m^3 were used as solid particles. The authors used tracer response technique to determine the liquid circulation velocity. The injection point was located in the downcomer and was kept from the liquid-solid fluidized section. Two conductivity probes were introduced at different locations vertically in the downcomer and saturated NaCl solution was used as the tracer. A computer was used to process the output signals from two conductivity probes. They investigated the change of liquid circulation velocity both in the packed bed regime and in the inverse fluidized bed regime. They observed that at a fixed loading the liquid circulation velocity was slightly increased with the increase of superficial gas velocity during the packed bed regime because of the flow resistance and was sharply increased with the increase of superficial gas velocity in inverse fluidized region as shown in Table 2.8. It was also shown that for a given superficial gas velocity, the liquid circulation velocity was decreased with the increase in solid particle loading. The reason was that the pressure drop was increased by increasing the solid particle loading which in turn decreased the liquid circulation velocity.

Table 2.8 Effect of superficial gas velocity and particle loading on liquid circulation velocity.

Superficial gas velocity (m/s)	Liquid velocity (m/s)			
	Particle loading height = 0.12 m	Particle loading height = 0.20 m	Particle loading height = 0.30 m	Particle loading height = 0.40 m
0.010	0.100	0.060	0.050	0.040
0.015	0.200	0.078	0.055	0.052
0.020	0.250	0.120	0.052	0.050

Loh and Liu (2001) proposed a novel external loop inversed fluidized bed airlift bioreactor for the treatment of high strength phenolic water. They installed a valve at the bottom between the riser and downcomer section to increase the gas holdup for better oxygen transfer. The hydrodynamics behaviour in this bioreactor was investigated in the presence and absence of solids in the downcomer. The tracer response technique was used to find the liquid circulation velocity. They found that at a fixed valve opening the liquid circulation velocity was increased with the increase in gas velocity as shown in Table 2.9. They also observed that by closing the valve at given gas velocity, the liquid circulation velocity was decreased which in turn increased the gas holdup in the riser.

Table 2.9 Effect of superficial gas velocity and valve opening on liquid circulation velocity.

Superficial gas velocity (m/s)	Liquid velocity for different valve openings (m/s)				
	20%	40%	60%	80%	100%
0.012	0.100	0.155	0.168	0.175	0.178
0.024	0.125	0.189	0.210	0.225	0.230
0.047	0.135	0.212	0.240	0.265	0.274
0.120	0.170	0.280	0.350	0.370	0.375

Kemblowski et al. (1993) investigated liquid circulation velocity in airlift bioreactor with external loop by using different sizes of downcomers. The flow follower method was used to measure the liquid circulation velocity. Because of the geometry of the gas-liquid separator, only liquid phase existed in the downcomer. This made it possible to measure the superficial liquid velocity in the riser by using continuity equation for liquid flow. The authors used both Newtonian and non Newtonian fluids as liquid for experiments and observed a strong influence of the reactor geometry and the properties of the liquid on the results obtained. The correlations used by Essadki et al. (2008), Vial et al. (2005), Hristov (2005), Loh and Liu (2001), Han et al. (2000), Kemblowski et al. (1993), Chisti and Moo-Young (1988), Popovic et al. (1988) and Bello et al. (1984) for liquid circulations are shown in Table 2.10.

Table 2.10 Models for liquid circulations in external loop airlift bioreactors.

Reference	Media	Conditions	Equations
Essadki et al., 2008	Mixture of 2- naphthoic acid and 2-naphtol	A_d/A_r= 0.286 H= 1.47m D_r= 0.094m D_d= 0.050m	$U_{lr}=\left[\frac{2gh_D(\varepsilon_r-\varepsilon_d)}{K_T(\frac{1}{1-\varepsilon_r})^2+\left(\frac{A_r}{A_d}\right)^2 K_B(\frac{1}{1-\varepsilon_d})^2}\right]^{0.5}$
Vial et al., 2005	Air, water	U_{gr}=0.01 – 0.25m/s A_d/A_r= 0.303, 0.286 H= 2.75m, 6.0m D_r= 0.1m, 0.15m D_d=0.05m, 0.08m	$U_{lr}=<U_{lr}>\frac{m+2}{m}(1-\emptyset^m)$
Hristov, 2005	Air, water and metallurgical dross	A_d/A_r= 0.128 H= 2m D_r= 0.14m D_d= 0.05m	$U_{lr}=[1+0.75(\frac{\mathbf{H}}{M_s})^{\frac{3}{2}}]\left(\frac{A_d}{A_r}\right)^{0.74}U_{gr}{}^{0.4}$
Loh and Liu, 2001	Air, water and expanded polystyrene beads(EPS)	A_d/A_r= 1 H= 0.786m D_r= 0.03m D_d= 0.03m	$U_{Lc}=\frac{4.88X10^4\,\Theta}{665+1755\Theta}U_{gr}{}^{0.248}$
Han et al., 2000	Air, water and spherical and hollow polyethylene particles	A_d/A_r= 1 H= 1.3m D_r= 0.06m D_d= 0.06m	$U_{lr}{}^2=\frac{2g\left[\varepsilon_g H_r-\left(1-\frac{\rho_s}{\rho_l}\right)\varepsilon_{s0}H_P\right]}{\frac{K_T}{(1-\varepsilon_g)^2}+K_B\left(\frac{A_r}{A_d}\right)^2}$
Kemblowski et al., 1993	Air, Water, Glycol, Sugar, Syrup, CMC	U_{gr}=0.001-0.15m/s A_d/A_r=1-1.33	$U_{lr}=\sqrt{\frac{2gh_D\varepsilon_r}{\frac{K_T}{(1-\varepsilon_r)^2}+K_B\left(\frac{A_r}{A_d}\right)^2+4h_D\left[\frac{f_r}{D_r}+\frac{f_d}{D_d}+\left(\frac{A_r}{A_d}\right)^2\right]}}$
Chisti and Moo-Young, 1988	Air, Water, NaCl	U_{gr}=0.01-2.0m/s A_r/A_d=0.5-9.1 H = 3.21m D_d = 0.142m	$U_{lr}=\left[\frac{2gh_{D(\varepsilon_r-\varepsilon_d)}}{K_B\left(\frac{1}{(1-\varepsilon_r)^2}+\left(\frac{A_d}{A_r}\right)^2\frac{1}{(1-\varepsilon_d)^2}\right)}\right]^{0.5}$
Popovic et al., 1988	Air, water, CMC solution, Sucrose solution	U_{gr}= 0.04 – 0.25m/s A_d/A_r= 0.111, 0.25, 0.444 D_d= 0.05m, 0.75m, 0.10m	$U_{lr}=0.23U_{gr}{}^{0.32}(\frac{A_d}{A_r})^{.97}\eta_{eff}{}^{-0.39}$
Bello et al., 1984	Air, Water, NaCl	U_{gr}=0.0137-0.086m/s A_d/A_r=0.11-0.69 H= 1.55m D_r = 0.152m D_d= 0.051m, 0.076m, 0.102m	$U_{lr}=1.55\left(\frac{A_d}{A_r}\right)^{0.74}U_{gr}^{0.33}$

2.3.5. Modeling

Dhaouadi et al. (1997) modeled the mass transfer in an external loop airlift bioreactor. They formulated the model of the external loop airlift reactor by dividing it into four sections: riser, gas-liquid separator, downcomer and bottom junction. Simple elementary models were used. They represented the flow in the riser as plug flow with axial dispersion, the flow in the downcomer as plug flow, and the flow in the gas-liquid separator and the bottom junction as continuous stirred tank reactors (CSTR). The gas flow in the riser was represented as plug flow. Navier-Stokes equations were used to derive all the model equations. The models were written in one velocity direction whereas the radial effects were ignored. The following is the basic equation used in phase k:

$$\frac{\partial(\rho\varepsilon\Phi)_k}{\partial t} = -\frac{\partial(\rho\varepsilon U\Phi)_k}{\partial z} + \frac{\partial(\frac{\mu_{eff}\varepsilon\frac{\partial\Phi}{\partial z}}{\sigma})_k}{\partial z} + S_\Phi \text{..... (2.8)}$$

where, ρ is the density, μ_{eff} is the effective viscosity, ε is the holdup, Φ is the variable, σ is the Schmidt number ($=\mu_{eff}/\rho D_{eff}$), D_{eff} is the effective diffusion coefficient, U is the axial velocity and S_Φ is the source term. The mass balances applied to the different sections of the external loop airlift reactor resulted into a system of differential equations. These differential equations were solved in the real-time domain using, an efficient commercial software (MODEST). The model parameters, volumetric coefficient of gas-liquid mass transfer ($K_L a$) and the dispersion coefficients in the riser (Di) were estimated by solving a set of ordinary second-order differential equation (ODE) and partial second-order differential equation (PDE) using the program package MODEST.

Axial dispersion coefficient is an important parameter used to describe the liquid mixing behaviour. Liu et al. (2008) used the Taylor dispersion model as the basis in their studies to

develop a model for axial dispersion coefficient in an external loop airlift bioreactor. The authors developed the following model for axial dispersion coefficient in external loop airlift bioreactor:

$$D_L = \frac{R^2}{4v_t(n+4)(n+2)} {U_L}^2 \varepsilon_L \approx k{U_L}^2 \varepsilon_L \text{..... (2.9)}$$

where, D_L is the axial dispersion coefficient, v_t is the turbulent viscosity coefficient, U_L is the cross-sectional averaged axial liquid velocity, ε_L is the liquid holdup, n is empirical constant which is dependent on both operating conditions and reactor structure parameters, R is the radius of the channel and

$$k = R^2 / 4\, v_t\, (n+4)(n+2) \text{ ..... (2.10)}$$

Sarkar et al. (2008) developed the hydrodynamic models using continuity equation in the riser, momentum equation in the downcomer and energy balance equation in the separator. The model was developed by using the following time-averaged, steady-state continuity equation in the riser:

$$\nabla . \rho u = 0 \text{..... (2.11)}$$

where, ρ is the liquid density and u is the liquid velocity. The definition of averaging volume was used to solve the equation. The liquid phase continuity equation gives the final differential form:

$$\frac{d}{dz}[< \rho > (1 - \acute{\varepsilon}) < \acute{\upsilon} >_z] = 0 \text{..... (2.12)}$$

where, d represents the differential form, z is the axial coordinate, <ρ> is the mean liquid density, έ is the area average phase holdup and <ύ> is the mean area average liquid velocity. Similarly the gas phase continuity equation gives the form:

$$\frac{d}{dz}[1 - < \rho > \acute{\varepsilon} < \acute{\upsilon}_g >_z] = 0 \text{..... (2.13)}$$

where, <ρ> is the mean density of liquid, ε is the area average phase holdup and <$\acute{v}_g$> is the mean area average gas velocity. The liquid phase flow in the separator was investigated by working on the mechanical energy balance. The final form of the macroscopic momentum balance obtained for the separator:

$$\frac{\acute{v}_{z\,d}^2}{2g}\left[\frac{3}{2}+\left[\frac{D_d}{(1-\acute{\varepsilon})D_r}\right]^2\left(\left[1-\left(\frac{D_r}{D_t}\right)^2\right]^2\left(\frac{D_d}{D_r}\right)^2-1\right)\right]+\frac{<P\prime>_r-P\prime_d}{\rho g}=0 \text{..... (2.14)}$$

where, $\acute{v}_d$ is the area average liquid velocity in the downcomer, z is the axial coordinate, g is the acceleration due to gravity, ε is the area average phase holdup, D_d is the diameter of the downcomer, D_r is the diameter of the riser, D_t is the diameter of separator, $<P`>_r$ is the mean area average pressure in the riser, $P`_d$ is the area average pressure in the downcomer. For the downcomer the mechanical energy balance equation was used and the final form of the macroscopic mechanical energy balance equation obtained:

$$\frac{\acute{v}_{z\,d}^2}{2g}\left[\left(\frac{D_d}{D_r}\right)^2-1\right]+\frac{<P>_r-P_d}{\rho g}-L+f_d\left(\frac{L}{D}\right)_d\frac{\acute{v}_{z\,d}^2}{2g}\{1.3+\left[1-\left(\frac{D_d}{D_r}\right)^2\right]^2\}+1.5\frac{<\acute{v}_{z\,r}^2>}{2g}=0 \text{..... (2.15)}$$

where, $\acute{v}_d$ is the area average liquid velocity in the downcomer, $\acute{v}_r$ is the area average liquid velocity in the riser, z is the axial coordinate, g is the acceleration due to gravity, f_d is the friction factor in the downcomer, D_d is the diameter of the downcomer, D_r is the diameter of the riser, L is the axial distance from sparger to riser, $<P>_r$ is the mean pressure in the riser, P_d is the pressure in the downcomer.

2.3.6. Computational Fluid Dynamics Modeling

In the last decades, Computational Fluid Dynamics (CFD) model development has been increased. Several investigators have carried out CFD simulations for external loop airlift bioreactors in order to study the hydrodynamic behaviour, mixing, mass transfer and axial dispersion in gas-liquid and gas-liquid-solid slurry systems (Roy et al., 2008, Roy et al., 2006, Dhanasekharan et al., 2005 and Wang et al., 2004).

Roy et al. (2008) solved the continuity, momentum-balance equations and passive tracer equation using the commercial software ANSYSCFX-10.0 for the development of the 3D flow pattern and mixing time in an external loop airlift reactor. The authors performed the steady-state simulations and solved the passive-tracer equation to get the mixing time. They solved numerically the set of steady-state governing equations. The transient mass balance equation for an inert tracer was then solved to estimate the mixing time by using the results of velocity profile and eddy diffusivity. A tetrahedral mesh along with prism mesh near the wall (80 000–500 000 nodes depending on the geometry) was used to carry out the simulations. In a 3D cylindrical coordinate system for multiphase flow the transient mass balance equation for a tracer substance was given as:

$$\frac{\partial(\varepsilon_L c)}{\partial t} + \nabla(\varepsilon_L u_L c) = \nabla(D_{eff}\varepsilon_L \nabla.c) \text{ ..... (2.16)}$$

where, ε_L is the liquid holdup, c is the instantaneous concentration of the tracer, u_L is the liquid velocity and D_{eff} is the effective diffusion coefficient.

Wang et al. (2004) developed the numerical simulations in the framework of Two-Fluid formulation along with a k-ε turbulence model. The equations in the Two-Fluid model were divided into three parts. The mass and momentum conservation equations were involved in the

first part where the effective viscosity was found. The interphase forces, including the drag force, virtual mass force and lateral forces were modeled in the second part. Lateral forces, transverse lift force, turbulent dispersion force and wall lubrication force had important effect on the radial profile of the gas holdup. The continuous- and dispersed-phase turbulence was considered in the third part. The authors used the standard k-ε turbulence model in order to model the turbulence in the liquid phase. In order to consider the effect of the gas phase on turbulence in the liquid phase they added extra source terms to the standard k-ε turbulence model. Dhanasekharan et al. (2005) used air-water system as a two-phase flow in external loop airlift reactor. The authors solved the mass and momentum balance equations for each phase in external loop airlift reactor. The population balance model was coupled to the mass and momentum balance equations and solved using computational fluid dynamics code FLUENT 6 that was based on the finite volume method.

2.3.7. Shear Rate

For viscous non-Newtonian systems, shear rate is used as an important parameter in the designing of an external loop airlift bioreactor. Some microorganisms are very sensitive to shear so the determination of average shear rate in the bioreactors involving these shear-sensitive microorganisms is very important. The physical properties of fluid and the hydrodynamics in the bioreactor can allow high shear rates which may damage these microorganisms and biofilms formation. The determination of average shear rate can be helpful to correlate hydrodynamics, and mass and heat transfer data in Newtonian and non-Newtonian systems.

In bioprocesses, the rheological behaviour of the culture fluid is characterised by measurement of the fluid consistency coefficient (K) and the flow behaviour index (n). Based on these

measurements, the culture fluid changes from a low viscosity Newtonian system early in the process, to a viscous Non-Newtonian (pseudoplastic) system (Kang et al., 2001). Values of K and n for any fluid depend on the concentration of solids in the broth, the morphology (length, diameter, shape, degree of branching) of the particles, the growth conditions (flexibility of cell wall and particles), the microbial species and the osmotic pressure of the suspending liquid, among other possible factors (Chavez-Parga et al., 2007). Power law model is usually used to present the shear rate relationship. The shear stress is given by:

$$\tau = K\gamma^{n} \text{..... (2.17)}$$

where, τ is the shear stress, K is the fluid consistency index, γ is the shear rate and n is the flow behaviour index.

$$\gamma = \left(\frac{\mu_{eff}}{K}\right)^{\frac{1}{(n-1)}} \text{..... (2.18)}$$

where, μ_{eff} is the effective viscosity.

Nishikawa et al. (1977) observed the following relation for the shear rate in bioreactors:

$$\gamma_{av} = 5000\, U_g \text{..... (2.19)}$$

where, $U_g \geq 0.04$ m/sec, γ_{av} is the average shear rate and U_g is the superficial gas velocity.

Al-Masry (1998) investigated the average shear rate in his studies. He developed a correlation for the average shear rate due to walls of the reactor by using the data from his work and those in the literature. The correlation showed that the average shear rate was a function of superficial gas velocity, geometry, and dispersion height:

$$\gamma_w = 3.36\,(1 - U_g)^{-32.56}\left(1 + \frac{A_d}{A_r}\right)^{0.89} {h_D}^{0.44} \text{.....(2.20)}$$

where, $0.0018 \leq U_g \leq 0.07$ m/sec, $0.11 \leq A_d/A_r \leq 1.0$ and $1.4 \leq h_D \leq 6$ m, γ_w is the average shear rate due to walls of the reactor, U_g is the superficial gas velocity, A_d is the cross-sectional area of the downcomer, A_r is the cross-sectional area of the riser and h_D is the dispersion height.

2.3.8. Sparger Design and Efficiency

Different types of sparger are used for the distribution of air in airlift bioreactors. Some spargers are shown in Figure 2.9. Different types of sparger have different efficiencies. Some of the types are discussed below.

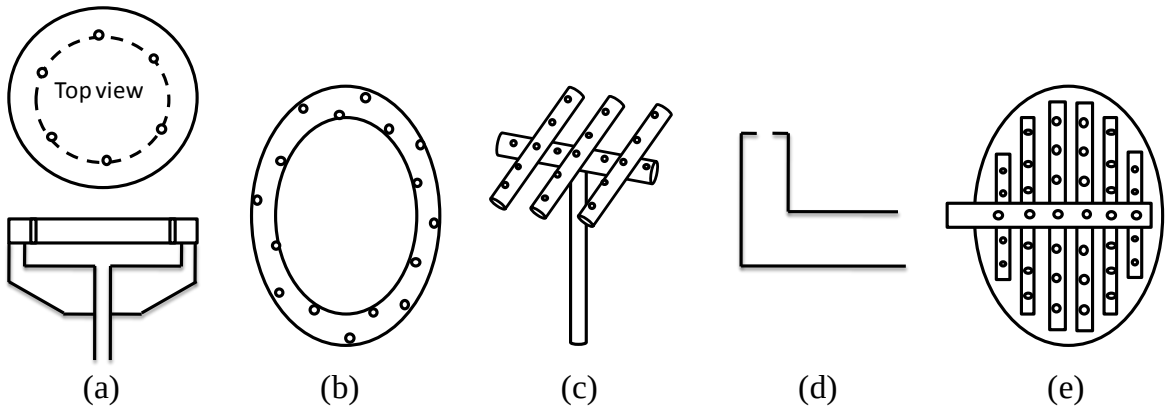

Figure 2.9 Different designs of sparger (a) Spinning sparger (b) Ring sparger, (c) Ladder type sparger, (d) Single orifice sparger, (e) Multi orifice sparger.

Becker et al. (1994) studied the gas-liquid flow in an external loop airlift bioreactor. The authors observed that the type of the sparger and its location in the riser influence the hydrodynamics of the bioreactor. They used two different spargers; a tube sparger and a frit sparger. The tube sparger had the diameter of 8mm with 45 holes of 0.3 mm bores and had its length over the

whole width of the riser. The tube sparger was placed above the downcomer end. The frit sparger consisted of sintered plastic with 40 mm disc diameter and 40 µm mean pore width. Two frits were mounted at the bottom of the riser, below the end of the downcomer. Different spargers showed different resulting flow structures, however both of these gas distributors produced similar bubble size distributions with a mean diameter of 3 mm. The investigation revealed that the flow structure of tube sparger was more uniform because the tube sparger was used in the riser just above point where the circulating liquid entered the riser. The frits showed a more heterogeneous flow pattern in the riser because of their location at the bottom of the riser. The circulating liquid coming from the downcomer pushed the bubbles to the left side of the riser which gave the asymmetry to the flow. This asymmetry of the gas flow was kept till about half the height of the riser and resulted in liquid circulation in the riser. The flow structures in the head and the downcomer were observed as similar to those in the case of the tube sparger.

Lin et al. (2004) investigated the influence of the gas distributor on the local hydrodynamic behaviour of an external loop airlift reactor. The authors used the air and tap water as the gas and liquid phases, respectively. They used two different types of gas distributor for the introduction of air into the reactor. One was a porous sinter distributor with holes of diameter 30 µm and the other was a perforated plate gas distributor with holes of diameter 1mm and a holed ratio of 0.25%. The air was supplied with a superficial gas velocity varying from 0.008 to 0.032 m/s. The gas holdup was measured and found to be increased with superficial gas velocity. It was observed that the gas holdup showed a wall-peaking radial profile for the porous sintered distributor. The perforated plate distributor gave a core-peaking radial profile of gas holdup due to the large bubbles formed. In case of perforated plate distributor, the relatively flatter radial profile of the gas holdup at low superficial gas velocities became more parabolic when the superficial gas velocity was increased. The radial profile of gas holdup in case of porous sintered

plate was much flatter than the one in perforated plate. This showed that the porous sinter plate sparger distributed the gas phase radially much better than the perforated plate sparger.

Randall and Hill (1993) studied the effect of spinning sparger in an external loop airlift bioreactor. The spinning sparger consisted of a flat plate with six orifices and was located below the downcomer connection in order to eliminate the generation of a high shear rates. A hollow shaft was used to support the sparger and a variable speed motor was used to rotate this shaft. The air flowed through this shaft to the sparger. The authors observed that the rotational speed of the sparger had a critical effect on the gas holdup. It was found that the spinning motion of the sparger generated bubbles of smaller diameter with higher gas holdups and interfacial areas.

2.3.9. Mass Transfer Coefficient

Providing an adequate amount of oxygen for microorganism growth is an important factor in the designing of a bioreactor. The oxygen transfer rate must exceed or at least be equal to the total oxygen consumption rate by cells under equilibrium conditions. The oxygen transfer rate depends on the volumetric mass transfer coefficient.

Dhanasekharan et al. (2005) calculated the volumetric mass transfer coefficient as the product of liquid-phase mass transfer coefficient (K_L) and the specific surface area *a*. The basis of Higbie's penetration theory was used to get K_L as:

$$K_L = \frac{2}{\sqrt{\pi}}\sqrt{D}\{\frac{\epsilon_L \rho_L}{\mu_L}\}^{0.25} \text{..... (2.21)}$$

where, K_L is the water turbulent dissipation rate which was predicted from the CFD simulation, ρ_L is the liquid density and μ_L is the liquid viscosity.

The interfacial area (a) was found directly from the predicted bubble size distribution as:

$$a = \sum_i \frac{6\propto_i}{d_i} \text{..... (2.22)}$$

where, α_i is the volume fraction of phase i, while d_i is the bubble diameter.

Jin et al. (2001) investigated the characterization and improvement of oxygen transfer in pilot plant external airlift bioreactor for mycelia biomass production. The solubility of oxygen in the cultivation was low and the dissolved oxygen was being consumed within few minutes. This demanded more supply of oxygen. In order to provide the required supply of oxygen, the authors used two spargers in the bioreactor. One sparger was used in the riser and the other was used in the downcomer. The two spargers played an important role in the improvement of the oxygen transfer efficiency. This created a full aeration environment in the bioreactor and increased the volumetric mass transfer coefficient. The following equation was used to calculate $K_L a$:

$$K_L a = \frac{G(y_1 - y_2)}{V(\frac{P_T y_1}{He} - DO)} \text{..... (2.23)}$$

where, G is the molar air flow rate, y_1 and y_2 are the oxygen content of inlet and exit air, V is the liquid volume in vessel, P_T is the total pressure in system, DO is the dissolved oxygen level in liquid and He is Henry's law constant = 8.345×10^2 litre.atm/mol.

Jin et al. (1999) studied the influence of geometry on the mass transfer characteristics in an external loop airlift reactor for the cultivation of filamentous fungi. The authors observed that the geometric parameter A_d/A_r had its effect on hydrodynamic and mass transfer characteristics in the reactor. They noticed that increasing the downcomer area at a given riser cross-sectional area, decreased the resistance for the fluid to flow in the downcomer. This resulted in the increase of the liquid circulation velocity which decreased the relative slip velocity between the gas bubbles

and the liquid in the riser. This process decreased the bubble average residence time which in turn reduced the gas holdup and the volumetric mass transfer coefficient. The authors also found that the increase in superficial gas velocity and height of gas separator resulted in the increase in gas holdup and mass transfer coefficient and decrease in mixing time. Equation 23 was used to calculate the volumetric mass transfer coefficient.

Mohanty et al. (2007) investigated an external loop airlift reactor operating in three stages. The continuous bubble generation, break-up and regeneration was induced hydro-dynamically for the staging effect by introducing rupture and expansion disks. These disks produced finer dispersion, which resulted in the increase of gas holdup in the reactor. This increase in gas holdup increased the mass transfer coefficient. The following equation was derived to determine $K_L a$:

$$R_a = K_L a C_A^* \text{..... (2.24)}$$

where, R_a is the rate of mass transfer per unit area, C_A^* is the dissolved oxygen concentration at equilibrium.

Zhang et al. (2006) studied the analysis and measurement of mass transfer in airlift loop reactors. The authors investigated different values of $K_L a$ for different solid loadings. They found that the volumetric mass transfer coefficient was reduced with the increase in solid loading. The bubble coalescence was increased with solid loading. This bubble coalescence decreased the gas holdup, which in turn decreased the interfacial area and volumetric mass transfer coefficient. They also showed that $K_L a$ was approximately linear increased with increasing superficial gas velocity. The following equation was derived:

$$\frac{C_L^* - C_m(t_e)}{C_L^* - C_m(0)} = \frac{1}{K_P - K_L a_w}\left[K_P \exp(-K_L a_w t_e) - K_L a_w \exp(-K_P t_e)\right] \text{..... (2.25)}$$

where, C_L^* is the oxygen saturated concentration in the liquid phase, C_m is the mean oxygen concentration, K_P is the sensor response coefficient, a_w is the interfacial area for the whole reactor and t_e is the time in Lagrange coordinate.

Ballica and Ryu (1993) have shown the effect of plant cell concentration on mass transfer rate in terms of volumetric oxygen transfer coefficients in their studies. The volumetric oxygen transfer coefficient decreases with increasing cell concentration while it increases with increasing aeration rate. The decrease in K_La with increasing cell concentration is because of the increasing apparent viscosity and insufficient mixing.

2.3.10. Mixing Characteristics

One of the most important parameters in the designing of an external loop airlift bioreactor is mixing. In some processes where non-uniform profiles of concentration or temperature can cause side reactions or reduce the chemical reaction rate, good mixing is very important. The dispersion coefficient, Peclet number, and mixing time are usually used in order to describe liquid mixing in an external loop airlift bioreactor. In external loop airlift bioreactors, sparged air is used to achieve the mixing. The mixing of gas phase is usually negligible because of the high velocity of gas bubbles in the airlift reactor.

Liu et al. (2008) investigated the axial dispersion coefficient in order to describe the mixing in an external loop airlift reactor. The authors used water as liquid phase, air as gas phase and FCC catalyst as solid phase. They found that when the superficial gas velocity, liquid velocity, or liquid level in the gas–liquid separator was increased, the liquid dispersion coefficient was also increased. They also noticed that when the concentration of fine particles or flowing resistance

was increased, the liquid dispersion coefficient was decreased. Jin et al. (2001) used the pulse tracer technique in order to measure the mixing time in an external loop airlift bioreactor. They used 1.0 ml injection of 4M NaOH as a tracer and measured the pH by using probes at four positions within the vessel. The signals from these probes were sent to the multichannel data logger which was connected to a micro computer. The mixing time was calculated as the time for the pH response to the initial peak. The time required to get the specific inhomogeneity (5%) after the injection of the tracer was also defined as mixing time. The inhomogeneity (I) after the tracer injection was calculated as the relative deviation of the actual maximum concentration (maximum pH) from the mean value (mean pH) which was achieved after perfect mixing:

$$I = \frac{C_a - C_m}{C_m} \text{..... (2.26)}$$

where, C_a is the actual maximum concentration (maximum pH) and C_m is the mean concentration (mean pH).

2.3.11. Flow Regimes

All flow regimes with different gas flow rates are directly dependent on the reactor configuration and the properties of the fluid used. The gas is usually sparged at the bottom of the reactor and with the increase of gas flow, different regimes can be observed. When the gas flow rate is low, the bubbles rise almost straight up the reactor with little or no interaction between them. This flow is called unhindered bubble flow or homogenous bubble flow or bubbly flow. This causes a larger surface area for mass transfer where as the velocity of the gas phase is equal to that of liquid phase giving less or no turbulence. Figure 2.10 (a) shows the unhindered bubble flow.

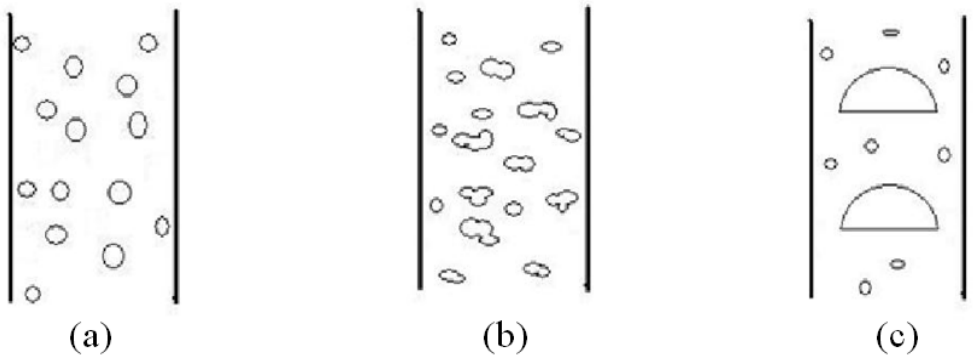

Figure 2.10 Flow regimes (a) Unhindered bubble flow, (b) Churn-turbulent flow and (c) Slug flow.

When the gas flow is increased, the bubbles of varying sizes are formed and the collision rate between bubbles increases. This flow is known as churn turbulent flow or heterogeneous turbulent flow. This flow can be observed with an increase in gas flow rate or with a greater diameter of reactor. The gas holdup will be low in heterogeneous turbulent flow and the mass transfer rates will be limiting (Kee et al. 1998). Figure 2.10 (b) shows the churn-turbulent flow.

The bubble size and shape may vary during turbulence. In highly viscous fluids at high flow rates, the size of the spherical cap bubbles varies. In small diameter column, the spherical cap bubbles may attain the dimension of the column in which they are rising, thus producing slug flow as shown in Figure 2.10 (c).

2.3.12. Coalescence and Shapes of Bubbles

Over the last four decades, considerable efforts have been made in order to find out the formation and growth of bubbles in a stagnant and moving liquid, shapes of bubbles in free rise, terminal velocity-volume or drag coefficient-Reynolds number relationship for single and ensemble of bubbles and coalescence and breakage of bubbles in different flow fields.

When the gas is sparged into the reactor, the bubbles may separate from each other or coalesce. The coalescence takes place in three stages. In the first stage, the two bubbles contact each other initially, which results in a film of thickness of few microns separating the bubbles. The second step is the thinning of film to a few Angstroms. In the third and final step, the film is ruptured leading to coalescence. This step is faster than the first and the second step. The coalescence depends on the rate of film drainage or thinning in the second step. If the time required to drain the film to rupturing thickness is longer than the period of contact, the two bubbles may separate than coalesce.

Studies of bubbles in non-Newtonian fluids have been investigated by several investigators (Kee and Chhabra, 1988; Astarita and Apuzzo, 1965; Popovic and Robinson, 1988). At very low Reynold numbers, the surface tension forces tend to maintain the spherical shape. Depending upon the physical properties and their volumes, bubbles can transform from one shape to another for example, from spherical to prolate-tear drop, to oblate cusped and finally to Davies-Taylor type spherical caps. Table 2.11 explains different shapes of bubbles in different concentrations of Polyacrylamide (PAAm) solution.

Table 2.11 Shapes of bubbles and their volumes in different concentrations of Polyacrylamide (PAAm) solution.

No. of Obs.	Concentration of PAAm	Volume of bubbles (m^3)			
		Spherical	Prolate teardrop	Oblate cusped	Spherical cap
1	0.5% PAAm	$< 4\times10^{-8}$	4×10^{-8} - 15×10^{-8}	15.10^{-8} - 250.10^{-8}	$> 250\times10^{-8}$
2	1.0% PAAm	$< 5\times10^{-8}$	5×10^{-8} - 50×10^{-8}	50×10^{-8} - 750×10^{-8}	$> 750\times10^{-8}$
3	1.5% PAAm	$< 7\times10^{-8}$	7×10^{-8} - 20×10^{-8}	20×10^{-8} - 1100×10^{-8}	$> 1100\times10^{-8}$

2.3.13. Different Configurations of External Loop Airlift Bioreactors

External loop airlift bioreactors have been used as gas-liquid contacting devices as well as gas-liquid-solid contacting devices in biotechnology processes at large scale due to their controllable liquid circulation velocity and gas holdup. Various investigators used different designs of external loop airlift bioreactors for the investigation of hydrodynamics behaviour. Different designs were offered for gas holdup, mass transfer, heat transfer and mixing. Some of the designs are discussed below:

Xu and Yu (2008) designed a multiple airlifting membrane bioreactor and investigated hydrodynamics and mass transfers. The vessel was separated into two compartments, a tube-side aerobic compartment and a shell-side anaerobic compartment, by installing four sintered stainless steel filter tubes between the top and the bottom sections as shown in Figure 2.11.

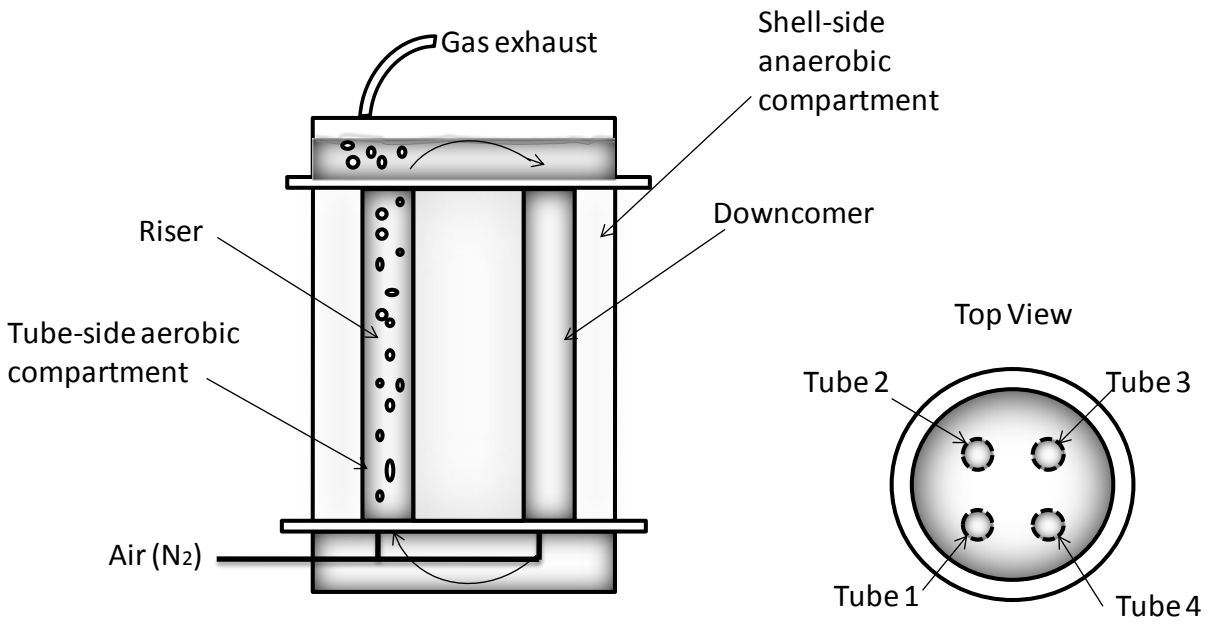

Figure 2.11 Multi-airlifting membrane bioreactor.

Air was sparged into the individual tubes at the bottom through a jet and liquid (water) was degassed at the top section. The degassed water flowed into the tubes that were not aerated, thus forming overall liquid circulations. To study hydrodynamics and mass transfer, the number of airlifting can be easily changed in this multiple airlifting membrane bioreactor as it can be operated with one, two or three risers with corresponding downcomers in order to control overall mixing and mass transfer. Molecular diffusion of substances such as nutrients and metabolic products across the porous walls of filter tubes under concentration gradients can be obtained in this type of bioreactor and it can efficiently integrate aerobic and anaerobic cultures in one single vessel.

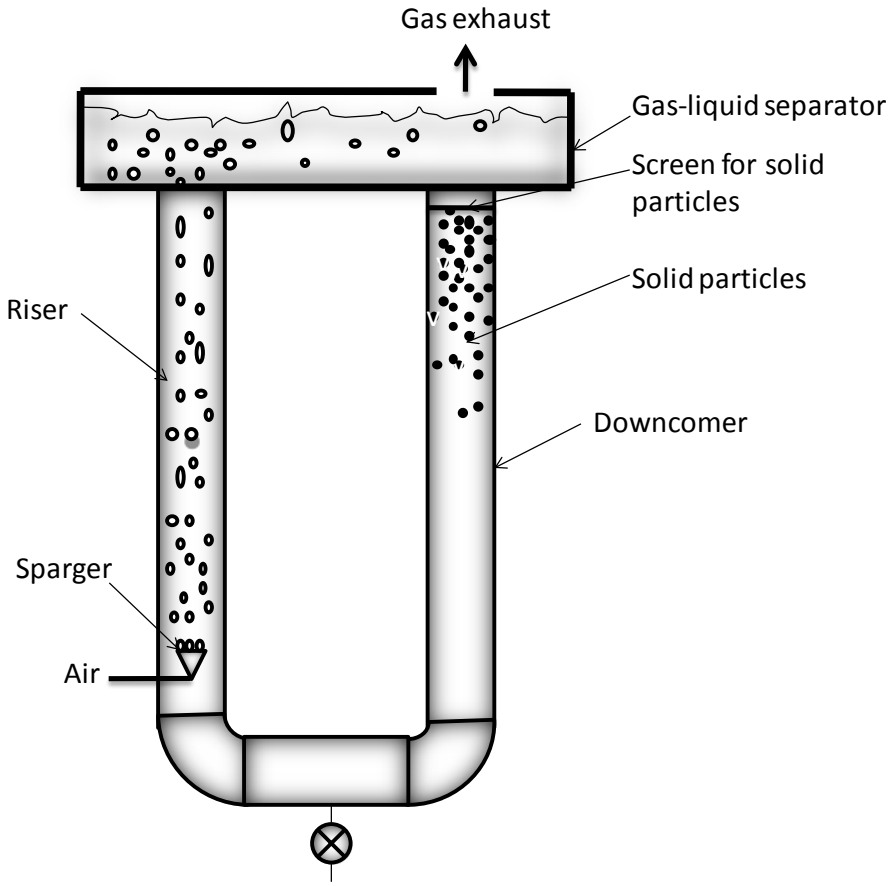

Figure 2.12 Gas-liquid-solid inverse fluidization airlift bioreactor.

Han et al. (2000) investigated hydrodynamic behaviour in a new gas-liquid-solid inverse fluidization airlift bioreactor. The bioreactor was made of Plexiglass materials and the air was introduced through a circular perforated plate sparger, mounted at one end of the pipe and located centrally along the riser axis. The investigators located a stainless steel screen between the gas-liquid separator and the downcomer in order to prevent the solid particles from rising from the downcomer to the gas-liquid separator as shown in Figure 2.12. The advantages of external loop reactors and inverse fluidized beds are combined to construct this novel external loop bioreactor. This bioreactor can be used for sensitive cells immobilized on solid particles. The death of sensitive cells by bubbles is eliminated because the liquid is degassed in the separator and almost no bubbles enter in the downcomer containing cells immobilized on solid particles under the screen while at the same time the turbulent gas-liquid contact can be achieved in the riser.

Loh and Liu (2001) proposed a novel external loop inversed fluidized bed airlift bioreactor by installing a valve at the bottom between the riser and downcomer sections for the treatment of wastewater containing high phenol concentrations as shown in Figure 2.13. In this configuration, for a given gas superficial velocity and a given solids loading, the gas holdup was fixed. In order to increase the gas hold up, either the solid particles loading or the gas superficial velocity was increased but both of these were limited by the extent to which fluidization could be carried out. For the purpose of maintaining high dissolved oxygen concentration in the treatment of wastewater with high phenol concentration, Loh and Liu used the adjusted valve opening in order to control the gas holdup by decoupling the liquid circulation velocity and bed fluidization from the gas velocity.

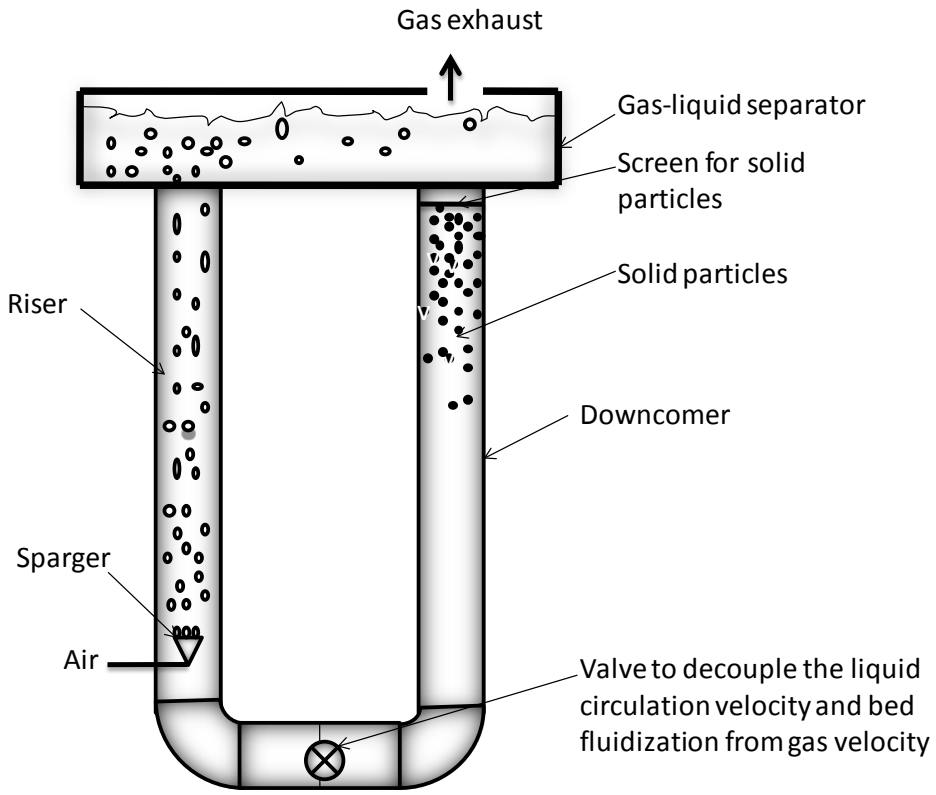

Figure 2.13 Gas-liquid-solid inverse fluidized bed airlift bioreactor with a valve at the bottom.

Zhang et al. (2005) designed a reactor internal for external loop airlift bioreactor. This internal was of 230mm in diameter and 100mm in height. The angle between the baffle of the internal and the vertical axis was 45◦ and each baffle was 30mm in width and 1mm in thickness. The internal also contained some semicircular holes and each hole had a tongue-like plate facing the upstream to break the bubbles. The investigators installed it in an external loop airlift bioreactor in order to enhance bubble breakup and flow redistribution and improve reactor performance as shown in Figure 2.14. A uniform radial profile of the gas holdup decreases bubble-bubble collisions and in turn bubble coalescence is decreased. The decrease in bubble coalescence offers more mass transfer because of the increase in interfacial area. The mounting of reactor internal improved the radial profile of the gas holdup and the liquid velocity and intensified the turbulence. The resistance in the circulation flow path was increased and the gas hold up was

consequently increased because of the decrease in liquid circulation velocity. This internal reduced the bubble size which intensified the mass transfer in the external loop airlift bioreactor.

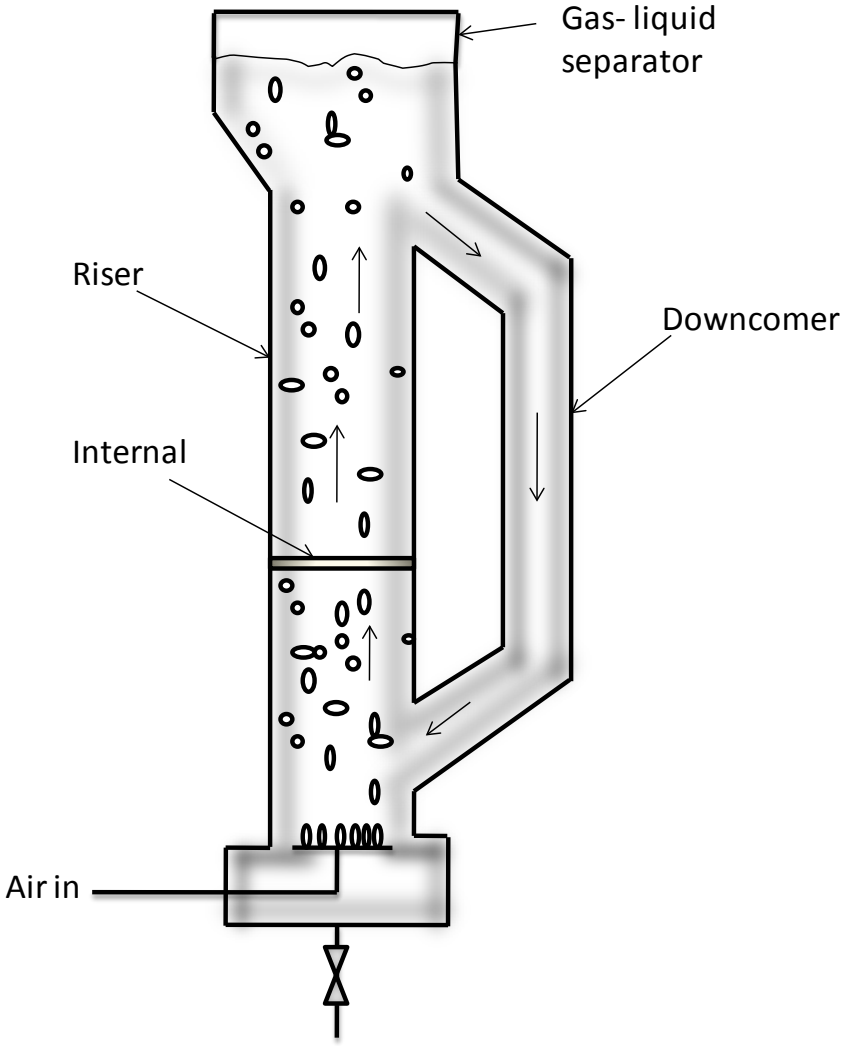

Figure 2.14 External loop airlift bioreactor with internal mounted in the riser.

Meng et al. (2002) combined the design strategies of external loop airlift bioreactor and packed bed bioreactor into one vessel in order to investigate the hydrodynamic behaviour of the combined system as shown in Figure 2.15. They used a woven nylon packing as a packed bed in the riser section of the airlift bioreactor. They observed that the gas holdup continuously increased by increasing the packing height and packing porosity over the range of 0.90-0.99 but

at a porosity of 1.0 (i.e., no packing), the gas holdup dropped at all gas flow rates. They also found that when the amounts of packing, whether in the form of height or packing density, was increased in the riser of external loop airlift bioreactor, the liquid circulation rate was decreased because of the increased frictional resistance. After passing through the packed bed, the bubble sizes were more uniform and had smaller diameters while the Bodenstein number was decreased that indicated greater axial dispersion and enhanced mixing.

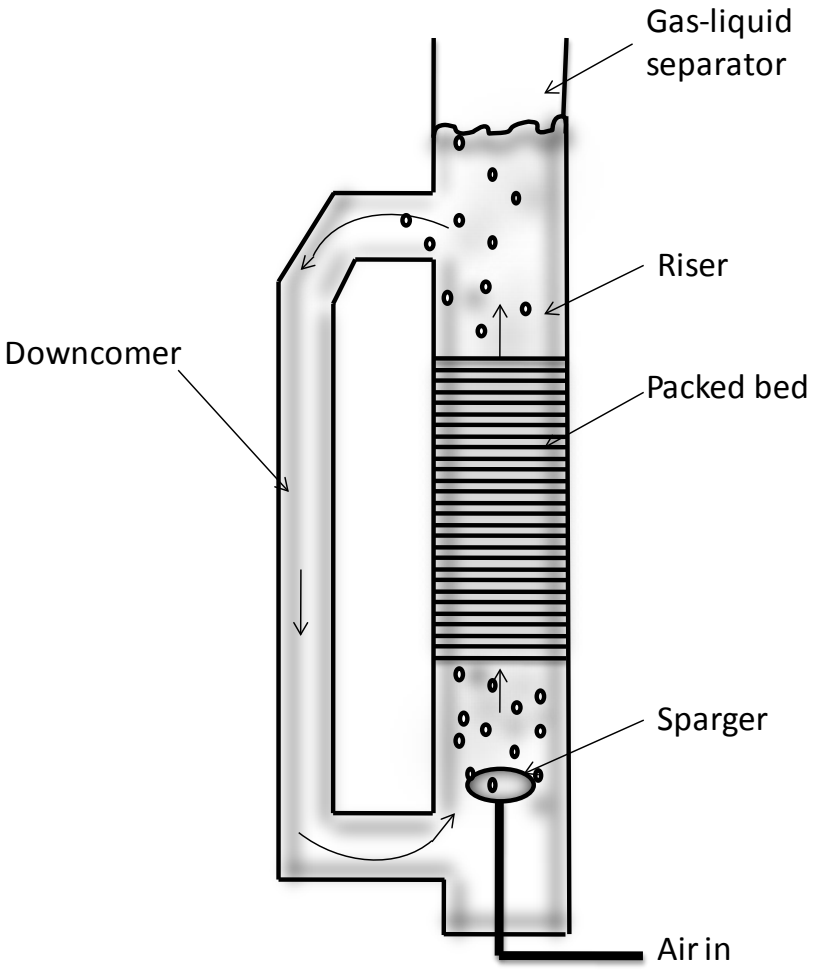

Figure 2.15 External loop airlift bioreactor with packed bed in the riser.

Mohanty et al. (2006) investigated the hydrodynamics of a novel external loop airlift bioreactor operating in three vertical stages which in effect operate in series. The vertical cylindrical column was fitted with a total of seven internals (four contraction disks and three expansion disks) as shown in Figure 2.16. The investigators placed all the contraction and expansion disks at equal distances from each other and threaded screws were used to support these disks. The downcomer at the top was connected to the gas–liquid separator. The downcomer was also connected to these three different stages through valves so that holdup can be measured in individual stages. This reactor was designed so that the hydrodynamic as well as the mass transfer characteristics could be improved without substantially increasing energy dissipation and also the removal of trace organic and inorganic pollutants from wastewater by means of adsorption onto activate carbon could be achieved.

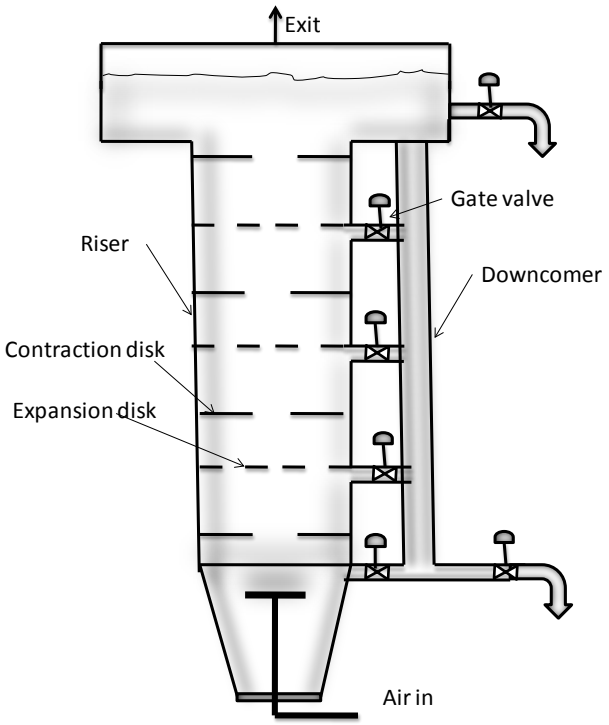

Figure 2.16 Multistage external loop airlift bioreactor.

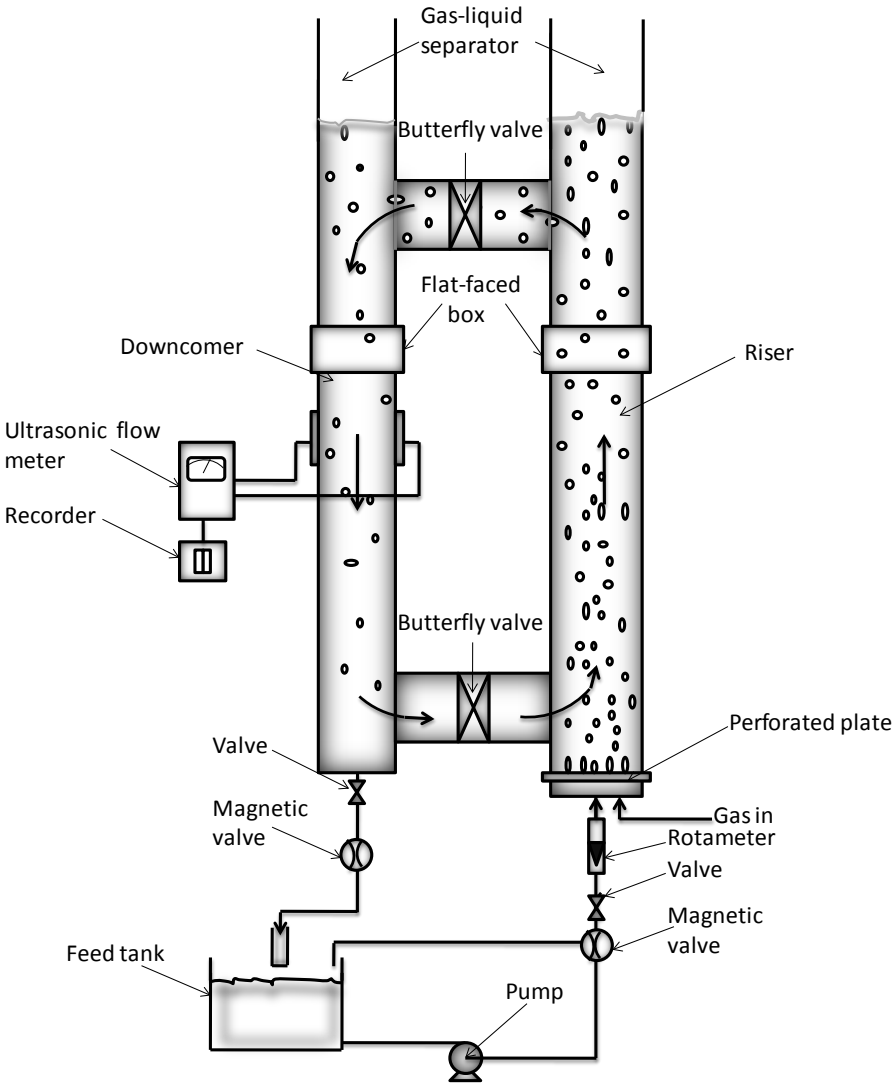

Figure 2.17 External-circulating-loop airlift bioreactor.

Popovic et al. (1988) studied the novel use of ultrasonic flow meter for the measurement of circulating liquid velocity in non-Newtonian systems in an external-circulation-loop airlift bioreactor. They used two butterfly valves in the bioreactor, one at the top connecting section and the other at the bottom connecting section between the riser and downcomer as shown in Figure 2.17. The top butterfly valve could be adjusted to control the circulation liquid velocity. When both butterfly valves at the top and the bottom connecting sections between riser and downcomer were closed, the external-circulation-loop airlift bioreactor could be used as a simple

bubble column. The setup for calibration of the ultrasonic flow meter was made by simultaneously closing of only the butterfly valve at the bottom connecting section and opening of drain at the bottom of the downcomer. Twin transducers were used in the ultrasonic flow meter and were placed at the bottom half of the glass downcomer pipe where the dispersion flow was uniform and laminar. One of the transducers contained a crystal which discharged a continuous ultrasonic wave passing through the pipe and entering the fluid stream. The bubbles in the downcomer reflected a small portion of the ultrasound, which was received by the receiving transducer. The meter dial showed the measured velocity.

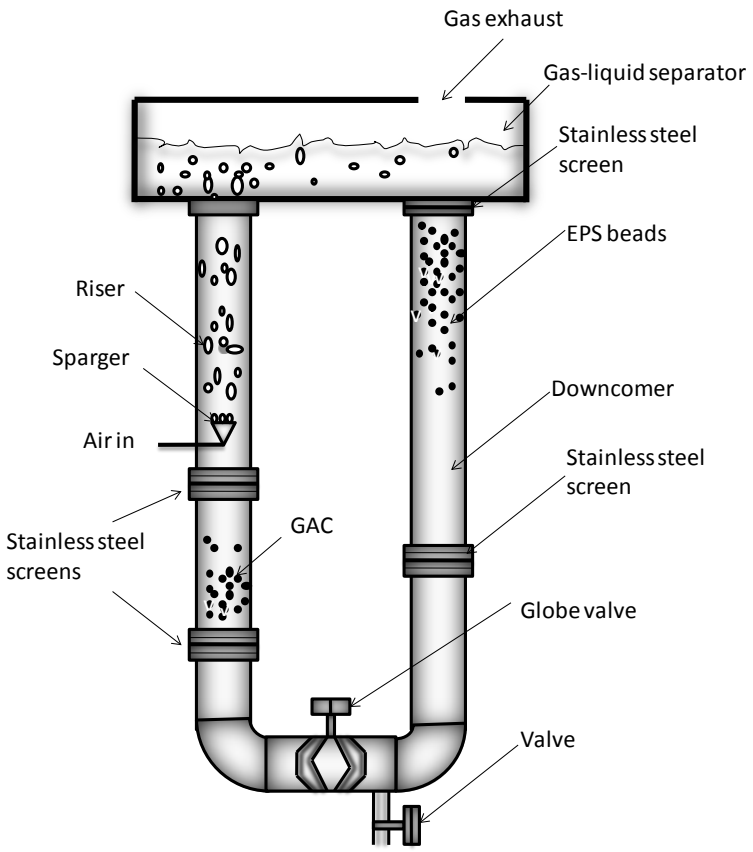

Figure 2.18 External-loop fluidized bed airlift bioreactor.

Loh et al. (2005) investigated the external-loop fluidized bed airlift bioreactor (EFBAB) for the cometabolic biotransformation of 4-chlorophenol (4-cp) in the presence of phenol. They used

two types of solid particles, one below the sparger in the riser and the other in the downcomer. Granular activated carbon (GAC) particles were used between two screens below the sparger in the riser and expanded polystyrene (EPS) beads were used between two screens in the downcomer as shown in Figure 2.18. Different gas velocities and solids loading (EPS and GAC) were used and the effect of the extent of valve opening on the gas holdup and liquid circulation velocity was observed to characterize the hydrodynamics of this bioreactor under cell free condition.

Different designs have been presented for external loop airlift bioreactors. Each of them has its own importance and applications in different chemical and biochemical process. Table 2.3.13 shows some designs of external loop airlift bioreactors with the conditions used, parameters measured and their applications.

Table 2.12 Different configurations of external loop airlift bioreactor.

Reference	Media	Conditions	Parameters Measured	Configuration of External Loop	Applications
Xu et al., 2008	Air Water	A_d/A_r= 1 H= 0.762m Vessel dia. = 0.28m External dia. Of tubes= 0.065m Average pore size= 10µm	Gas holdup, liquid circulation velocity, circulation time, mixing time	Multiple-airlifting membrane bioreactor (MAMBR): A vessel was separated into two compartments by installing four sintered stainless steel filter tubes between the top and the bottom sections. One, two or three tubes could be used as risers and rest of the tubes could be used as downcomers.	This bioreactor can be used in bioprocesses where two different biological systems such as aerobic and anaerobic fermentations can be integrated using the multiple risers and downcomers made from porous stainless steel filter tubes. Through these porous membranes molecule diffusion occurs under concentration gradients.
Mohanty et al., 2006	Air Water	Gas flow rates = 3.33 – 13.3x10 $^{-4}$ m/s D_r= 0.2199m Opening of contraction disk = 0.1099m Single opening on expansion disk = 0.00635m	Gas holdup, liquid circulation velocity	Multi-stage external loop airlift reactor (ELALR): A vertical cylindrical column was fitted with a total of seven internals (four contraction disks and three expansion disks) making three stages. The downcomer at the top was connected to the gas–liquid separator. The downcomer was also connected to these three different stages through valves.	This bioreactor can be efficiently used for the treatment of waste water containing phenol by using the method of adsorption onto the surface of activated carbons. Because of continuous agitation by rupture and bursting of bubbles, turbulence is created. This turbulence increases the transfer of trace pollutants to the active sites of the solid adsorbents where the pollutants are adsorbed.

Zhang et al., 2005	Air Water	U_{gr}=0.0067-0.535m/s A_d/A_r= 0.68 H= 4.8m D_r= 0.23m D_d= 0.19m Dia. of reactor internal = 0.230m Height of reactor internal = 0.100m	Gas holdup, bubble rise velocity, bubble sauter diameter, bubble size distribution, liquid velocity	A reactor internal was installed in an external loop airlift bioreactor in order to enhance bubble breakup and flow redistribution and improve reactor performance. The semicircular holes in the internal had a tongue-like plate facing the upstream to break the bubbles.	The internal used in this airlift bioreactor is very useful in the application of airlift bioreactors where higher gas-liquid mass transfer is required. It also improves the flow distribution.
Loh et al., 2005	Air Phenol 4-Chlorophenol Expanded polystyrene beads (EPS) Granular activated carbon (GAC)	A_d/A_r= 1 H= 0.786m D_r= 0.03m D_d= 0.03m	Gas holdup, liquid circulation velocity	External-loop fluidized bed airlift bioreactor (EFBAB): Granular activated carbon (GAC) particles were used between two screens below the sparger in the riser and expanded polystyrene (EPS) beads were used between two screens in the downcomer. A valve was used in the bottom section connecting the riser and the downcomer.	This bioreactor can be used for enhanced cometabolic biotransformation of 4-cp in the presence of phenol.
Meng et al., 2002	Air Water	U_{gr}= $3.1x10^{-3}$ – $1.6x10^{-2}$m/s Liquid height above the sparger = 1.44m Packing height = 0.05 - 0.8m Packing porosity = 0.90 – 1.0	Gas holdup, liquid velocity, axial dispersion, bubble size	The design strategies of external loop airlift bioreactor and packed bed bioreactor were combined into one vessel. A woven nylon packing was used as a packed bed in the riser section of the airlift bioreactor.	This design of external loop airlift bioreactor can be used for processes where the cells immobilized on packing particles are not very sensitive.

Loh et al., 2001	Air Water Expanded polystyrene beads(EPS)	A_d/A_r= 1 H= 0.786m D_r= 0.03m D_d= 0.03m Bead density = 713 kg/m Dia. of beads = 0.001 – 0.00118	Gas holdup, liquid circulation velocity	External loop inversed fluidized bed airlift bioreactor: A standard 0.0254m globe valve was installed at the bottom connection between the riser and downcomer sections.	This bioreactor can be used for the treatment of high strength phenolic wastewater.
Han et al., 2000	Air Water Spherical and hollow polyethylene particles	A_d/A_r= 1 H= 1.3m D_r= 0.06m D_d= 0.06m Dia. of solid particles = 0.01m Density of solid particles = 388 kg/m^3	Gas holdup, bed expansion of inverse fluidization, minimum fluidization velocity in the downcomer, liquid circulation velocity	Gas-liquid-solid inverse fluidization airlift bioreactor: The bioreactor was made of Plexiglass materials. A stainless steel screen was located between the gas-liquid separator and the downcomer in order to prevent the solid particles from rising from the downcomer to the gas-liquid separator.	This bioreactor can be used for the processes where very sensitive cells are immobilized on the solid particles. The design of these bioreactors eliminates the potential problems such as cell death by bubbles.
Popovic et al., 1988	Air Water CMC solution Sucrose solution	U_{gr}= 0.04 – 0.25m/s A_d/A_r= 0.111, 0.25, 0.444 D_d= 0.05m, 0.75m, 0.10m	Gas holdup, mean (sauter) bubble diameter, liquid circulation velocity	External-circulation-loop airlift bioreactor: Ultrasonic flow meter was used for the measurement of circulating liquid velocity. Two butterfly valves were installed in the bioreactor, one at the top connecting section and the other at the bottom connecting section between the riser and downcomer.	The non-invasive ultrasonic flow velocity meter in this design can be used for viscous non-Newtonian systems because the viscosity of these systems is sensitive to most of the standard methods used for measuring liquid velocity.

2.4. Research Objectives

A thorough search of the literature suggests that even though a wide variety of experiments have been performed on the mixing characteristics of external loop airlift bioreactor, the knowledge of mixing characteristics inside this bioreactor can be further enhanced. The literature review also demonstrates that there is still a lack of information on improving hydrodynamic parameters in order to enhance the quality of the product from these bioreactors. For this purpose, new configurations of external loop airlift bioreactor are required and new measurement techniques must be employed in order to better define the mixing characteristics inside the bioreactor in the field of biotechnology. Mohanty et al. (2006) investigated the hydrodynamics in a multi-stage external loop airlift reactor operating in three stages with hydro-dynamically induced continuous bubble generation, breakup through rupture and regeneration. They employed contraction-expansion disks in the riser for better mass transfer. The authors observed that the gas holdup was increased with increasing superficial gas velocity, at a constant superficial liquid velocity. Mohanty et al. (2006) increased the mass transfer rate during the time of mixing by increasing the gas holdup after the installation of contraction and expansion disks in the bioreactor. However, no information was provided for the increase of mass transfer in processes where cell immobilization is employed for the manufacturing of the required product. A new configuration of external loop airlift bioreactor with a packed bed was needed to design in which, during the time of mixing, a higher mass transfer rate could be achieved.

The electrical resistance tomography (ERT) has been employed in many chemical engineering applications and has been becoming a very popular technique in order to evaluate the mixing performance inside the reactors (Gumery et al., 2011; Ishkintana and Bennington, 2010; Hosseini

et al., 2010; Jin et al., 2007; Jin et al., 2006). This measuring technique is non-intrusive to flow processes and it provides information on flow characteristics inside the process vessel. This technique is based on the measurement of conductivity variations within the reactor.

Different investigators used different measurement techniques to measure the hydrodynamic parameters in packed bed external loop airlift bioreactor (Nikakhtari and Hill, 2005; Meng et al., 2002), but nobody has used ERT technique to find the hydrodynamic parameters in a packed bed external loop airlift bioreactor. However, this technique is very useful because it is not only a non-intrusive technique but this technique can be also used to see the material flowing inside the bioreactor.

Following are the objectives for this research work in order to evaluate the mixing performance of a novel external loop airlift bioreactor.

- To evaluate the feasibility of employing ERT in characterization of the hydrodynamic of an external loop airlift bioreactor.
- To design a new configuration of external loop airlift bioreactor in order to improve the reactor hydrodynamics for a better quality product.
- To measure the gas holdup, mixing time and liquid circulation velocity in an external loop airlift bioreactor, using ERT.
- To evaluate the effect of the gas flow rate, bioreactor liquid height, riser internal gas distributor (perforated plate), and riser packing on hydrodynamic parameters.

CHAPTER 3

EXPERIMENTAL SETUP AND PROCEDURE

3.1. Experimental Setup

In the present work, a novel packed bed external loop airlift bioreactor with an internal gas distributor (perforated plate) between two rolls of packing in the riser was designed and built. This novel approach combines advantages of packed bed and external loop airlift bioreactors. Geometries and design of the bioreactor were based on a variety of literatures (Masry et al., 1999 and Al-Masry et al., 2004, Bentifraouine et al., 1997, Benyahia et al., 1997, Han et al, 2000, Loh et al., 2001, Meng et al., 2002, Mohanty et al, 2006, Nikakhtari et al., 2005). The schematic diagram of the experimental setup is shown in Figure 3.1.

3.1.1. Design of Airlift Bioreactor

Polyvinyl chloride material was used to construct this bioreactor. As shown in Figure 3.1, the inner diameters of riser and downcomer were 0.248 m and 0.102 m respectively. The height of the bioreactor was 1.996 m. The height of each packing was 0.234 m and the diameter of internal gas distributor (perforated plate) was 0.248 m. The distance between the internal gas distributor and the top of lower packing was 0.117 m. The distance between the internal gas distributor and the bottom of upper packing was the same as of the distance between the internal gas distributor and the top of lower packing (i.e., 0.117 m). The inner diameter of the upper connecting tube was same as of the inner diameter of lower connecting tube that was 0.102 m. The distance between

the riser and downcomer was 0.305 m. Figure 3.1 shows all the dimensions of the bioreactor. Fibre glass packing was used in this bioreactor. A sparger was installed at the bottom of the riser and the air flow was controlled using a rotameter. The superficial gas velocity in the riser was varied between 0.01087 and 0.03264 m/s. Different configurations of bioreactor were used in order to find hydrodynamic parameters such as gas holdup, mixing time and liquid circulation velocity. This includes installing an internal gas distributor (without any packing) in the riser, installing one packing in the riser and installing an internal gas distributor (perforated plate) between two packings in the riser. In order to build a novel bioreactor, two rolls of packing (fibre glass packing) were installed in the riser and an internal gas distributor (perforated plate) was installed between these two rolls of packing. The function of this perforated plate was to break and regenerate the gas bubbles exiting the lower packing and before entering the upper packing in the riser.

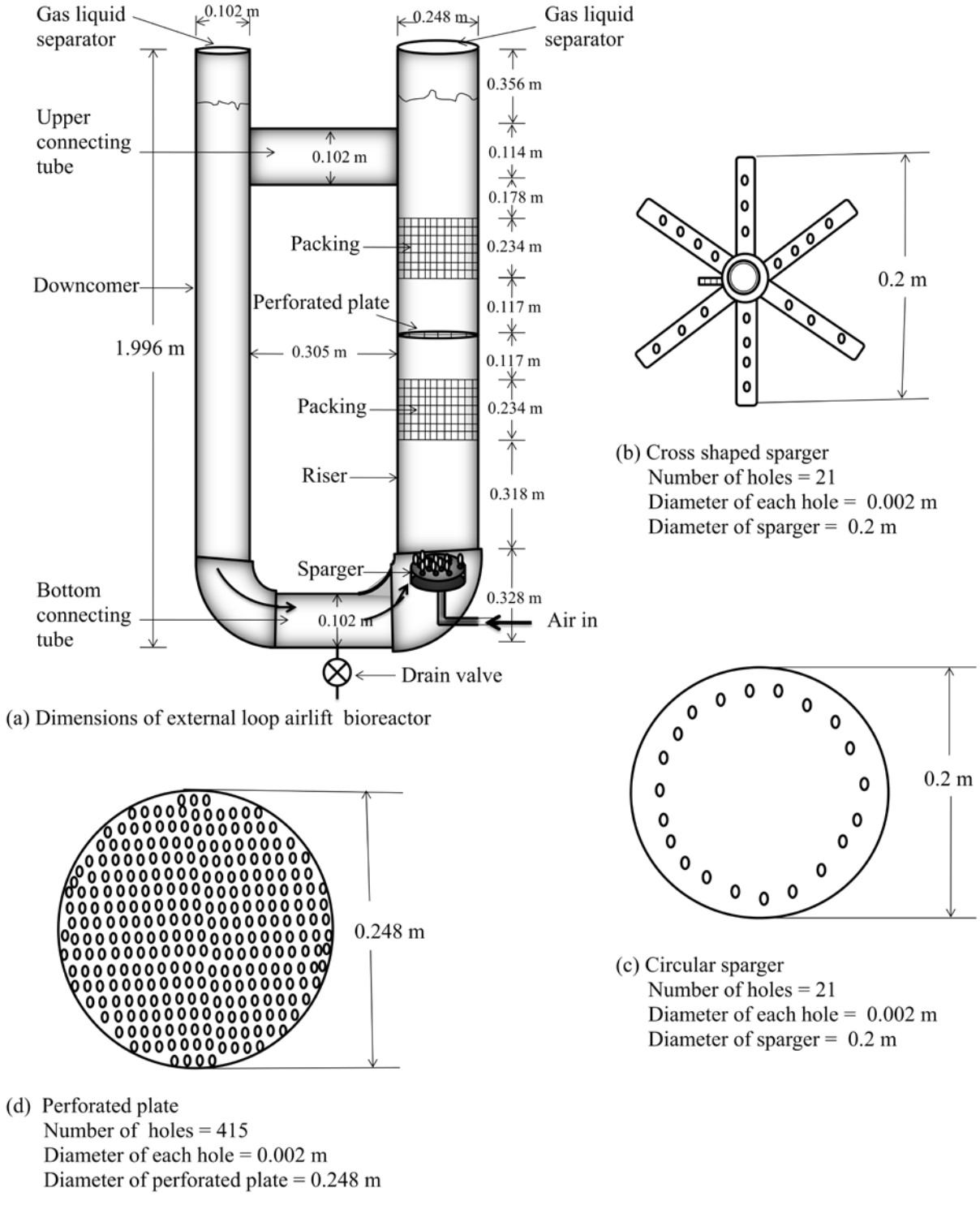

Figure 3.1 Schematic diagram of the external loop airlift bioreactor utilized in this study.

3.1.1.1. Sparger and Perforated Plate Design

Two types of sparger, cross shaped sparger and circular sparger, were used in the present study. In order to design a sparger it is important to know the number of holes in the sparger. For this purpose, the velocity of gas through each hole in the sparger must be known. The Weber number (*We*) proposed by Mersmann (1978) was used to prevent weeping. Mersmann (1978) proposed that Weber number for the sparger with a hole diameter between 1 mm and 5 mm must be 2. Many investigators used the Weber criterion in order to find the superficial gas velocity through each hole in the sparger (Gumery, 2010; Ruff *et al.*, 1978):

$$W_e = \frac{\rho_G d_0 U_G^2}{\sigma_L} = 2 \quad \text{..... (3.1)}$$

$$U_G^2 = \frac{2\sigma_L}{\rho_G d_o} \quad \text{..... (3.2)}$$

where, d_o is the diameter of each hole on sparger, ρ_G is the density of gas, σ_L is the surface tension of liquid and U_G is the superficial gas velocity through each hole in the sparger. Figure 3.1 shows the cross shaped sparger and the circular sparger. The gas velocity through each hole in the sparger was based on the following parameters:

d_o= 2 mm, ρ_G= 1.206 kg/m^3 and σ_L= 0.0724 Kg/s^2.

$$U_G = \sqrt{\frac{2 \times 0.0724}{1.206 \times 0.002}}$$

$$U_G = 7.75\ m/s$$

In order to find the maximum number of holes on the sparger, the lowest superficial gas velocity in the riser (U_{gr}) was calculated according to the following general formula:

$$U_{gr} = \frac{4Q}{\pi D_r^2} \quad \text{..... (3.3)}$$

where, D_r is the inner diameter of the riser and Q is the gas flow rate. The inner diameter of the riser was 0.248 m and the lowest gas flow rate was 0.0005249 m^3/s.

Therefore,

$$U_{gr} = \frac{4 \times 0.0005249}{\pi \times 0.248^2} = 0.01087 m/s$$

The overall volumetric flow rate of air is equal to volumetric flow rate of air through holes in sparger:

$$\frac{\pi}{4} D_r^2 U_{gr} = \frac{\pi}{4} d_o^2 U_G N \quad \text{..... (3.4)}$$

Number of holes, $$N = \frac{D_r^2 U_{gr}}{d_o^2 U_G} = \frac{0.248^2 \times 0.01087}{0.002^2 \times 7.75} \cong 21 \text{ holes}$$

The size of each hole in the perforated plate distributor was taken as 2 mm, which was the size of the each hole in the sparger. Polyvinyl chloride material was used for the manufacturing of this perforated plate because this material is non conductive, which allows the use of electrical resistance tomography. Figure 3.1 shows the schematic diagram of internal gas distributor (perforated plate). The diameter of the perforated plate was equal to the inner diameter of the riser. The number of holes that were drilled on the perforated plate was 415 holes, which is the

maximum number of holes of 2 mm diameter that allows maintaining the integrity of the plate. Increasing the number of holes on the perforated plate could break the plate.

3.1.2. Electrical Resistance Tomography Technique

Electrical Resistance Tomography (ERT) technique was used in the present study to analyze mixing characteristics in the packed bed external loop airlift bioreactor. In a process vessel containing liquid and gas mixture, this technology can create a tomographic image of the inside of the vessel showing liquid phase and gas phase separately in the form of different colours in the tomographic image (Holder, 2005). This technology manipulates data obtained from non-intrusive sensors in order to get the precise quantitative information from locations where it is hard to reach. The tomographic technology involves the installation of a number of electrodes on the periphery of an object to be imaged, such as process vessel or pipeline. The acquisition of measurement signals from these sensors gives the information on the nature and distribution of components within the sensing zone (Williams and Beck, 1995). The applications of process tomography have been increased in recent years as a robust non-invasive tool for direct analysis of the characteristics of multiphase flows. There are different techniques used in electrical tomography in order to find the distribution of electrical properties such as conductivity or resistance (electrical resistance tomography), magnetic inductance (electrical inductance tomography) and capacitance (electrical capacitance tomography). Electrical resistance tomography (ERT) is a non-intrusive measurement technique to determine the electrical conductivity from measurements of voltage around the periphery of a vessel (Mann et al., 1997). The electrodes used for this tomography technique are small and are fitted into the vessel

periphery in such a way that they can contact the material of the vessel but they do not disturb the flow in the vessel. Figure 3.2 shows that the ERT setup for experimental work that includes the electrodes, ITS P2000 (Manchester, UK) data acquisition system (DAS) and a host computer.

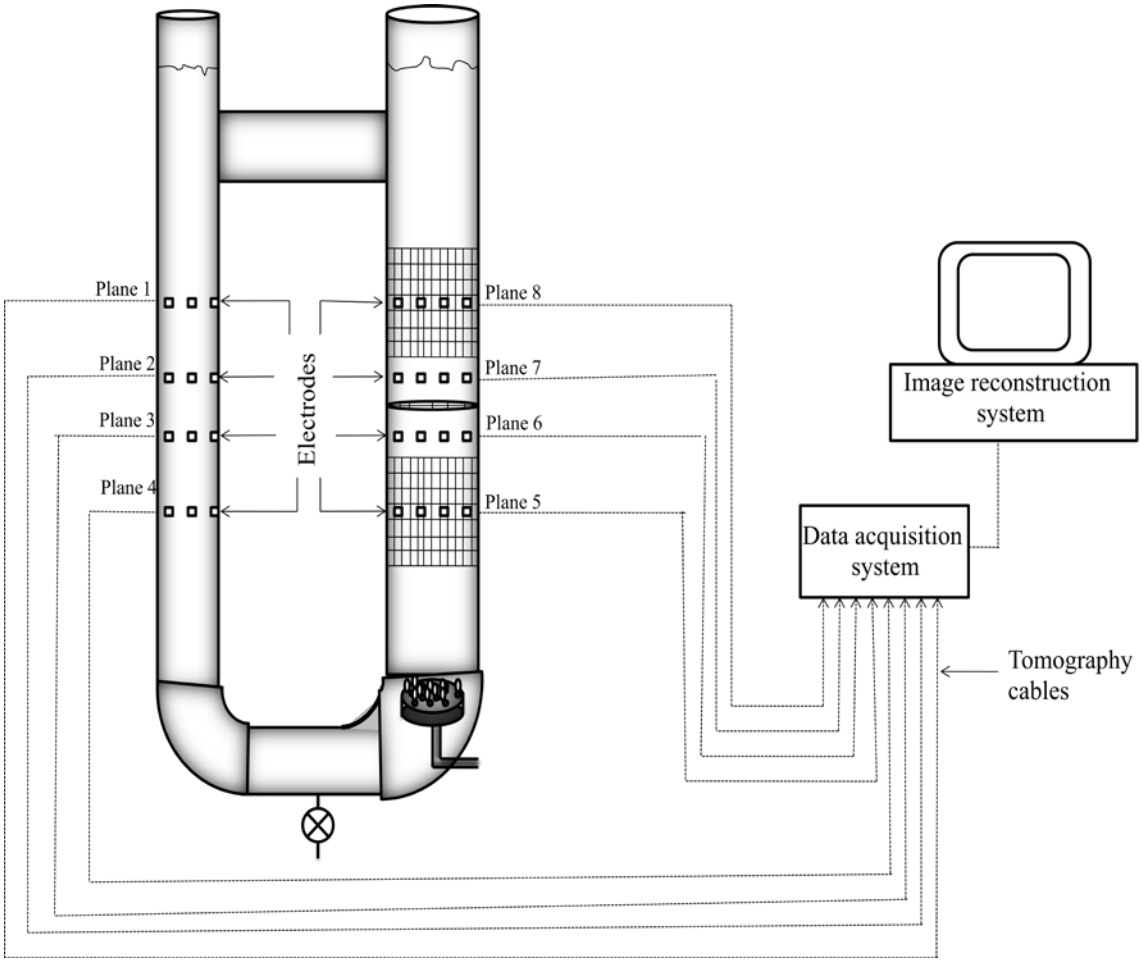

Figure 3.2 Airlift bioreactor equipped with ERT.

3.1.2.1. Electrodes

Sixteen equally spaced stainless steel rectangular electrodes were fitted on the periphery of the bioreactor (riser and downcomer) in one array (plane) and there were four planes on the downcomer and four planes on the riser. Figure 3.3 shows the position and dimensions of

electrodes located on the bioreactor. Each rectangular electrode used on the downcomer was dimensioned as 15 mm high by 10 mm wide with 1 mm thick, while each rectangular electrode used on the riser was dimensioned as 15 mm high by 20 mm wide with 1 mm thick. Plane 5 was constructed on the middle of the axial height of the lower packing, while plane 6 was constructed on the middle of the axial distance between the top of lower packing and the bottom of perforated plate. Plane 7 was constructed on the middle of the axial distance between the bottom of upper packing and the top of perforated plate, while plane 8 was constructed on the middle of the axial height of the upper packing. The distance between plane 5 and plane 6 was 0.175 m, the distance between plane 6 and plane 7 was 0.117 m and the distance between plane 7 and plane 8 was 0.175 m. The distance between plane 5 and the bottom of the bioreactor was 0.764 m. Plane 1, plane 2, plane 3 and plane 4 were constructed on the downcomer at the same level from the bottom of the bioreactor as of plane 8, plane 7, plane 6 and plane 5, respectively. All these electrodes were connected to the ITS P2000 data acquisition system via co-axial cables.

3.1.2.2. Data Acquisition System (DAS)

The data acquisition system was used to send current to the electrodes fitted on the internal walls of the bioreactor. DAS was controlled by using the software ITS P2000 which was installed in the host computer. Different measurement strategies are used to get the electrical measurements using electrodes. These strategies include the adjacent strategy, the opposite strategy, the diagonal or cross method strategy, and the conducting boundary strategy. The adjacent measurement protocol was utilized in this study. The electrical current was applied between an adjacent pair of electrodes using the DAS. The DAS then measured the voltage difference

between all other pairs of adjacent electrodes. Other combinations of adjacent electrode pairs went through the same procedure until the full rotation was obtained on the bioreactor. The frequency of 9600 kHz and injection current of 1.5 mA were the main specifications of ITS P2000 DAS used for all the experiments in this study. The data were collected to calculate the conductivity values within the bioreactor using ITS P2000 software, installed in the host computer, after the air supply and after the injection of saline solution. The mean values of maximum and minimum conductivities for each plane were used to determine the gas holdup, mixing time and liquid circulation velocity.

3.1.2.3. Host Computer

A host computer was used to connect the DAS through a communication port in order to collect and store the data obtained from DAS. After the acquisition of voltage measurements from the electrodes using the DAS, it was necessary to process this data using an appropriate image reconstruction algorithm. The image reconstruction algorithms for straight-ray transmission (e.g., X-ray, γ-ray) do not work in electrostatic fields because when the current lines come across by an interface of different conductivities, the current lines deflect. In industries, the image reconstruction algorithm is chosen as an exchange between the accuracy of image and time required for reconstruction. The ITS 2000 used a qualitative, non-iterative algorithm based on linear back-projection which converted the voltage measurement to conductivity values. This algorithm required a low computational time and was quick and simple because a single, pre-calculated matrix was simply multiplied by the measurements in order to produce the average conductivity readings or signals. This algorithm gave the average conductivity values that

showed the cross-sectional distribution of the electrical conductivity of the contents within the same measurement plane.

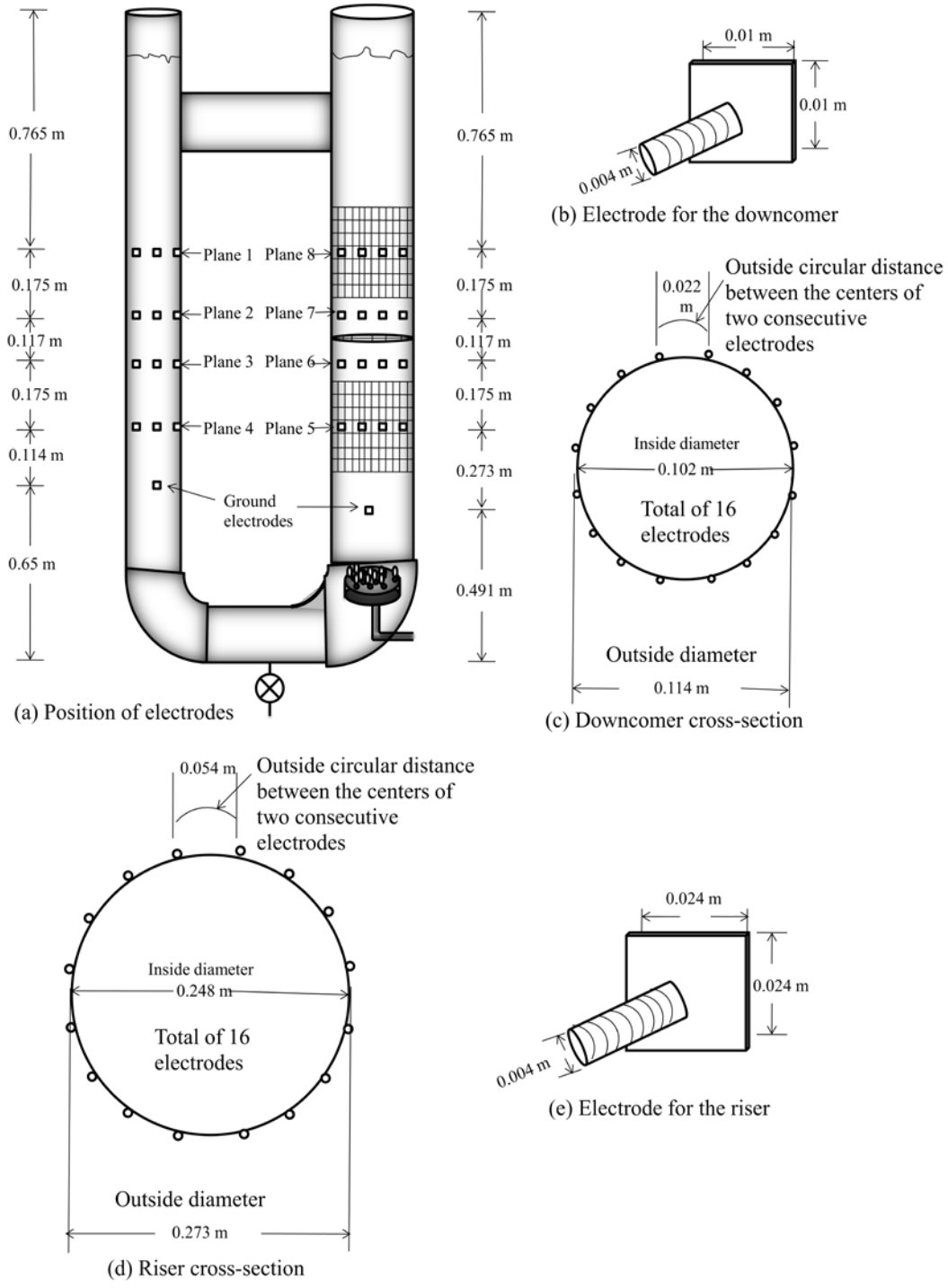

Figure 3.3 Position and size of the tomography electrodes.

3.2. Experimental Procedure

Gas holdup, mixing time and liquid circulation velocity were measured by the ERT for the external loop airlift bioreactor depicted in Figure 3.1. These hydrodynamic parameters can be determined by first finding the change in fluid conductivity in the bioreactor (Gumery et al., 2011; Ishkintana and Bennington, 2010; Jin et al., 2007; Jin et al., 2006).

3.2.1. Gas Holdup Measurement

Tests were performed to determine the effect of changes in air flow rate on gas holdup in the bioreactor. Tap water and air were used as the liquid and gas phases respectively in these experiments. Spargers were fitted in the external loop airlift bioreactor at the bottom of the riser. The bioreactor was filled with water to a constant height. The ERT system was employed to measure the conductivity of water. Air was then introduced using the sparger at the bottom of the bioreactor with a constant flow rate until steady state conditions were reached. The conductivity of the air-water mixture was monitored using ERT system (Ishkintana and Bennington, 2010; Jin et al., 2007; Jin et al., 2006). Data collection was stopped when the steady state condition was reached. The gas flow rate was measured using a rotameter. Same procedure was repeated for different gas flow rates. The local gas holdup fraction in the riser and the downcomer was then measured using the conductivity data obtained from the ERT system. The following Maxwell equation was applied to find the gas holdup (ε_g):

$$\varepsilon_g = \frac{2\sigma_1+\sigma_2-2\sigma_{mc}-\sigma_{mc}{}^{\sigma_2}/_{\sigma_1}}{\sigma_{mc}-{}^{\sigma_2}/_{\sigma_1}+2(\sigma_1-\sigma_2)} \quad \text{..... (3.5)}$$

where, σ_1 is the conductivity of the liquid phase, σ_2 is the conductivity of the gas phase and σ_{mc} is the local value of the mixture conductivity distribution of the two phases. In the present work the second phase (air) is a non-conductive material. By substituting $\sigma_2 = 0$ in equation 3.5, the equation is simplified as follows:

$$\varepsilon_g = \frac{2\sigma_1 - 2\sigma_{mc}}{2\sigma_1 + \sigma_{mc}} \quad \text{..... (3.6)}$$

In order to measure gas holdup in the downcomer, the average value of mean conductivities taken from all four planes on downcomer for water and for air-water mixture in the downcomer were first determined using ERT images. Gas holdup in the riser was estimated by then substituting these mean values in equation 3.6. Same method was used to determine the gas holdup in the riser. A graph was plotted between the mean conductivity values and time for all the eight planes located on downcomer and riser (Figure 3.4). Figure 3.4 shows that when the air was supplied at superficial gas velocity of 1.087×10^{-2} m/s, the conductivity of the air-water mixture was sharply decreased because of the gas holdup in the riser. It can also be seen from Figure 3.4 that the conductivity in down comer was also slightly decreased due to presence of fewer bubbles in the downcomer.

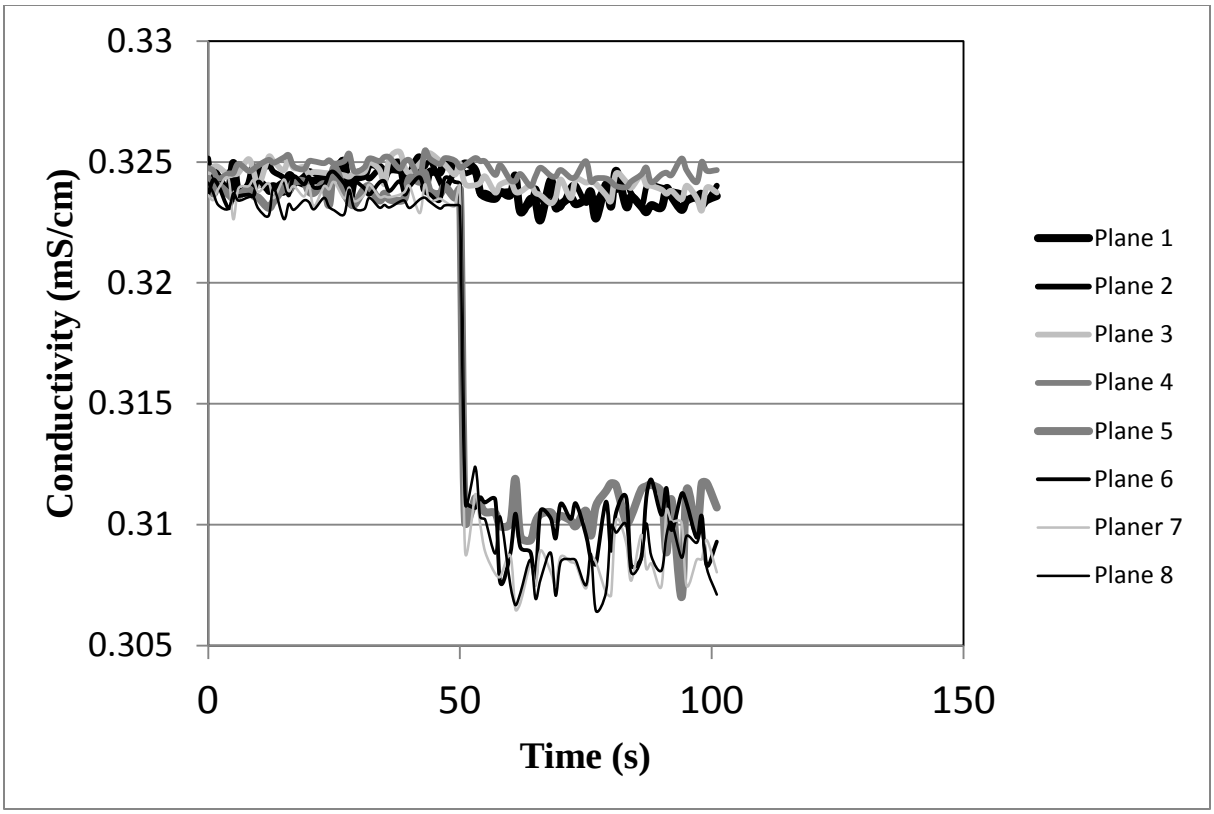

Figure 3.4 Variations in conductivity with time on plane 1, plane 2, plane 3, plane 4 (located in the downcomer), plane 5, plane 6, plane 7 and plane 8 (located in the riser) of ERT system with liquid height = 1.63 m due to the injection of air at U_{gr} = 1.087 × 10^{-2} m/s using cross shaped sparger.

3.2.2. Mixing Time Measurement

The tracer response technique was used to obtain the mixing time in the bioreactor. For this purpose 100 ml of 4% saline solution (NaCl) was used as a tracer. Air was sparged into the bioreactor using a sparger at the bottom of the riser with a constant flow rate. The conductivity of the air-water mixture was monitored using ERT system. After 50 seconds of air supply, the steady state was reached because the conductivity of air-water mixture became stable. After reaching the steady state, the tracer injection was applied in the downcomer above the liquid level. The variations in mean conductivity signals generated by the ERT system were observed

on the host computer. The data collection was stopped when the variations in mean conductivity values taken from all the four planes on the downcomer and all the four planes on the riser became ±1%. The air was then discontinued and water was drained out. Same procedure was repeated for different gas flow rates (Gumery et al., 2011). A graph was plotted between the mean conductivity values taken from all the eight planes and time (Figure 3.5). Figure 3.5 shows the change in the mean conductivity of air-water mixture with time at a riser superficial gas velocity of 1.087×10^{-2} m/s following the injection of tracer. Mixing time (t_m) was measured from the plot (Figure 3.5) by subtracting the time when the conductivity just started increasing, after the injection of tracer, from the time when the variation in mean conductivity values became ±1%. Mixing time was found as 30 seconds as shown in Figure 3.5.

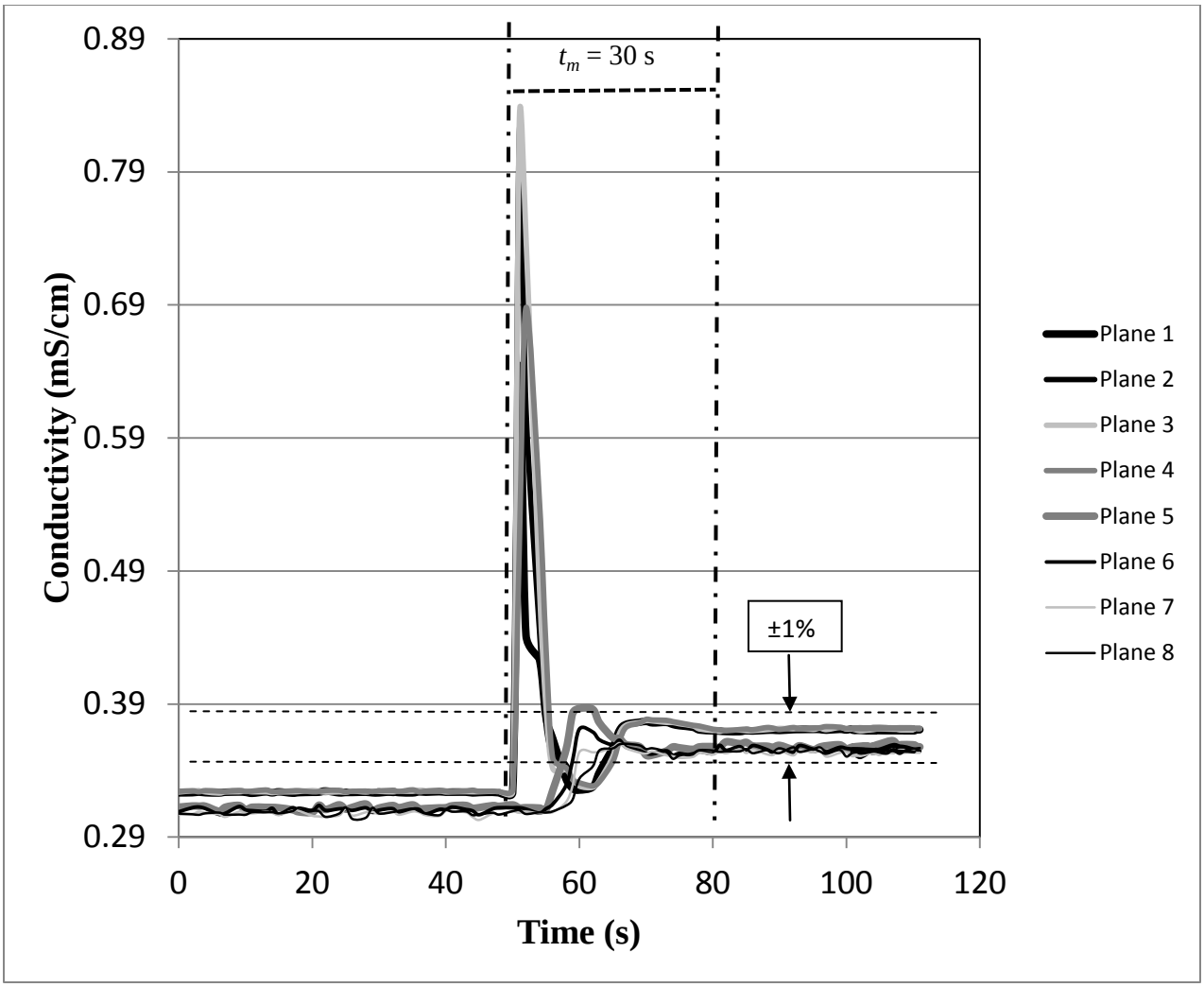

Figure 3.5 Measurement of the mixing time at U_{gr} = 1.087 × 10^{-2} m/s for cross shaped sparger with liquid height = 1.63 m.

3.3. Calculation of Riser Superficial Liquid Velocity

Same experimental procedure was used to find the superficial liquid velocity in the riser as was employed for mixing time (Han et al., 2000; Loh and Liu, 2001; Liu et al., 2008). The riser superficial liquid velocity was calculated using the ratio of the riser liquid circulation height to the riser liquid residence time (Bello et al., 1984; Bello, 1981). The following formula was used to find the superficial liquid velocity in the riser:

$$U_{lr} = \frac{H_r}{t_r}(1 - \varepsilon_{gr}) \text{ ..... (3.7)}$$

where, H_r is the circulating liquid height in the riser, t_r is the liquid residence time in the riser and ε_{gr} is the gas holdup in the riser. The residence time of liquid in the riser (t_r) was determined by the following formula:

$$t_r = \frac{t_c}{\varphi} \text{..... (3.8)}$$

where, t_c is the circulation time and φ is the dimensionless factor. Figure 3.6 represents the change in conductivity with time at riser superficial gas velocity of 1.087×10^{-2} m/s on plane 2 (located in downcomer) of ERT system using cross shaped sparger with liquid height of 1.63 m following the injection of saline solution. The liquid circulation time in the bioreactor can be determined from the plot (Figure 3.6). The circulation time of the tracer was observed as t_c = 20 s on this plot. The circulation time on this plot was measured as the time between two consecutive peaks (Figure 3.6). The circulation time is defined as the time required for an elemental volume of liquid to circulate through the whole path-length of the bioreactor. The dimensionless factor φ can be measured by using the following equation:

$$\varphi = 1 + \frac{1-\varepsilon_{gd}}{1-\varepsilon_{gr}}\left[\frac{A_d}{A_r} + \frac{A_{bc}}{A_r}\frac{H_{bc}}{H_r}\right] + \frac{A_{tc}}{A_r}\frac{H_{tc}}{H_r} \text{ ..... (3.9)}$$

where ε_{gd} is the gas holdup in the downcomer, ε_{gr} is the gas holdup in the riser, A_d is the cross-sectional area of the downcomer, A_r is the cross-sectional area of the riser, A_{bc} is the cross-sectional area of the bottom connecting section, A_{tc} is the cross-sectional area of the top connecting section, H_r is the circulating liquid height in the riser, H_{bc} is the circulating liquid length in the bottom connecting section and H_{tc} is the circulating liquid length in the top

connecting section. By putting the values of A_d, A_{bc}, A_{tc}, H_r, H_{bc} and H_{tc} from the bioreactor geometry in equation 3.9 we get:

$$\varphi = 1 + \frac{1-\varepsilon_{gd}}{1-\varepsilon_{gr}}[0.224] + 0.0551 \quad \text{..... (3.10)}$$

The superficial liquid velocity in the downcomer (U_{ld}) can be determined from a mass balance on the liquid phase (Essadki et al., 2008; Popovic, 1993):

$$U_{ld} = \frac{A_r}{A_d} U_{lr} \quad \text{..... (3.11)}$$

where, U_{lr} is the superficial liquid velocity in the riser, A_d is the cross-sectional area of the downcomer and A_r is the cross-sectional area of the riser.

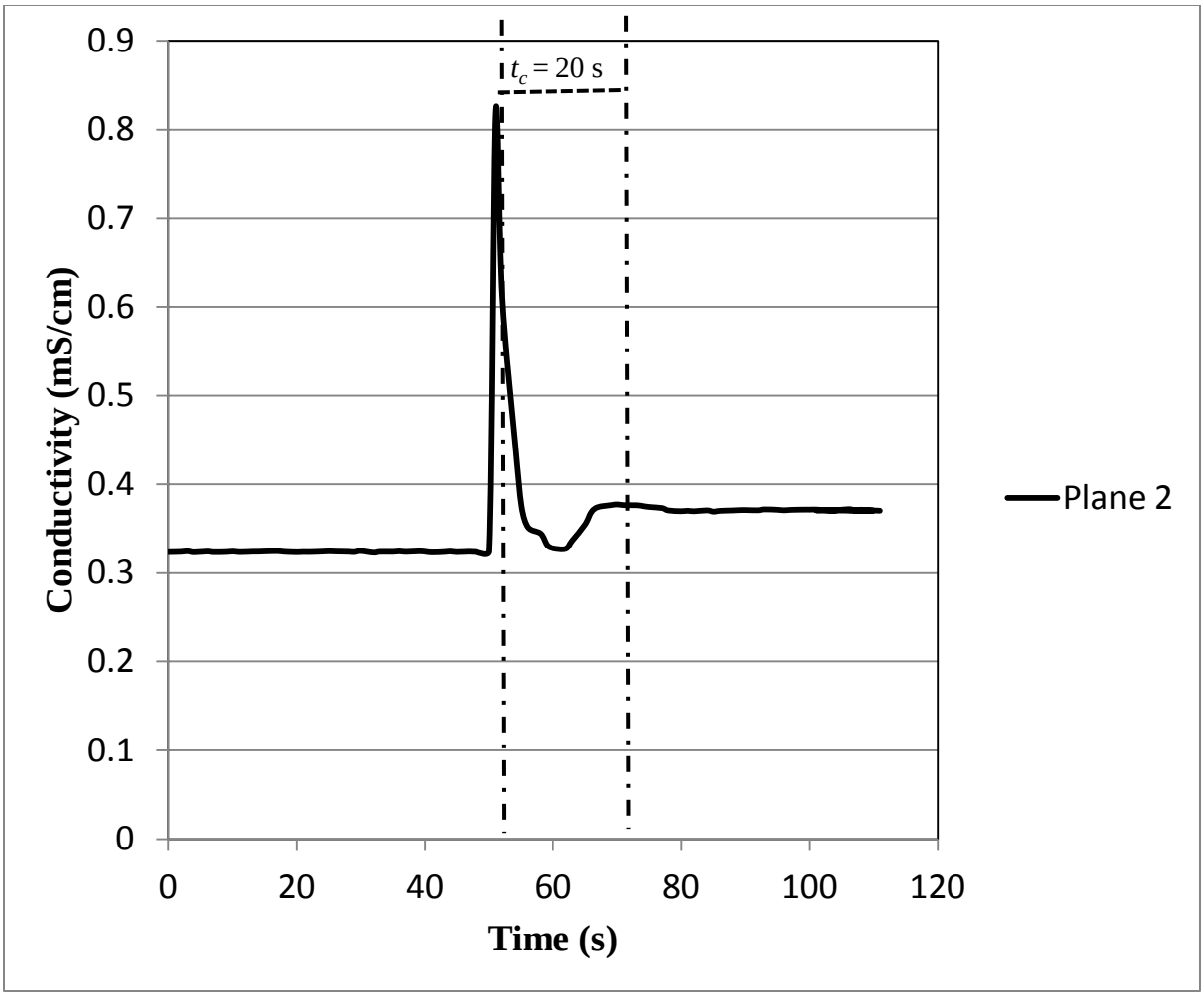

Figure 3.6 Measurement of the circulation time at U_{gr} = 1.087 × 10^{-2} m/s using ERT plane 2 (located in downcomer) for cross shaped sparger with liquid height = 1.63 m.

CHAPTER 4

RESULTS AND DISCUSSION

The effect of gas flow rate, bioreactor liquid height, sparger configuration and bioreactor configuration on gas holdup, mixing time and liquid superficial velocity will be discussed in this chapter.

4.1. Gas Holdup

The gas holdup plays a significant role in the design and scale up of external loop airlift bioreactors. The gas holdup controls the residence time of the gas in the liquid. In combination with the bubble size, it has a greater impact on the gas-liquid interfacial area per unit volume, the mass transfer efficiency from gas to liquid and the circulation liquid velocity in airlift reactors. The impact of gas holdup on the bioreactor design has been given much importance because the rate of mass transfer depends on the gas holdup in the bioreactor. Thus, for any range of operating conditions, the maximum required gas holdup in the bioreactor must be accommodated in the total design volume of the bioreactor. Han et al. (2000) investigated the gas holdup in a new gas-liquid-solid inverse fluidized airlift bioreactor. These investigators employed the inverted U-type manometers connected to pressure taps located at different positions axially to determine the gas holdup. Ishtinkana and Benington (2010) investigated the gas holdup in a bubble column bioreactor. They employed three different techniques in order to measure the gas holdup: height difference technique, pressure difference technique, and electrical resistance tomography technique. They noticed that the technique, which was based on the height

difference between gassed and ungassed operation, measured the overall gas holdup to an accuracy of 75%. They also observed that the differential pressure measurements along the column axis made it possible to determine both the average and axial holdup profiles. When the electrical resistance tomography was used to measure the gas holdup in the bubble column bioreactor, it allowed the average, axial and radial holdup profiles to be measured. Electrical resistance tomography also made it possible to diagnose the flow of air bubbles in the column by creating tomography images. Jin et al. (2010) used electrical resistance tomography technique in order to measure the gas holdup in an external loop airlift bioreactor without packing. They noticed that the phase holdups and radial holdups were successfully measured using ERT technique. These investigators found that the ERT application in three phase system (solid, liquid and gas) was limited to the measurement of phase holdups because they were only able to measure the gas holdups and solid holdups together as two non-conductive phases. In order to solve that problem they had to employ the pressure difference technique.

4.1.1. Effect of Superficial Gas Velocity and Liquid Height

Figure 4.1 illustrates the effects of gas flow rate and liquid height on the riser gas holdup using a cross shaped sparger. It can be observed from this figure that the gas holdup in the riser increased with increasing superficial gas velocity in the riser. At lower gas flow rate, a smaller number of bubbles were formed, which gave lower gas holdup. The increase in gas flow rate resulted in the formation of larger number of bubbles which in return gave higher gas holdup. These results are in agreement with previously reported results in the literatures (Yazdian et al., 2009; Liu et al., 2008; Mohanty et al., 2006; Han et al., 2000).

Figure 4.1 also shows that the gas holdup in the riser increased with the decrease in liquid height in the bioreactor. Apparently, with decreasing the liquid height in the bioreactor, the flowing resistance in the upper connecting tube is increased, which decreases the liquid superficial velocity. The decreased liquid superficial velocity contributes to higher gas holdup in the bioreactor (Loh and Liu, 2001). Several investigators used external loop airlift bioreactor to find the effect of liquid height in the bioreactor on gas holdup and they found the same trend for the gas holdup as was noticed in the present experimental study (Liu et al., 2008; Al-Masry, 2004; Al-Masry, 1999; Bentifraouine et al., 1997).

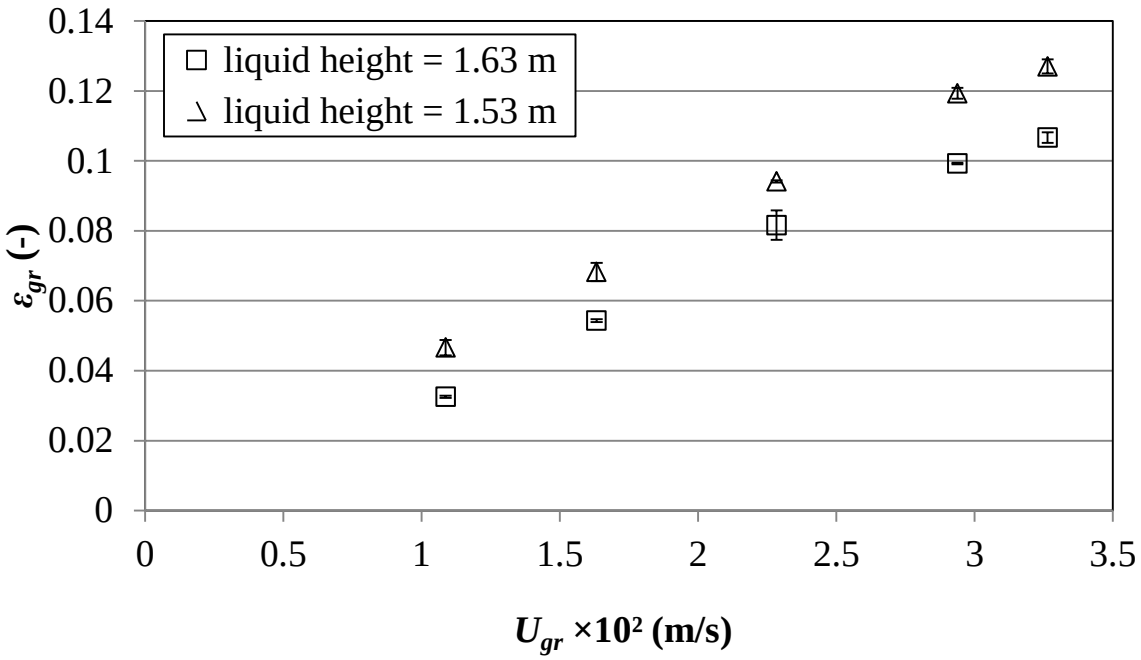

Figure 4.1 Effect of gas flow rate and liquid height on gas holdup in the riser using cross shaped sparger (average standard deviation = 0.0015).

Figure 4.2 depicts the time series of tomographic images collected from 8 measurement planes of ERT system following the air supply at a constant superficial gas velocity of 3.264×10^{-2} m/s in the riser using cross shaped sparger with a constant liquid height of 1.63 m. Planes 1, 2, 3 and 4

were located from top to bottom on the downcomer, while planes 5, 6, 7 and 8 were located from bottom to top on the riser (See Figure 3.2). As shown in the scale bar in Figure 4.2, the blue colour in these tomographic images indicates the lower conductivity and the red colour shows the higher conductivity of the fluid in the bioreactor.

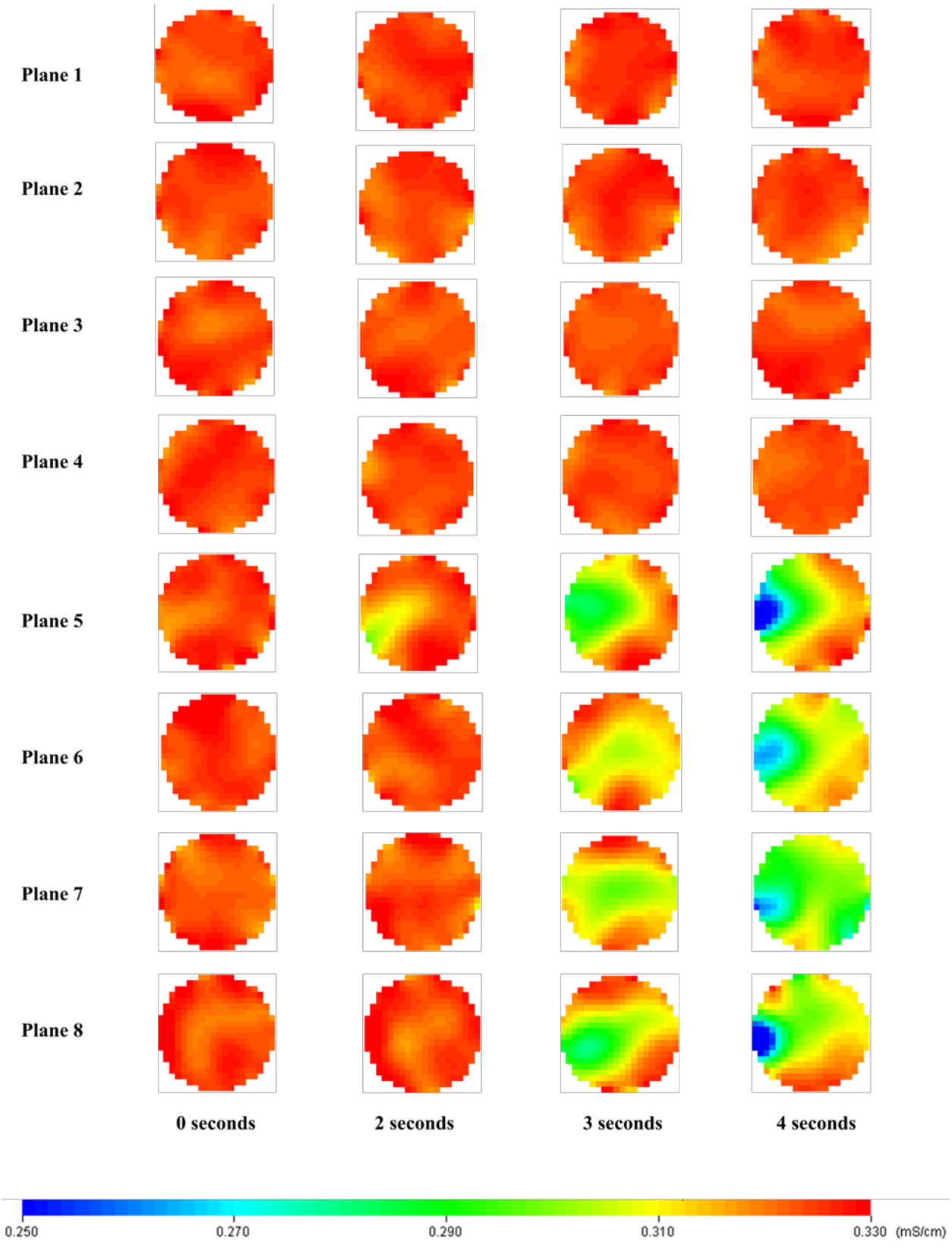
Plane 1
Plane 2
Plane 3
Plane 4
Plane 5
Plane 6
Plane 7
Plane 8
0 seconds
2 seconds
3 seconds
4 seconds
0.250
0.270
0.290
0.310
0.330
(mS/cm)

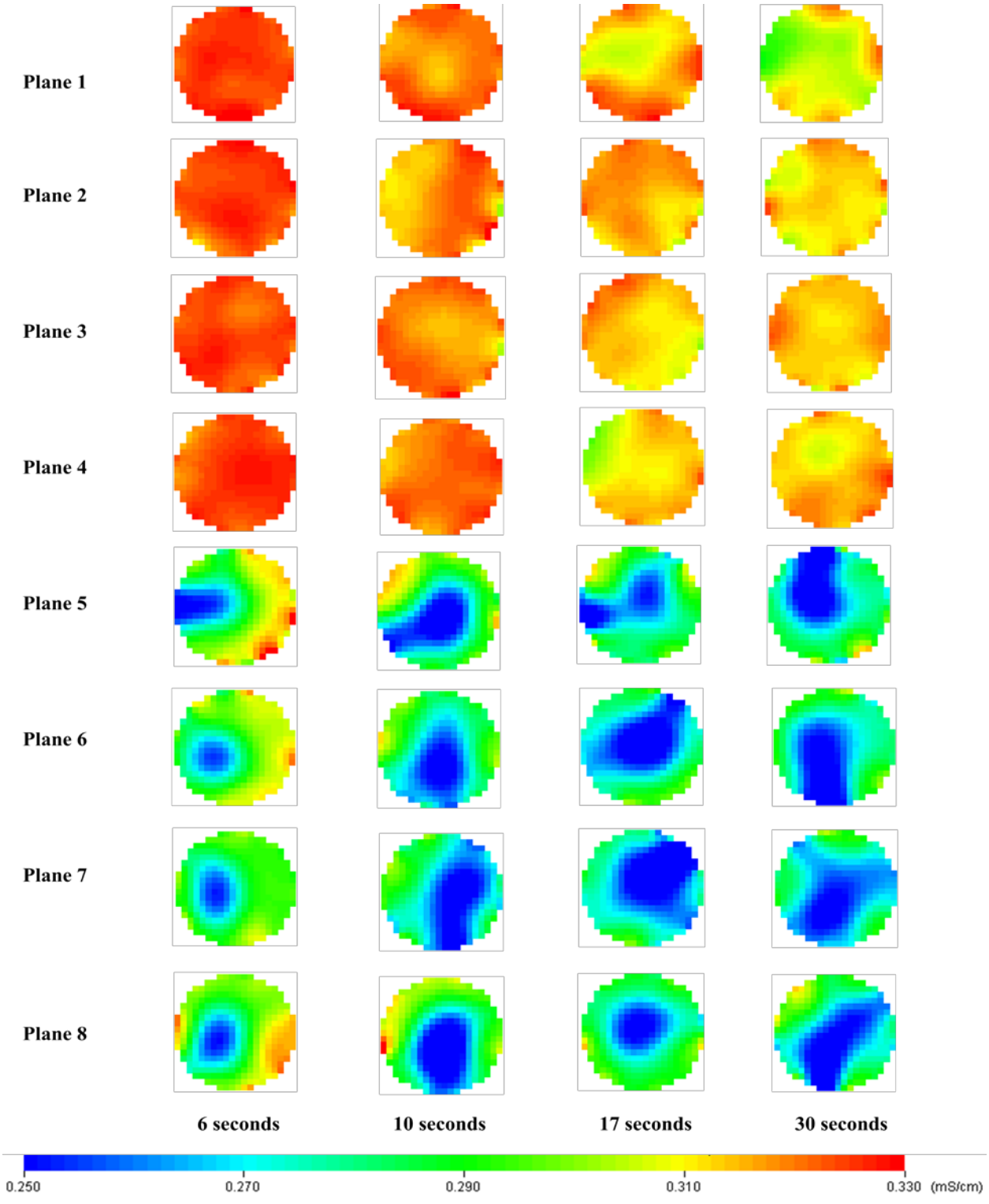

Figure 4.2 Time series of tomographic images collected from 8 measurement planes of ERT system (plane 1, plane 2, plane 3 and plane 4 located on downcomer and plane 5, plane 6, plane 7 and plane 8 located on riser) following the supply of air at $U_{gr} = 3.264 \times 10^{-2}$ m/s into the water using a cross shaped sparger with a liquid height of 1.63 m.

Examining this Figure shows that when air was introduced at the bottom of the riser for 2 seconds the colour of the tomographic image from plane 5 (closest to sparger) changed. After 3 seconds, the colours of the tomographic images of planes 6, 7 and 8 also changed to green and yellow (i.e., representing lower conductivity). The lower conductivity was due to the presence of air bubbles in the riser, which increased the gas holdup in the riser. It is a known fact that the air has zero conductivity, thus the region with lower conductivity depicts the accumulation of air bubbles in the bioreactor (Ishkintana and Bennington, 2010). Figure 4.2 also illustrates that the colours of the tomographic images from planes 1, 2, 3 and 4 located in the downcomer changed after 10 seconds of air purging. This change in colour is due to the decrease in the fluid conductivity in the downcomer, which again is due to the increase in gas holdup in the downcomer. In general, the minimum conductivity value of the fluid in the bioreactor does not reach zero, even when air is supplied to the water in the bioreactor, because the ERT system gives the conductivity of the mixture of air and water flowing in the bioreactor instead of air separately. In previous investigations (Ishkintana and Bennington, 2010; Jin et al., 2010; Jin et al., 2007; Jin et al., 2006), investigators used ERT in order to find the gas holdup in their bioreactors. They found that the conductivity values of the fluid in the bioreactors were decreased when the air was supplied into these bioreactors, which is in agreement with the present experimental result.

In order to get the knowledge of mixing characteristics inside the bioreactor, the riser and the downcomer of bioreactor were sliced vertically from two different positions; $X = 0$ and $Y = 0$. The origins were taken as zero at the centres of the riser and the downcomer (see Figure 3.1). Figure 4.3 represents the vertical slice tomographic images and 3D tomographic images of the fluid contained in riser and downcomer of the bioreactor at different riser superficial gas

velocities using a cross shaped sparger at a constant liquid height of 1.63 m in the bioreactor. Figure 4.3 also illustrates that, when no air was supplied in the bioreactor, the conductivity of the liquid in the bioreactor was high (red colour). When the air was supplied at a lower superficial gas velocity of 1.087×10^{-2} m/s in the riser, most part of the red coloured tomographic image in the riser turned yellow and green. This change in colour is due to the presence of gas bubbles and thus the presence of gas holdup in the riser. The change in colour of the tomographic image in the downcomer is so small that it cannot be easily seen with naked eyes because of the presence of very few bubbles in the downcomer. It can also be seen from Figure 4.3 that when the air was supplied at a higher superficial gas velocity of 3.264×10^{-2} m/s in the riser of the bioreactor, the colour in the riser turned blue (lower conductivity). The colour in the downcomer was also changed to yellow and green because of the presence of more bubbles in the downcomer. This change in colour indicates the lower conductivity and thus the presence of higher gas holdup in the downcomer (Figure 4.3).

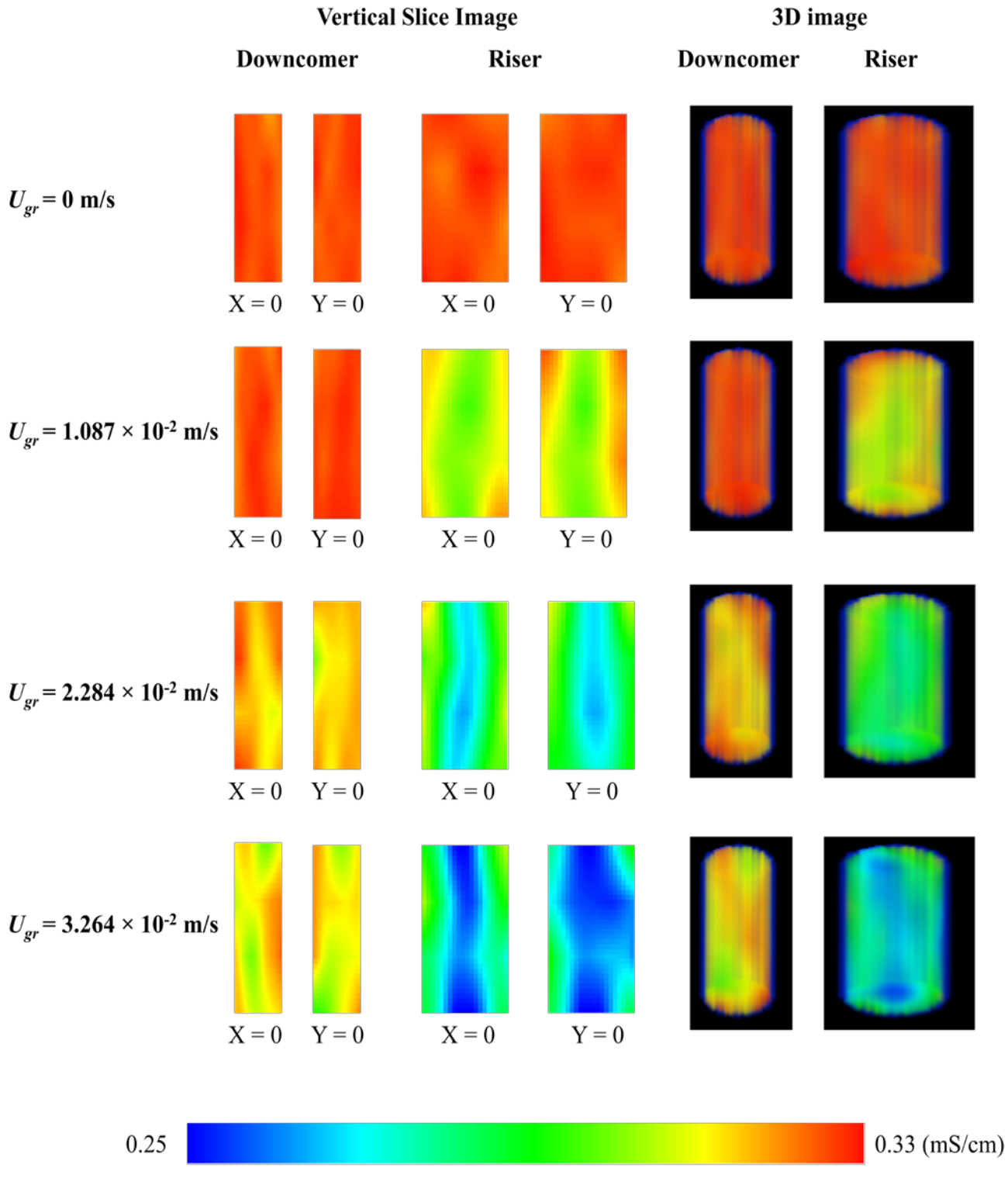

Figure 4.3 Vertical slice tomographic images and 3D tomographic images of the fluid (air-water system) in riser and downcomer of the bioreactor at different riser superficial gas velocities using a cross shaped sparger at constant liquid height of 1.63 m in the bioreactor.

4.1.2. Effect of Sparger

The effect of sparger configurations was pursued in an empty column with no packing or gas distributor. Two different sparger configurations that include cross shaped and circular sparger were examined. Figure 4.4 shows the effect of the sparger type on gas holdup at different superficial gas velocities with a constant liquid height of 1.63 m in the bioreactor. The results illustrate that the gas holdup was slightly higher at constant riser superficial gas velocity when the circular sparger was used over a cross shaped sparger of same diameter and with same number and size of holes. This can be related to that the circular sparger offers more resistance in the flow of liquid than a cross shaped sparger with same diameter and same size and number of holes on it. It has been revealed by previous investigators that the increase in resistance in the flow path of the liquid contributes to a lower liquid superficial velocity in the bioreactor (Loh and Ranganath, 2005; Han et al, 2000; Guo et al, 1997). A cross shaped sparger consists of six perforated small diameter tubes (Figure 3.1). These small diameter circular tubes offer much more space and hence lower resistance for the water to pass around them. On the other hand, the circular sparger consists of a circular solid plate with lesser space between riser and sparger, hence offers more resistance for the water to pass through that space.

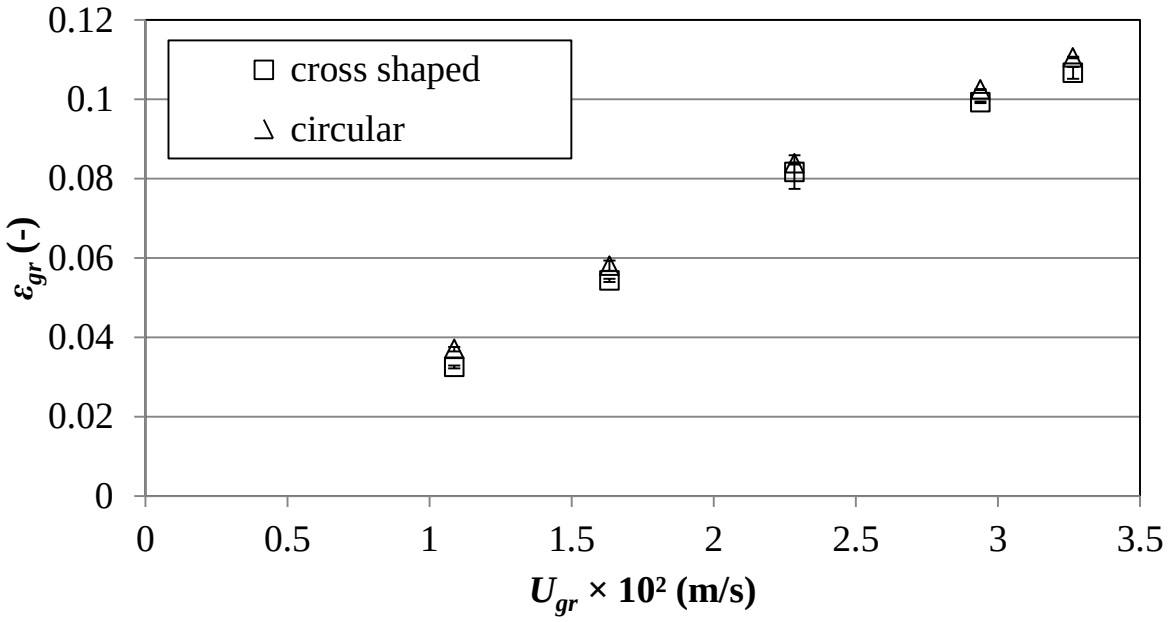

Figure 4.4 Effect of sparger configuration on gas holdup in the riser with a constant bioreactor liquid height of 1.63 m with no packing (average standard deviation = 0.000912).

4.1.3. Effect of Packing

Figure 4.5 represents the effect of packing in the riser on the riser gas holdup at different gas flow rates using a cross shaped sparger with a constant liquid height of 1.63 m in the bioreactor. This figure demonstrates that when a packing was installed in the riser of an external loop airlift bioreactor, the gas hold up was slightly increased, at a constant riser superficial gas velocity. This slightly increased gas holdup is partially due to the resistance of the packing in the riser and partially due to the decrease in the size of gas bubbles (Nikhakhtari and Hill, 2005). Meng et al. (2002) also reported that the impacts of gas bubbles with packing material can change the hydrodynamic parameters including the gas holdup. Meng and his coworkers also found that when they used packing in the riser of an external loop airlift bioreactor, the gas holdup was slightly increased.

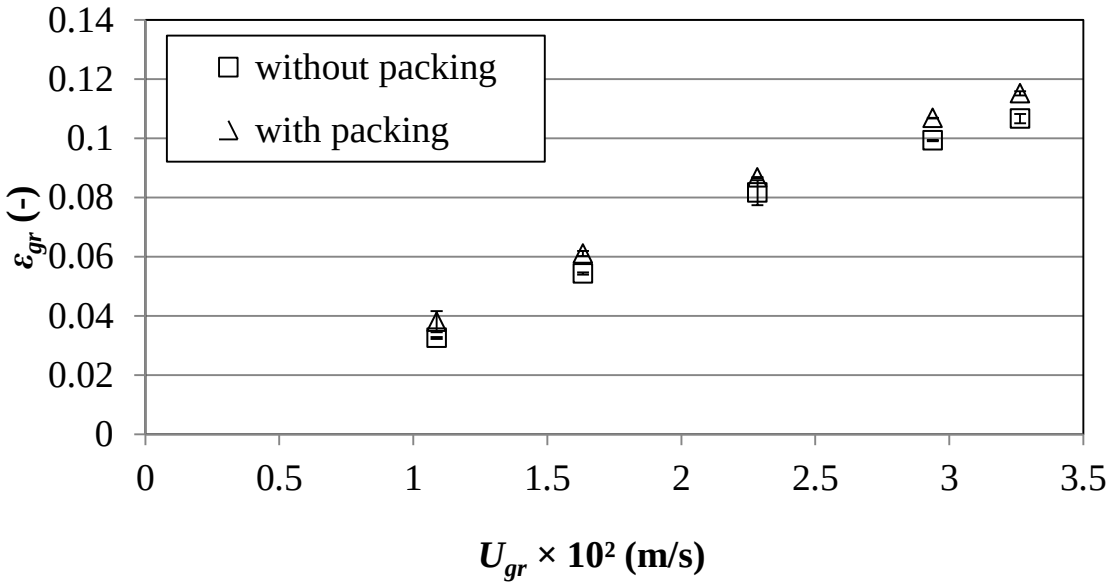

Figure 4.5 Effect of a riser packing (packing height = 0.234 m) on riser gas holdup with a constant liquid height of 1.63 m in the bioreactor using a cross shaped sparger configuration (average standard deviation = 0.00122).

4.1.4. Effect of Internal Gas Distributor (Perforated Plate)

Figure 4.6 shows the influence of installing an internal gas distributor on gas holdup in the riser with no packing installed versus riser superficial gas velocity, using a cross shaped sparger with a liquid height of 1.63 m in the bioreactor. As shown in Figure 4.6, the gas holdup in the riser was increased when the perforated plate was installed in the riser. This higher gas holdup can be related to the finer dispersion of gas bubbles achieved in the bioreactor when an internal gas distributor is installed. When the liquid flows through the perforated plate, the turbulence intensity in the riser is enhanced; this effectively forces the bubble breakup. This leads to the decrease in bubble size and an increase in gas holdup. The installation of an internal gas distributor in the riser results in extra flow resistance, which decreases the liquid superficial velocity and increases the gas holdup in the bioreactor. Mohanty and his co-workers (2006)

investigated the presence of internal perforated plates in the riser of an external loop airlift bioreactor and they observed that the gas holdup was increased when internal perforated plates were installed in the riser of the bioreactor.

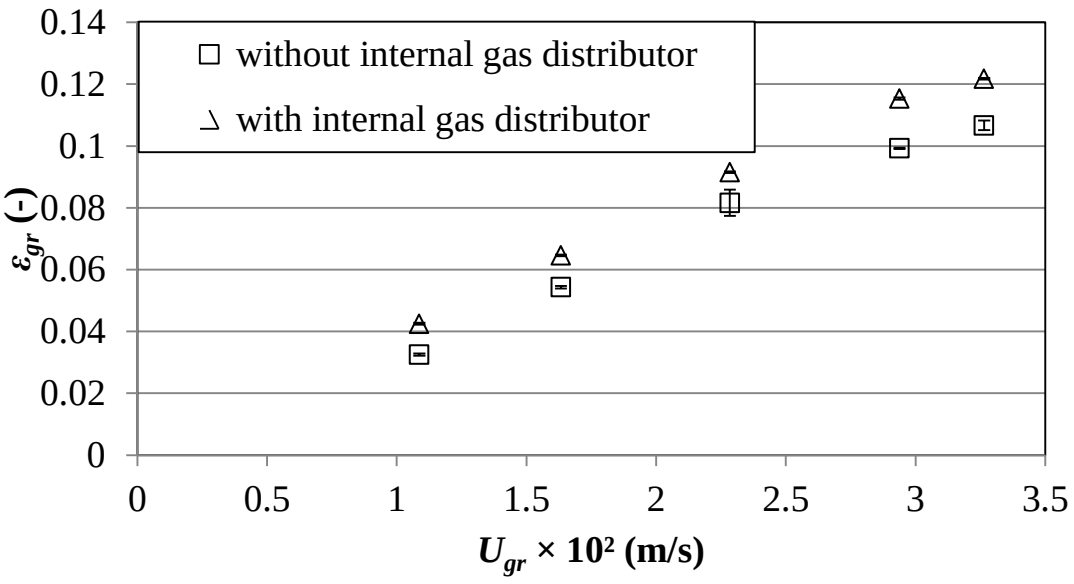

Figure 4.6 Effect of riser internal gas distributor (perforated plate) on gas holdup in the riser with a bioreactor liquid height of 1.63 m using cross shaped sparger configuration with no packing (average standard deviation = 0.000814).

Figure 4.7 shows the effect of installing the gas distributor in the riser between the two packings on the riser gas holdup versus an empty riser, both cases with a constant liquid height of 1.63 m in the bioreactor using a cross shaped sparger configuration (Figure 3.1). It is clear from Figure 4.7 that the gas holdup was increased in the riser in the presence of the perforated plate in the riser together with the two packings. These packings offer more resistance in the flow of liquid which in turn decreases the liquid superficial velocity and ultimately increases the gas holdup. The gas holdup also increases due to the decrease in the size of the gas bubbles passing through these packings (Nikhakhtari and Hill, 2005; Meng et al., 2002). Zhang and his co-workers (2005)

used an internal gas distributor in the riser of an external loop airlift bioreactor. They noticed that when the air bubbles and the liquid passed through the internal gas distributor, the size of the air bubbles was reduced. They also observed that the air bubbles were also redistributed after passing through the internal gas distributor. The function of the perforated plate is to break and redistribute the gas bubbles after exiting the lower packing and before entering the upper packing, which results in the increase in gas holdup.

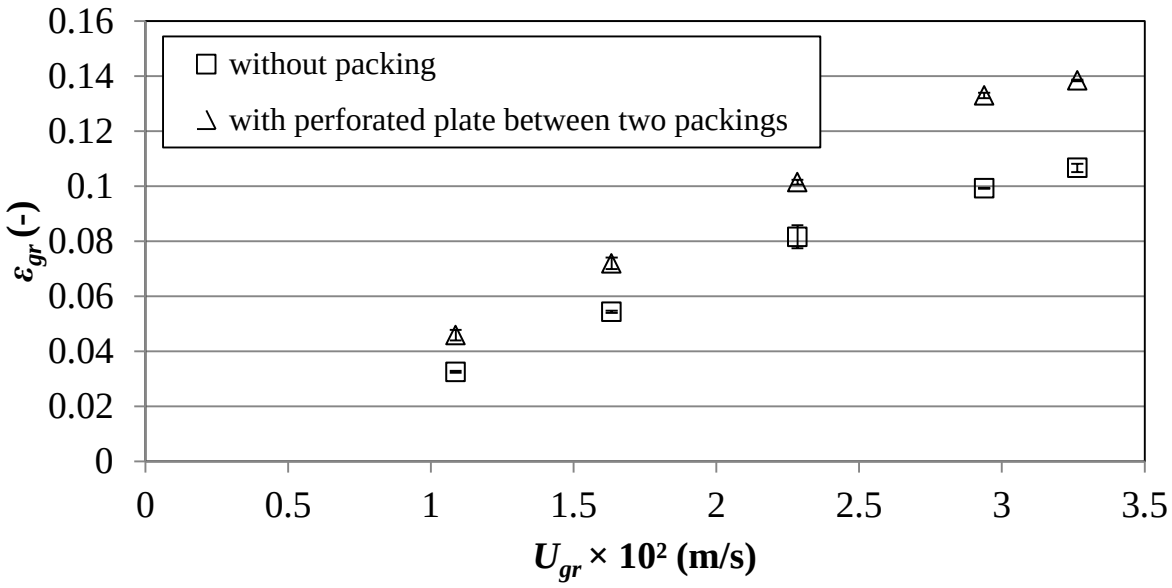

Figure 4.7 Effect of a perforated plate between two packings in the riser (height of each packing = 0.234 m) on riser gas holdup with a constant liquid height of 1.63 m in the bioreactor using a cross shaped sparger configuration (average standard deviation = 0.0013).

All experiments showed that the gas holdup in downcomer was found very low as compared to the gas holdup in the riser because most of the gas bubbles escaped from the top of the riser and the top of the downcomer of bioreactor. The range of gas holdup in the downcomer was 1.7% to 30% of that in the riser. Douek et al. (1994) investigated the downcomer gas holdup and riser gas

holdup in an external loop airlift bioreactor. The investigators found that downcomer gas holdup was 0 to 29% of the riser gas holdup.

4.2. Mixing Time

Mixing time is one of the most important parameters in the designing and scale up of an external loop airlift bioreactor. Non-uniform profiles of concentration or temperature can cause side reactions or reduce the chemical reaction rate in some process. In these processes, it is very important to have good mixing. Jin et al. (2001) investigated the mixing time by using the pulse tracer technique in an external loop airlift bioreactor. These investigators injected 1.0 ml 4M NaOH as a tracer in the bioreactor and measured the pH by using probes at four positions within the vessel. These probes sent signals to the multichannel data logger which was connected to a micro-computer. The mixing time was calculated as the time for the pH response to the initial peak. The mixing time was defined as the time required achieving the specific inhomogeneity (5%) after the injection of the tracer. Kawase et al. (1994) added a pulse of HCl solution from the entrance of the downcomer and the top of the dispersed height in an external loop airlift bioreactor. They placed a pH electrode near the exit of the downcomer in the bioreactor. The pH responses were recorded with a chart recorder. They defined mixing time as the time required to achieve 95% homogeneity. Gumery et al. (2011) investigated the mixing characteristics in an internal loop airlift bioreactor using electrical resistance tomography (ERT). They injected the 50 ml saline tracer (NaCl) into the bioreactor. Mixing was monitored by means of variations in average conductivity signals that were generated by the ERT system using four planes of electrodes. The investigators discontinued the data collection once the changes in average

conductivity were less than ±1%. The mixing time was measured by subtracting the time when the conductivity just started increasing, after the injection of tracer, from the time when the variation in mean conductivity values became ±1%. Unlike other mixing time measuring techniques, the electrical resistance tomography has not only been used to determine the mixing time but it also has been employed as an efficient technique to visualize the flow pattern inside vessel (Bolton et al., 2004). By employing this technique, the pulse injection of high conductivity tracer can be imaged as multiple tomographic images or 3D solid-body images (Bolton et al., 2004; Mann et al., 2001).

4.2.1. Effect of Superficial Gas Velocity and Liquid Height

Figure 4.8 shows the effects of superficial gas velocity and liquid height on mixing time in the bioreactor using a cross shaped sparger configuration in an empty riser (no packing or gas distributor). It was found that the mixing time in the bioreactor was decreased with increasing superficial gas velocity in the riser; see Figure 4.8. A lower riser superficial gas velocity results in lower riser superficial liquid velocity, which allows a longer mixing time in the bioreactor. When the superficial gas velocity in the riser is increased, the riser superficial liquid velocity is increased, which reduces the mixing time in the bioreactor. Figure 4.8 also reveals that the mixing time in the riser increased with the decrease in liquid height in the bioreactor. The decrease in liquid height in the bioreactor gives a higher resistance in the flow path of the liquid in the upper connecting tube, which results in a decrease in liquid superficial velocity. This decrease in liquid superficial velocity allows a higher mixing time in the bioreactor (Gavrilescu and Tudose, 1997).

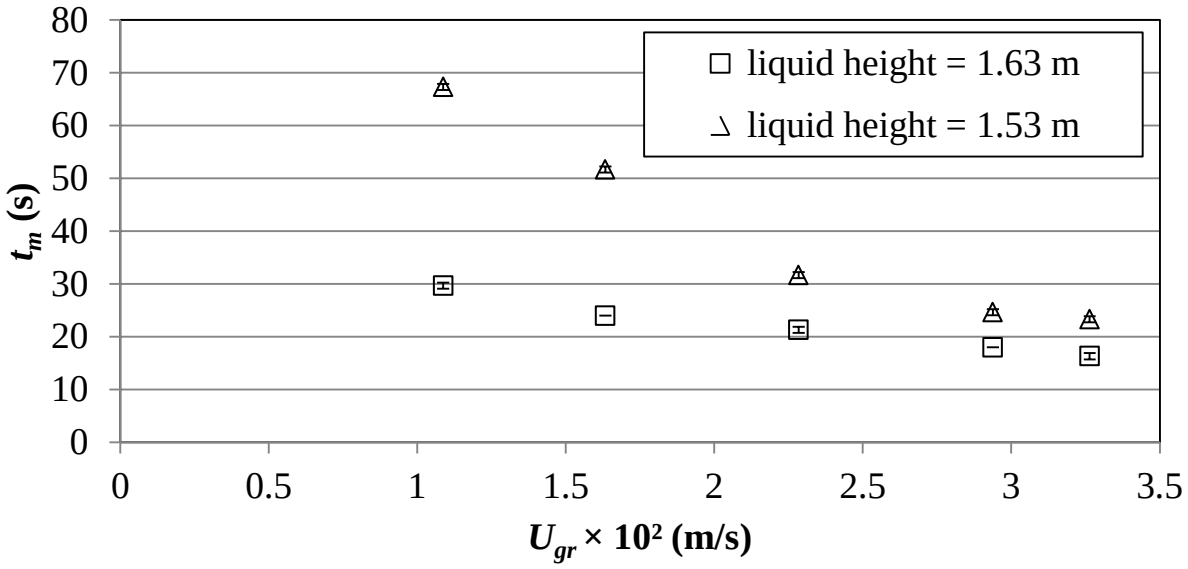

Figure 4.8 Effect of gas flow rate and liquid height on mixing time using cross shaped sparger (average standard deviation = 0.46 s).

Figure 4.9 illustrates the time series of tomographic images taken from 8 measurement planes of ERT system following the injection of 100 ml of 4% saline solution at a constant riser superficial gas velocity of 3.264×10^{-2} m/s using cross shaped sparger with a constant liquid height of 1.63 m. The blue colour in Figure 4.9 signifies the lower conductivity and the red colour shows the higher conductivity.

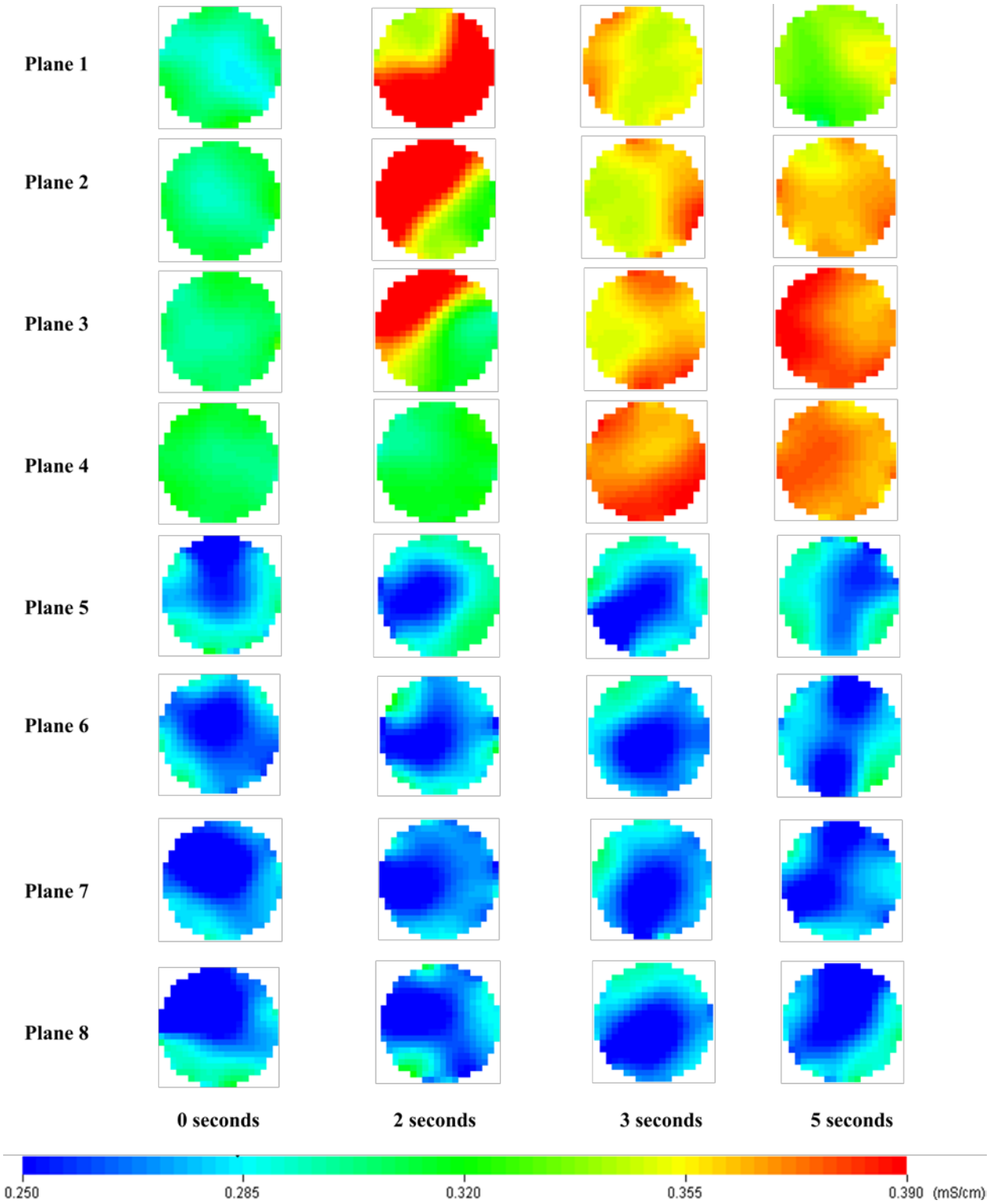
Plane 1
Plane 2
Plane 3
Plane 4
Plane 5
Plane 6
Plane 7
Plane 8
0 seconds
2 seconds
3 seconds
5 seconds
0.250
0.285
0.320
0.355
0.390
(mS/cm)

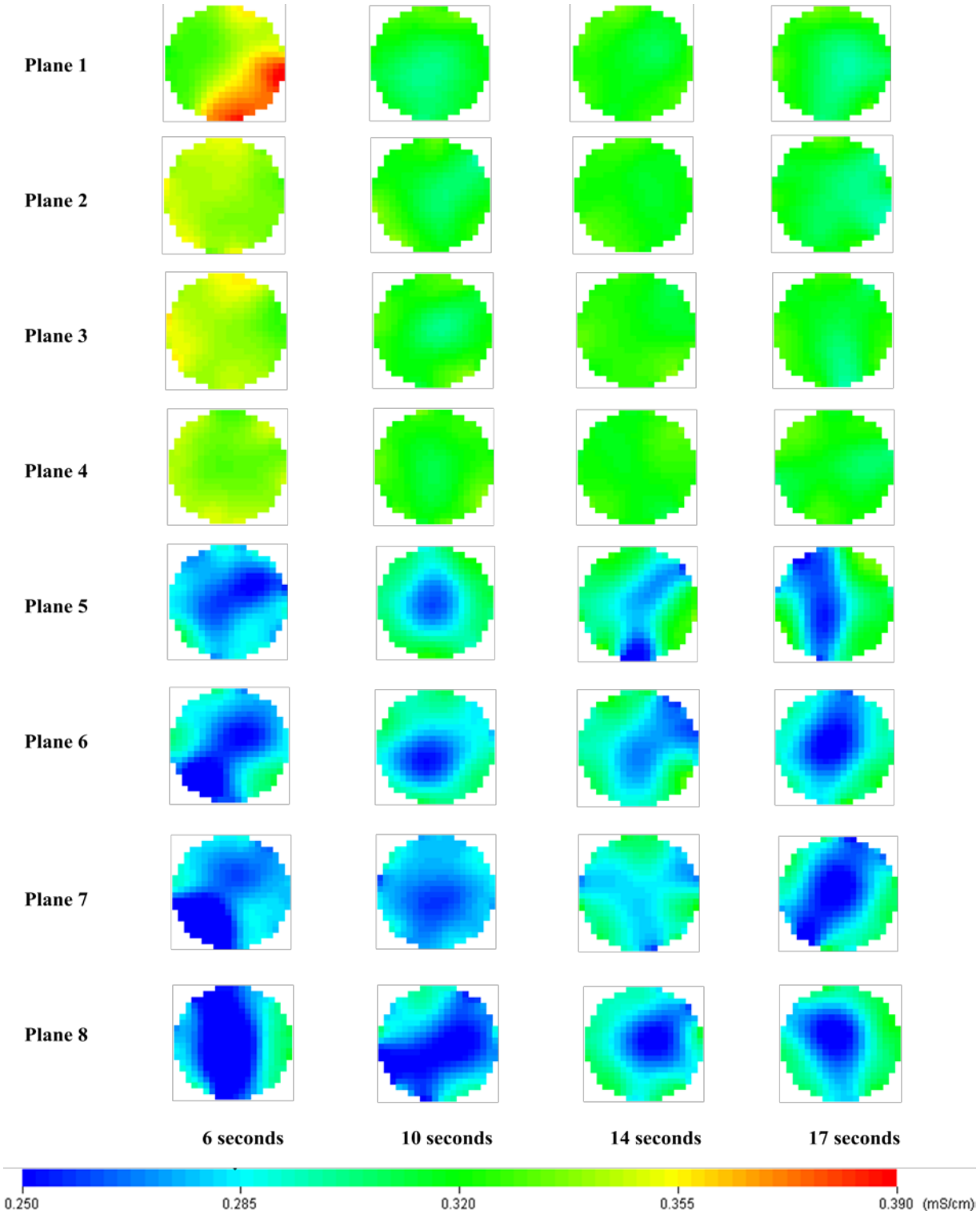

Figure 4.9 Time series of tomographic images collected from 8 measurement planes of ERT system (plane 1, plane 2, plane 3 and plane 4 located on downcomer and plane 5, plane 6, plane 7 and plane 8 located on riser) following the injection of saline solution into the air-water mixture using a cross shaped sparger with $U_{gr} = 3.264 \times 10^{-2}$ m/s and liquid height = 1.63 m.

It can be seen from Figure 4.9 that the saline solution was injected from the top of the downcomer near plane 1 located on the downcomer at 0 second and the colour of the tomographic images of planes 1, 2 and 3 located on the downcomer was changed at 2 seconds. At 3 seconds, the colour of the tomographic image of plane 4 located on downcomer was also changed in Figure 4.9. This change in colour is due to the increase in conductivity of the fluid in the downcomer. At 6 seconds, most regions of the tomographic images of planes 1, 2, 3 and 4 changed to green because of the dispersion of saline solution in the downcomer. After passing through the downcomer, the saline solution enters into the riser using bottom connecting tube. However, since the gas holdup in the riser is much higher, the red regions on tomographic images of planes 5, 6, 7 and 8, located on the riser from the bottom to top, were not observed. This variation in conductivity indicates the presence of saline solution in the bioreactor. The ERT images show that the mixing time under these circumstances was about 17 seconds. In previous investigations (Gumery et al., 2011; Bolton et al., 2004), investigators used ERT technique in order to find the mixing time in their bioreactors. They used high-conductivity tracers in their bioreactors and found that the conductivity of the fluid was first suddenly increased in some regions of the bioreactor and then decreased because of the mixing in the bioreactor, which is in agreement with the present experimental result.

Figure 4.10 demonstrates the vertical slice tomographic images and 3D tomographic images of air-water mixture in riser and downcomer of the bioreactor following the injection of 100 ml of 4% saline solution from the top of the downcomer at a constant riser superficial gas velocity of 3.264×10^{-2} m/s using a cross shaped sparger at constant liquid height of 1.63 m in the empty bioreactor (no packing or gas distributor). The red colour signifies the higher conductivity and the blue colour indicates the lower conductivity in the bioreactor. It is a known fact that the

conductivity of saline solution is higher than the conductivity of water in the bioreactor, thus the region with higher conductivity depicts the accumulation of saline solution in the bioreactor (Gumery et al., 2011; Pakzad et al., 2008; Bolton et al., 2004). It can be seen from Figure 4.10 that when no saline solution was present in the downcomer at 0 second, the colour in the downcomer was green. The green colour in the downcomer was due to the lower gas holdup in the downcomer than that in the riser. Thus, the blue region was not observed in the downcomer. At 0 seconds, the saline solution was injected into the bioreactor from the top of the downcomer, while at 2 seconds the colour in the downcomer turned red (highest conductivity). The color changes in Figure 4.10 indicate the presence of saline solution in the downcomer. At 10 seconds, the colour in the downcomer changed to green (lower conductivity) because of the fact that the saline solution had left the downcomer and entered into the riser through the bottom connecting tube. Figure 4.10 also demonstrates that, at 10 seconds, the blue colour (lower conductivity due to air bubbles) in the riser was slightly changed to green colour, indicating the presence of saline solution in the riser. The tracer was uniformly dispersed throughout the bioreactor after 17 seconds.

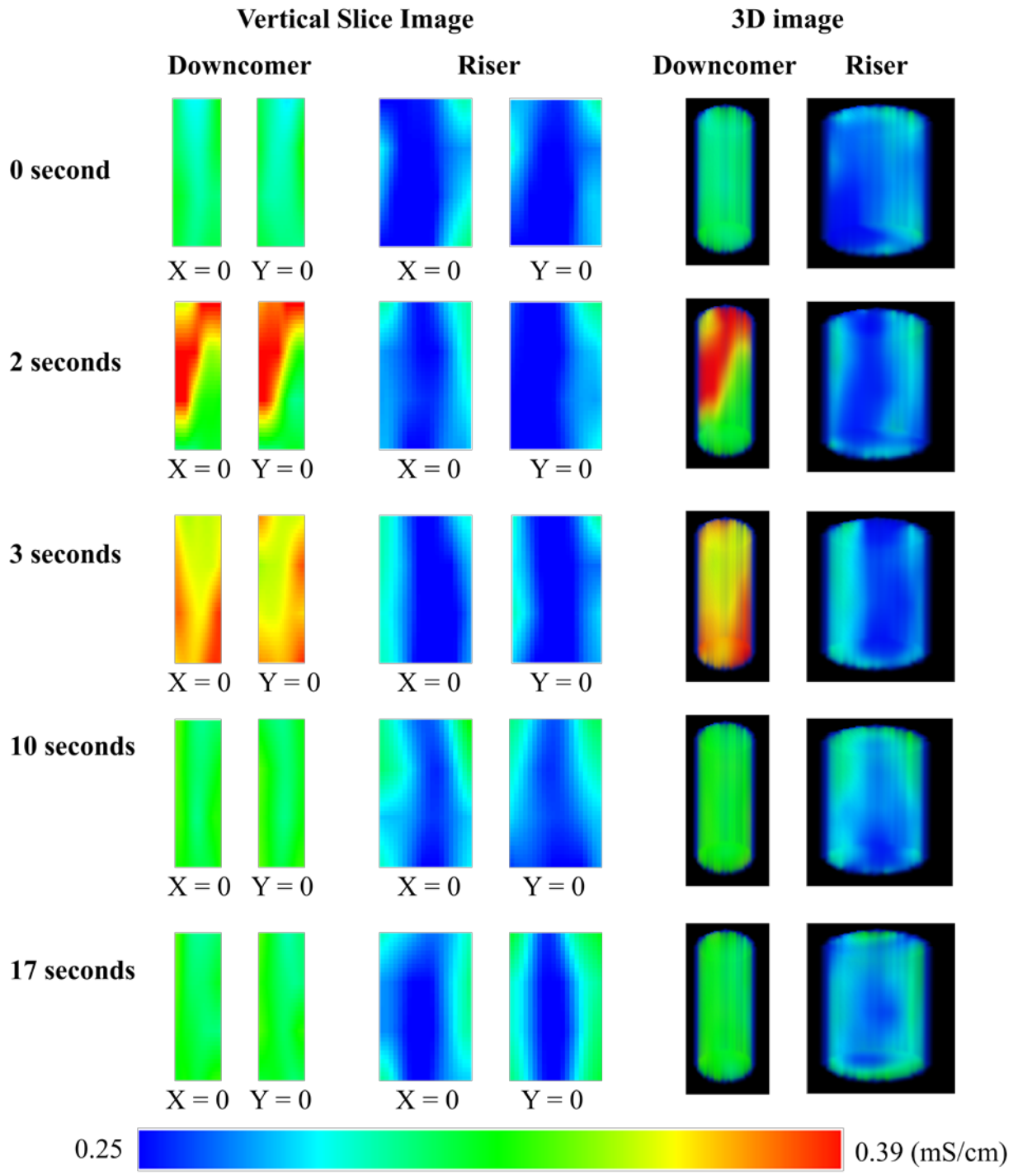

Figure 4.10 Vertical slice tomographic images and 3D tomographic images of air-water mixture in riser and downcomer of the bioreactor following the injection of saline solution at a constant riser superficial gas velocity of 3.264×10^{-2} m/s using a cross shaped sparger at a constant liquid height of 1.63 m in the bioreactor.

4.2.2. Effect of Sparger

Figure 4.11 compares the mixing time profiles of a cross shaped sparger and a circular sparger using different riser superficial gas velocities with a constant liquid height of 1.63 m in the empty bioreactor. These results demonstrate that at a constant riser superficial gas velocity, the mixing time was increased when a circular sparger was used over a cross shaped sparger of same diameter and with same number and size of holes on it. The increase in mixing time is due to the presence of more resistance in the flow. The cross shaped sparger consists of six circular tubes of small diameter. The liquid can easily pass through the space between these circular tubes. While a circular sparger consists of a circular plate which offers less space between the riser and the sparger for the liquid to pass and hence offers more resistance to flow path of the liquid. It is a known fact that the increase in resistance results in a lower liquid superficial velocity (Loh and Ranganath, 2005; Han et al, 2000; Guo et al, 1997), which in turn increases the mixing time in the bioreactor.

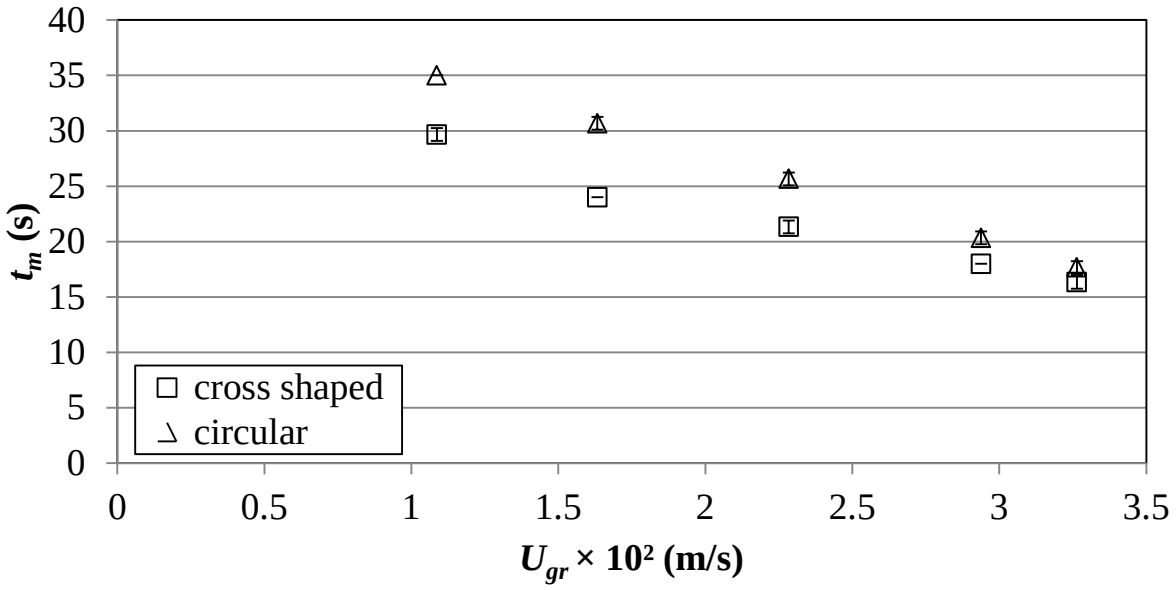

Figure 4.11 Effect of sparger configuration on mixing time with a constant liquid height of 1.63 m in the bioreactor (average standard deviation = 0.4 s).

4.2.3. Effect of Packing

Figure 4.12 represents the effect of the packing in the riser on the mixing time in the bioreactor by using a cross shaped sparger with a constant liquid height of 1.63 m in the bioreactor. It was observed that, at a constant riser superficial gas velocity, the mixing time was increased when a packing was installed in the riser. The installation of packing in the riser offers more resistance to the flow path of the liquid in the riser which results in the decrease in the liquid superficial velocity (Nikhakhtari and Hill, 2005; Meng et al., 2002). This decrease in liquid superficial velocity in turn increases the mixing time in the bioreactor. However, it is still important to install packing in a bioreactor for processes where packing is used as a support for immobilized microorganisms or enzymes (Horiuchi et al., 2000).

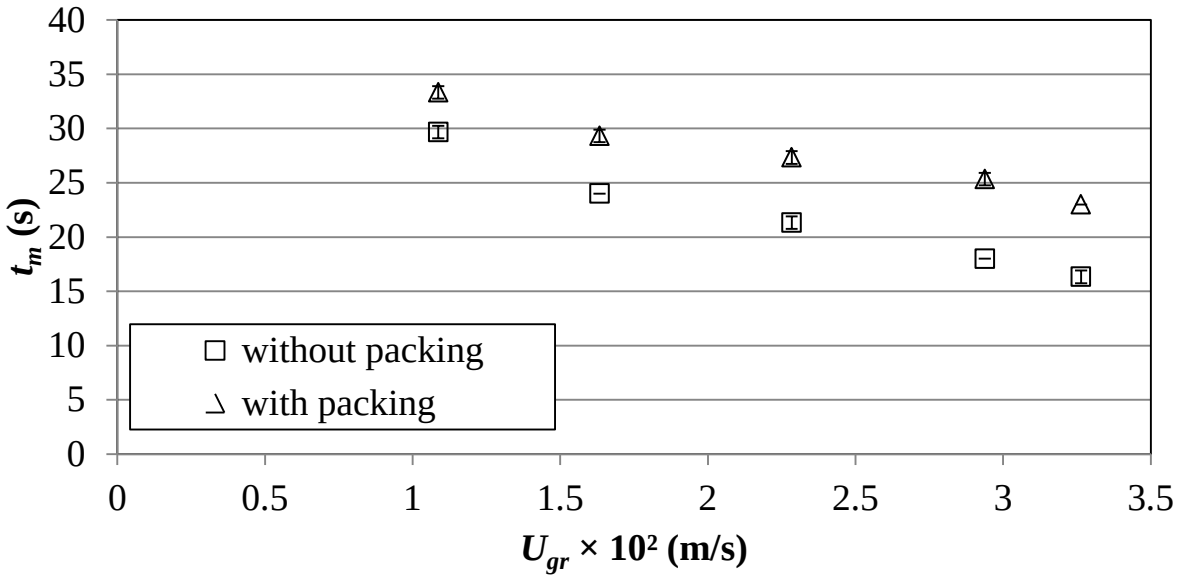

Figure 4.12 Effect of the packing in the riser (packing height = 0.234 m) on mixing time with a constant liquid height of 1.63 m using a cross shaped sparger configuration (average standard deviation = 0.4 s).

4.2.4. Effect of Internal Gas Distributor (Perforated Plate)

Figure 4.13 represents the effect of superficial gas velocity on mixing time in the bioreactor, with and without the perforated plate (no packings). It can be noticed from Figure 4.13 that, at a constant riser superficial gas velocity, the mixing time in the bioreactor installed with the internal gas distributor was higher than in the bioreactor without internal gas distributor. Several investigators studied the liquid velocity in fluidized bed and inverse fluidized bed external loop airlift bioreactors (Loh and Ranganath, 2005; Han et al, 2000; Guo et al, 1997). These investigators observed that the liquid velocity in the bioreactor with fluidized bed was lower than that without any fluidized bed. This lower liquid velocity was due to the fact that when a fluidized bed is provided in the bioreactor, the resistance in the flow path of the liquid is increased which in turn decreases the liquid velocity in the bioreactor. It is believed that when an

internal gas distributor is installed in the riser of the bioreactor, it enhances the flow resistance, which in turn decreases the liquid superficial velocity. This decrease in liquid superficial velocity delays the time required for mixing in the bioreactor. This delay results in the increase in mixing time in the bioreactor.

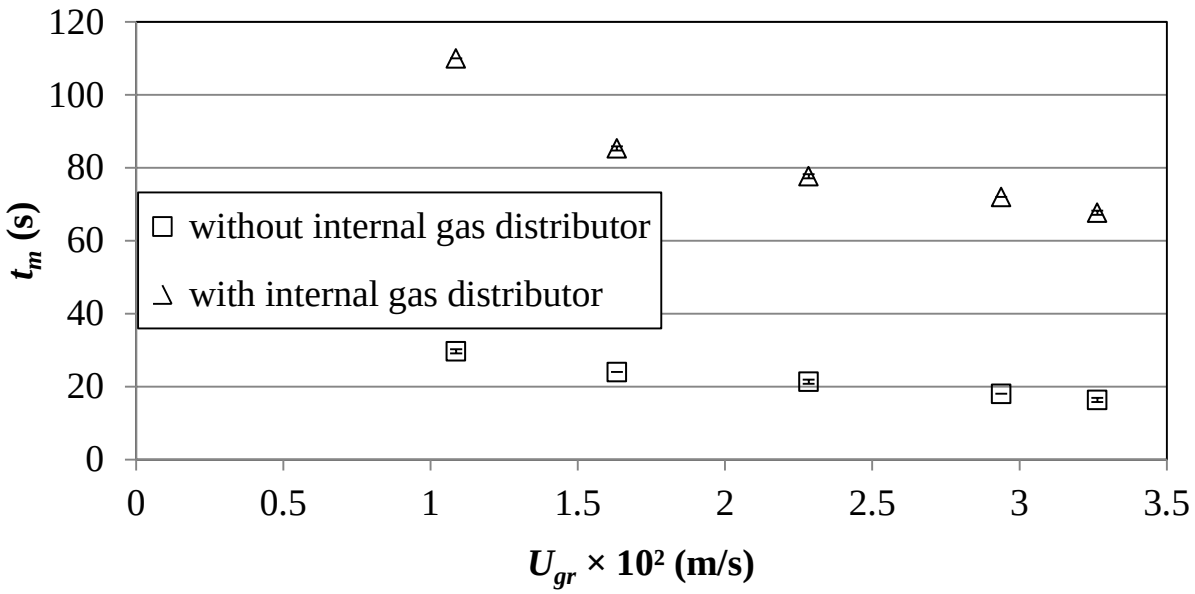

Figure 4.13 Effect of riser internal gas distributor (perforated plate) on mixing time with a constant liquid height of 1.63 m using cross shaped sparger configuration (average standard deviation = 0.35 s).

Figure 4.14 depicts the effect of an internal gas distributor installed in the riser between two packings on mixing time in the bioreactor with a constant liquid height of 1.63 m using a cross shaped sparger configuration in the bioreactor. It was noticed that the mixing time was increased when an internal gas distributor was installed in the riser between two packings at a constant superficial gas velocity in the riser. This increase in mixing time is due to the presence of more resistance in the form of packings and a perforated plate in the flow path of the liquid in the riser. The presence of this resistance in the liquid flow contributes to lower liquid superficial velocity

(Nikhakhtari and Hill, 2005; Meng et al., 2002; Loh and Ranganath, 2005; Han et al, 2000; Guo et al, 1997) which in turn increases the mixing time in the bioreactor.

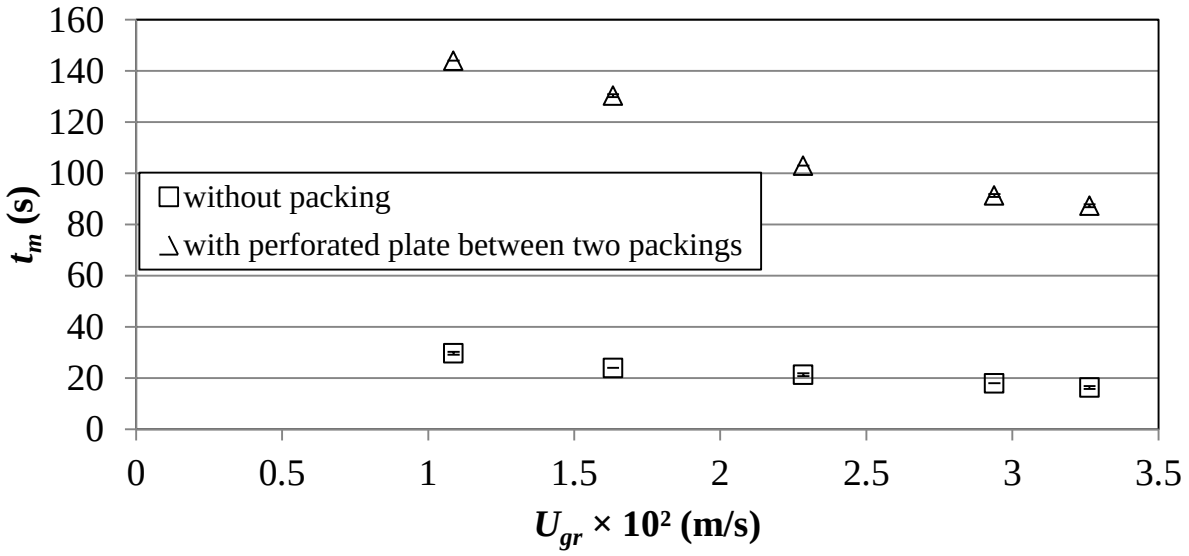

Figure 4.14 Effect of a perforated plate between two packings in the riser (height of each packing = 0.234 m) on mixing time with a constant liquid height of 1.63 m using a cross shaped sparger configuration (average standard deviation = 0.35 s).

4.3. Superficial Liquid Velocity

4.3.1. Effect of Superficial Gas Velocity and Liquid Height

Figure 4.15 represents the effects of superficial gas velocity and liquid height on the superficial liquid velocity in the riser using a cross shaped sparger. It was found that the superficial liquid velocity in the riser was increased with increasing superficial gas velocity in the riser (Figure 4.15). The superficial liquid velocity in the bioreactor depends on the hydrostatic pressure difference between the riser and the downcomer of the bioreactor. When the gas flow rate is increased in the riser, the hydrostatic pressure difference between the riser and the downcomer is

increased, which in turn increases the superficial liquid velocity in the riser. In the earlier investigations of Mohanty et al. (2006), Loh and Liu (2001), Han et al. (2000) and Kemblowski et al. (1993), they all agreed on that when the gas flow rate in the bioreactor is increased, the superficial liquid velocity is also increased.

It can also be seen from Figure 4.15 that the superficial liquid velocity in the riser was decreased with decreasing liquid height in the bioreactor. At constant riser superficial gas velocity, when the liquid height in the bioreactor is decreased, the resistance in the path of the liquid flowing in the upper connecting tube of the bioreactor is increased. This increased resistance, in turn, decreases the liquid superficial velocity in the bioreactor (Liu et al., 2008; Al-Masry, 2004; Al-Masry, 1999; Bentifraouine et al., 1997).

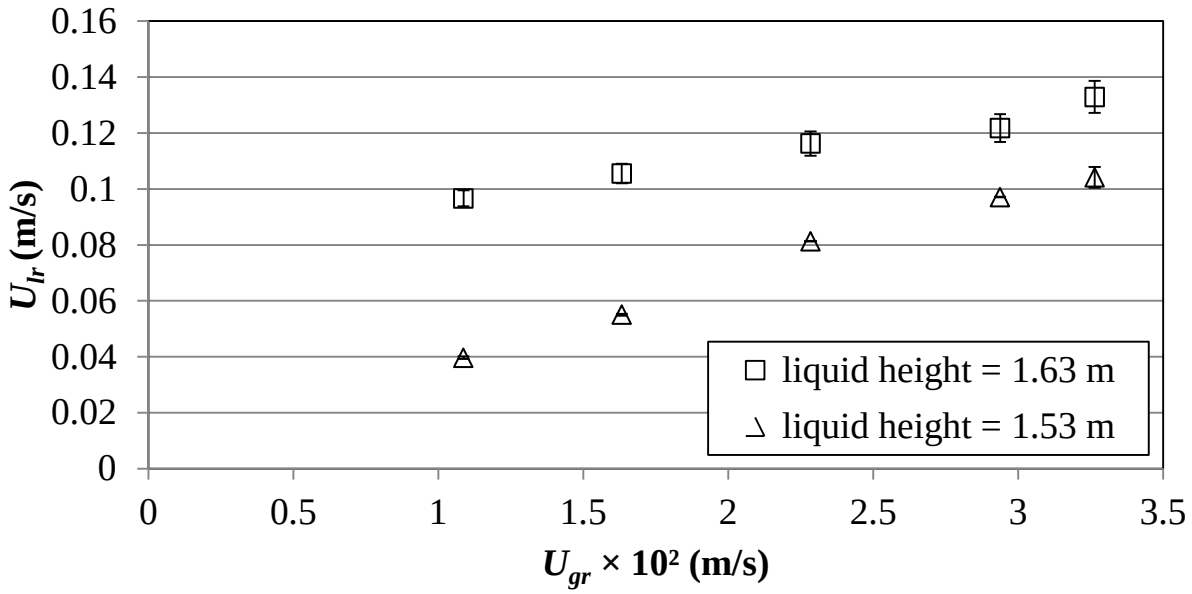

Figure 4.15 Effect of gas flow rate and liquid height on superficial liquid velocity in the riser using a cross shaped sparger (average standard deviation = 0.0026 m/s).

4.3.2. Effect of Sparger

Figure 4.16 illustrates the effect of gas sparger types on the superficial liquid velocity in the riser at different riser superficial gas velocities using a constant liquid height of 1.63 m in the bioreactor. It was noticed that the riser superficial liquid velocity was decreased at constant riser superficial gas velocity when a circular sparger was used over a cross shaped sparger of same diameter and with same number and size of holes on it (Figure 4.16). This decrease in superficial liquid velocity in the riser is due to the fact that circular sparger consists of a circular solid plate, which offers more resistance than its counterpart (cross shaped sparger). A cross shaped sparger consists of six small diameter circular tubes. These small diameter tubes have much more space between each other for the water to pass easily without much resistance. It is believed that the increase in resistance in the flow path of the liquid contributes to lower superficial liquid velocity in the bioreactor (Loh and Ranganath, 2005; Han et al., 2000; Guo et al., 1997).

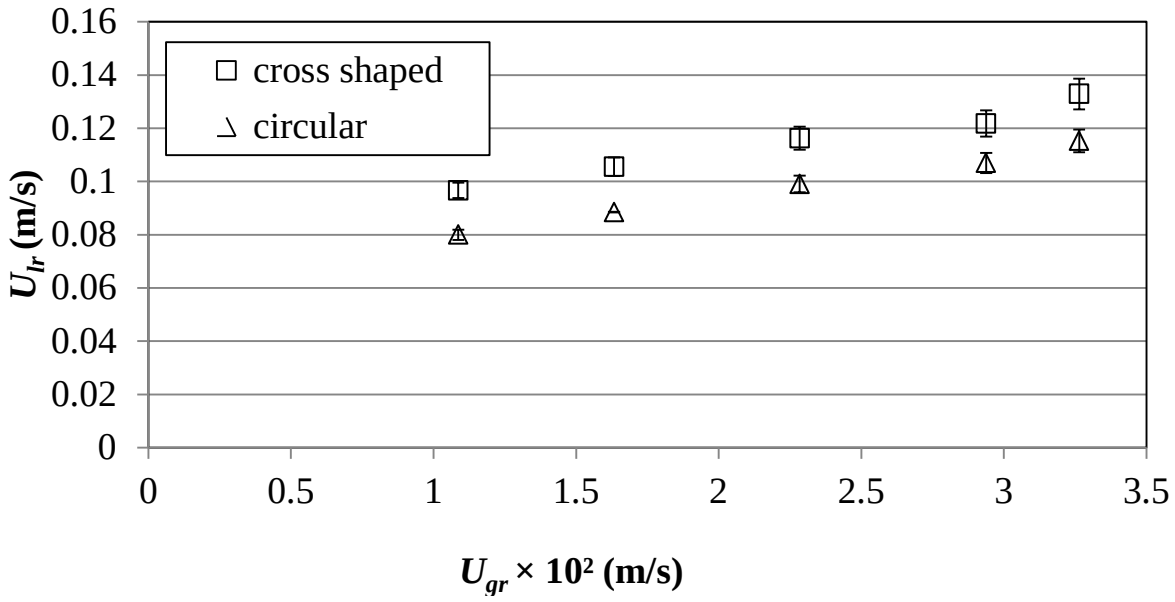

Figure 4.16 Effect of sparger configuration on riser superficial liquid velocity with a constant liquid height of 1.63 m in the bioreactor (average standard deviation = 0.0034 m/s).

4.3.3. Effect of Packing

Figure 4.17 demonstrates the effect of packing on the superficial liquid velocity in the riser using a cross shaped sparger with a constant liquid height of 1.63 m in the bioreactor. It was observed that, at a constant riser superficial gas velocity, the superficial liquid velocity in the riser is decreased when a packing is installed in the riser (Figure 4.17). The installation of packing in the riser offers more resistance to the flow path of liquid, which results in the decrease in liquid superficial velocity (Nikhakhtari and Hill, 2005; Meng et al., 2002).

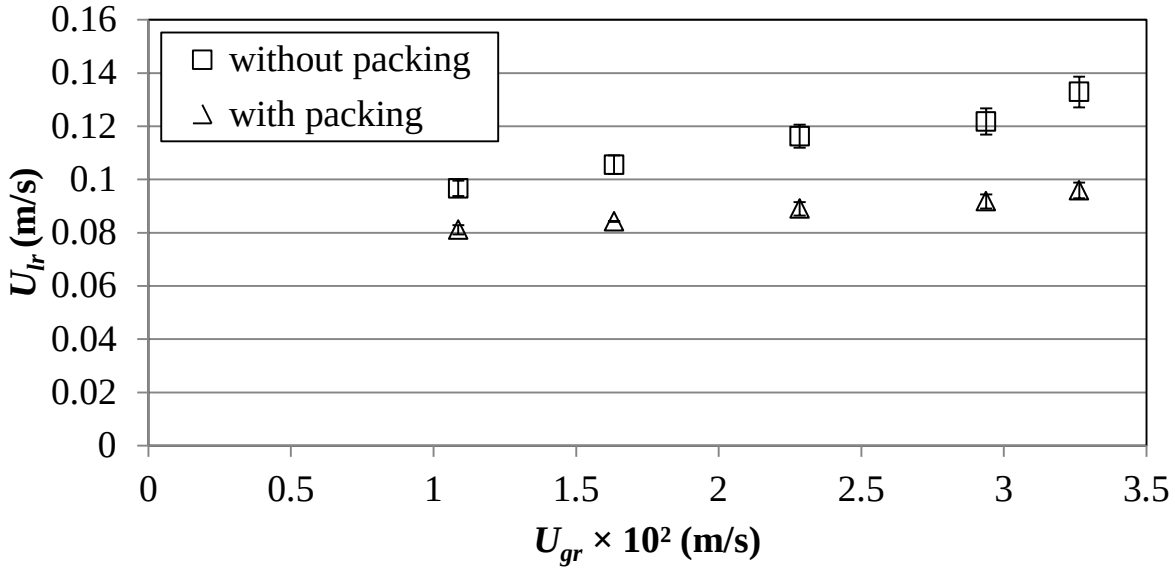

Figure 4.17 Effect of packing installed in the riser (packing height = 0.234 m) on the riser superficial liquid velocity with a constant liquid height of 1.63 m using a cross shaped sparger configuration in the bioreactor (average standard deviation = 0.0032 m/s).

4.3.4. Effect of Internal Gas Distributor (Perforated Plate)

Figure 4.18 is a typical plot showing the effect of riser superficial gas velocity on riser superficial liquid velocity in the bioreactor, with and without the perforated plate. It can be seen

from Figure 4.18 that the superficial liquid velocity in the riser for the bioreactor fitted with the internal gas distributor, at a constant riser superficial gas velocity, was lower than that measured for the bioreactor without internal gas distributor. The lower superficial liquid velocity in the riser is due to the increase in flow resistance in the bioreactor fitted with the internal gas distributor (Loh and Ranganath, 2005; Han et al, 2000; Guo et al, 1997).

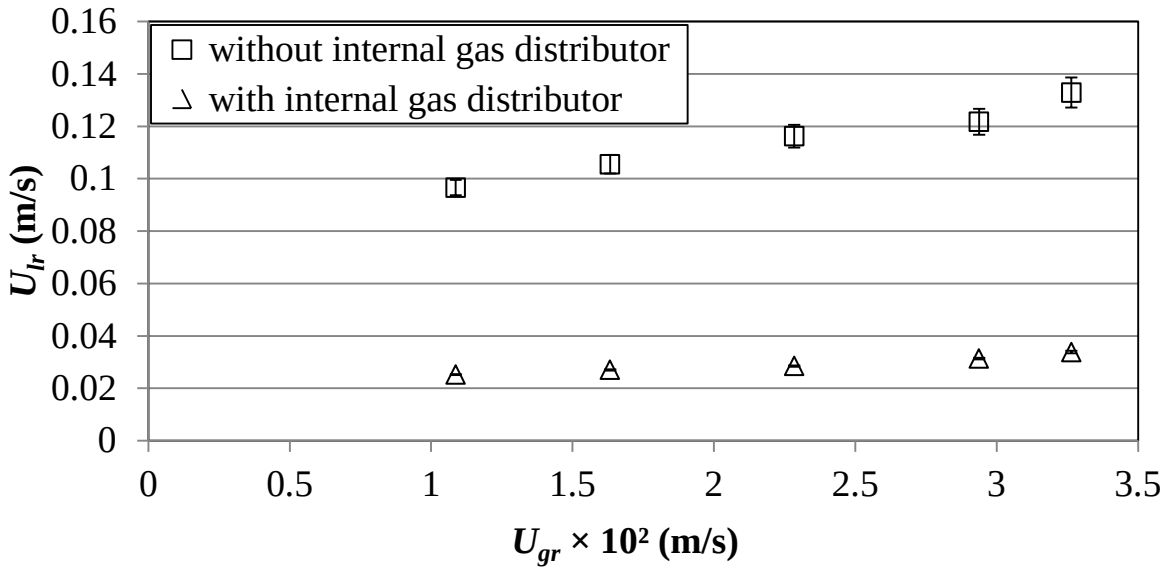

Figure 4.18 Effect of the perforated plate installed in the riser on the superficial liquid velocity in the riser with a constant liquid height of 1.63 m for a cross shaped sparger configuration (average standard deviation = 0.0023 m/s).

Figure 4.19 illustrates the effect of an internal gas distributor (perforated plate) installed in the riser between two packings on the superficial liquid velocity in the riser with a constant liquid height of 1.63 m for a cross shaped sparger configuration in the bioreactor. It was noticed that the riser superficial liquid velocity was decreased, at constant riser superficial gas velocity, when an internal gas distributor was installed between two packings in the riser (Figure 4.19). A bioreactor with an internal gas distributor between two packings offers much more resistance in

the flow path of the liquid than a bioreactor without internal gas distributor and packings. It is believed that, this increase in resistance in the flow path of the liquid contributes to lower liquid superficial velocity in the bioreactor (Nikhakhtari and Hill, 2005; Meng et al., 2002; Loh and Ranganath, 2005; Han et al, 2000; Guo et al, 1997).

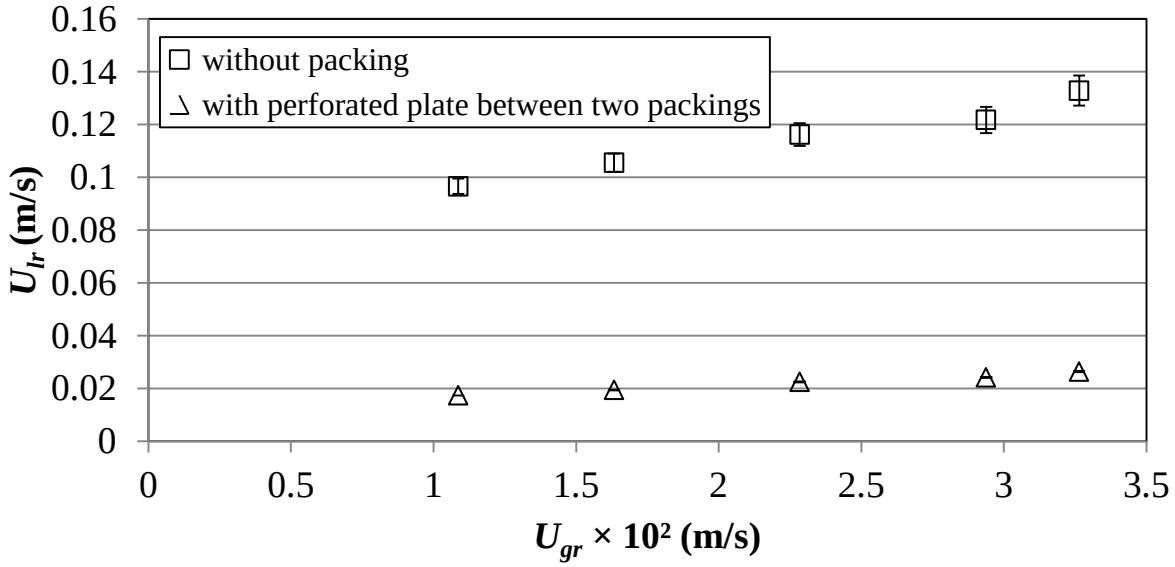

Figure 4.19 Effect of using a perforated plate between two packings in the riser (height of each packing = 0.234 m) on riser superficial liquid velocity with a constant liquid height of 1.63 m using a cross shaped sparger configuration in the bioreactor (average standard deviation = 0.0022 m/s).

In general, the superficial liquid velocity in the downcomer was higher than the superficial liquid velocity in the riser because of the smaller diameter of the downcomer. The range of superficial liquid velocity found in the downcomer was 0.103 to 0.785 m/s.

CHAPTER 5

CONCLUSIONS AND RECOMMENDATIONS

5.1. Conclusions

In this work, a novel external loop airlift bioreactor was designed by installing an internal gas distributor (perforated plate) between two packings in the riser. This novel configuration can be used in fermentation industries where microorganisms or enzymes are immobilized on packing and where during the process of mixing, the achievement of a higher mass transfer rate is required. The effects of different design parameters and operating conditions such as employing an internal gas distributor in the riser, using a packing in the riser, installation of an internal gas distributor between two packings in the riser, sparger configuration, gas flow rate, and liquid height in the bioreactor on the different hydrodynamic parameters (gas holdup, mixing time, and liquid circulation velocity) were explored for an air-water system. Electrical resistance tomography system was successfully utilized to measure the gas holdup, mixing time, and liquid circulation velocity in the bioreactor.

The experimental results demonstrated that the riser superficial gas velocity had a very significant effect on the hydrodynamic parameters. The gas holdup in the riser was significantly increased with increasing superficial gas velocity in the riser. The lower gas flow rate resulted in the formation of smaller number of bubbles, which contributed to a lower gas holdup. When the gas flow rate was increased, large number of bubbles were formed, which contributed to a higher gas holdup. It was also noticed that the mixing time in the bioreactor was decreased with increasing superficial gas velocity in the riser. The lower riser superficial gas velocity resulted in a lower riser superficial liquid velocity, which resulted in a longer mixing time in the bioreactor.

When the gas flow rate was increased in the riser, the hydrostatic pressure difference between the riser and the downcomer was increased, which in turn increased the superficial liquid velocity in the riser. This increase in superficial liquid velocity in the riser decreased the mixing time in the bioreactor.

The liquid height in the bioreactor also played a very important role in order to affect the hydrodynamic parameters. The results revealed that the riser gas holdup and mixing time were increased while the riser superficial liquid velocity was decreased with reducing the liquid height in the bioreactor, at constant riser superficial gas velocity. This increase in gas holdup was due to the fact that, with decreasing liquid height in the bioreactor, the resistance in the flow path of liquid in upper connecting tube of the bioreactor was increased, which in turn decreased the liquid circulation velocity. This decreased liquid circulation velocity contributed to a higher gas holdup and longer mixing time in the bioreactor.

Installation of an internal gas distributor (perforated plate) meaningfully influenced the gas holdup, mixing time and liquid circulation velocity. The internal gas distributor employed in this work has a good performance for the growth of gas-liquid mass transfer rate and because of this increase in mass transfer rate it has an outstanding application in airlift reactors. This configuration of reactor can be used in chemical and biochemical industries where higher mass transfer rate is required because greater gas holdup means achieving a greater mass transfer rate. It was observed that the gas holdup in the riser was significantly increased when an internal gas distributor was installed in the rise. This higher gas holdup was due to the finer dispersion of gas bubbles achieved because of internal gas distributor in the bioreactor. The turbulence intensity in the riser was increased when the liquid flowed through the internal gas distributor. This increased turbulence intensity effectively resulted in the bubble breakup, which led to decrease in

bubble size and an increase in gas holdup. Installation of an internal gas distributor in the riser also gave rise to an extra flow resistance, which in turn decreased the liquid circulation velocity. This decreased liquid circulation velocity increased the gas holdup and mixing time in the bioreactor.

The experimental results also disclosed the influence of sparger configuration on hydrodynamic parameters. The results demonstrated that the gas holdup was slightly increased, at constant riser superficial gas velocity, when a circular sparger was used over a cross shaped sparger of same diameter and with same number and size of holes on it. This increased gas holdup was due to the fact that the circular sparger offered more resistance in the flow of liquid than a cross shaped sparger with same diameter and same size and number of holes on it. The increase in resistance also resulted in the decrease in liquid circulation velocity which led to a longer mixing time in the bioreactor.

Installing a packing in the riser also had a significant impact on hydrodynamic parameters. It was noticed that, at a constant riser superficial gas velocity, the riser superficial liquid velocity was decreased when a packing was installed in the riser. The installation of packing in the riser contributed to higher resistance in the flow path of the liquid in the riser which resulted in the decrease in the liquid circulation velocity. This decrease in liquid circulation velocity in turn increased the mixing time and gas holdup in the bioreactor. The gas holdup was also increased because the packing decreased the size of the gas bubbles.

The impact of the novel design parameter (installing an internal gas distributor (perforated plate) between two packings) on hydrodynamic parameters was significantly noticeable. The experimental results illustrated that the riser superficial liquid velocity was decreased, at constant riser superficial gas velocity, when an internal gas distributor was installed between two

packings in the riser. This design parameter offered greater resistance in the flow path of the liquid. It is believed that, this increase in resistance in the flow path of the liquid contributed to lower liquid circulation velocity in the bioreactor, which in turn increased the gas holdup and the mixing time in the bioreactor.

5.2. Recommendations

Following are the recommendations for future studies:

- The proposed bioreactor can be further investigated for other Newtonian solutions (sugar solutions) and non-Newtonian solutions (xanthan gum solutions).
- The packed bed external loop bioreactor can be converted into a fluidized bed external loop bioreactor by removing the packing from the riser and installing a screen in the downcomer. The screen can be installed in the downcomer just below the point where upper connecting tube and downcomer are connected.
- Computational fluid dynamics (CFD) modeling can be used to simulate and validate the mixing processes.

NOMENCLATURE

A	cross sectional area (m^2)
A_{bc}	cross-sectional area of the bottom connecting section (m^2)
A_{tc}	cross-sectional area of the top connecting section (m^2)
A_d	downcomer cross sectional area (m^2)
A_r	riser cross sectional area (m^2)
a	interfacial area (m^2)
a_w	interfacial area for the whole reactor (m^2)
C	distribution factor (-)
C_m	mean concentration ($kmol/m^3$)
C_a	actual maximum concentration ($kmol/m^3$)
C_A^*	dissolved oxygen concentration at equilibrium ($kgmol/m^3$)
C_L^*	oxygen saturated concentration in the liquid phase (mol/m^3)
c	instantaneous concentration of the tracer ($kmol/m^3$)
Dr	diameter of riser (m)
Dd	diameter of downcomer (m)
Di	dispersion coefficient in the riser (m^2/s)
D_L	axial dispersion coefficient (m^2/s)
D	inner diameter of riser or downcomer (m)
D_t	diameter of separator (m)
D_{eff}	effective diffusion coefficient (m^2/s)
DO	dissolved oxygen level in liquid (mol/litre)
d_i	bubble diameter (m)

d	derivative (-)
f	fanning friction factor (-)
f_r	fanning friction factor in the riser (-)
f_d	fanning friction factor in the downcomer (-)
Fr_G	Froude number of gas (-)
g	acceleration due to gravity (m/s^2)
G	molar air flow rate (mol/h)
He	Henry's law constant (litre.atm/mol)
H	reactor height (m)
H_r	circulating liquid height in the riser (m)
H_{bc}	circulating liquid length in the bottom connecting section (m)
H_{tc}	circulating liquid length in the top connecting section (m)
H	magnetic field intensity (A/m)
H_D, h_D	dispersion height (m)
H_L	liquid (bubble free) height (m)
H_p	packed bed height (m)
H_o	distance between two measured points of manometer (m)
ΔH	level difference in the inverse U-type manometer (m)
I	degree of inhomogeneity (-)
K_T, K_B	energy loss coefficients (-)
K	fluid consistency index (Pa s^n)
K	kinetic energy (m/sec^2)
$K_L a$	volumetric mass transfer coefficient (m^2/s)

K_L liquid phase mass transfer coefficient (s^{-1})

K_P sensor response coefficient (s^{-1})

L axial distance from sparger to riser (m)

L_{rd} gas-separator characteristic length (m)

Ln natural log (-)

M_o generalized Morton number for power law fluids (-)

M_s magnetization at saturation (A/m)

M exponent (-)

N fluid behavior index (-)

N empirical constant (-)

P_T total pressure in system (atm)

P pressure (Pa)

P_b Pressure at the bottom (Pa)

P_t Pressure at the top (Pa)

$<P`>_r$ mean area average pressure in the riser (N/m^2)

$P`_d$ area average pressure in the downcomer (N/m^2)

$<P>_r$ mean pressure in the riser (N/m^2)

P_d pressure in the downcomer (N/m^2)

Q volumetric flow rate (m^3/s)

Q_L, Q_l volumetric liquid flow rate (m^3/s)

Q_g volumetric gas flow rate (m^3/s)

Re Reynolds number (-)

R_a rate of absorption per unit area (kg mole/m^3 s)

S	separator to downcomer volume ratio, dimensionless
S_Φ	source term (-)
T	time (s)
t_r	liquid residence time in the riser (s)
t_c	circulation time (s)
U	superficial velocity (m/s)
U_{lr}	superficial liquid velocity in the riser (m/s)
U_{ld}	superficial liquid velocity in the downcomer (m/s)
$U_{ld,apparent}$	apparent superficial liquid velocity in the downcomer (m/s)
U_{st}	terminal velocity of solid (m/s)
U_{bt}	terminal rise velocity of a single bubble (m/s)
U_g	superficial gas velocity (m/s)
U_{gr}	superficial gas velocity in the riser (m/s)
U_{bt}	terminal rise velocity of single bubble (m/s)
U_{Lc}	liquid circulation velocity (m/s)
u, u_L	liquid velocity (m/s)
V, V_l	liquid volume in vessel (L)
V_g	gas volume in vessel (L)
V_s	solid volume in vessel (L)
y_1	oxygen content of inlet air (mol %)
y_2	oxygen content of exit air (mol %)
Z	distance coordinate (m)

Greek Symbols

α_i	volume fraction of phase i (-)
Θ	percentage of valve opening (-)
$\emptyset$	radial coordinate (-)
σ_1	conductivity of the liquid phase (mS/cm)
σ_2	conductivity of the gas phase (mS/cm)
σ_{mc}	local value of the mixture conductivity distribution of the two phases (mS/cm)
φ	dimensionless factor (-)
μ	viscosity (Pa s)
μ_L	liquid viscosity (Pa s)
Γ	shear rate (s^{-1})
γ_{av}	average shear rate (s^{-1})
γ_w	average shear rate due to walls of the reactor (s^{-1})
τ	shear stress (Pa)
$\sum$	summation (-)
∂	partial derivative (-)
υ_g	kinematic gas viscosity (Pa s)
υ_{N_2}	kinematic nitrogen viscosity (Pa s)
ε	phase holdup (-)
ε_L	liquid holdup (-)
ε_g	gas holdup (-)
$\varepsilon_r, \varepsilon_{gr}$	gas holdup in the riser (-)

$\varepsilon_{d,}\ \varepsilon_{gd}$	gas holdup in the downcomer (-)
ε_s	solid holdup (-)
ε_{sr}	solid holdup in the riser (-)
ε_{so}	solid holdup in the packed bed (-)
έ	area average phase holdup (-)
K_L	water turbulent dissipation rate (m^2/s^3)
ρ, ρ_L	liquid density (kg/m^3)
$<\rho>$	mean liquid density (kg/m^3)
ύ	area average liquid velocity (m/s)
$ύ_d$	area average liquid velocity in the downcomer (m/s)
$ύ_r$	area average liquid velocity in the riser (m/s)
<ύ>	mean area average liquid velocity (m/s)
$<ύ_g>$	mean area average gas velocity (m/s)

Subscript

av	Average
b	Bottom
bu	Bubble
c	circulation
D, d	Down comer
g	Gas
L,l	Liquid
m	mean

R, r	Riser
s	Solid
t	top of the riser
w	whole reactor
z	axial coordinate

REFERENCES

Allen, D. G. and Robinson, C. W.: Communication to the Editor. Comments on the communication: On the calculation of shear rate and apparent viscosity in airlift and bubble column bioreactors, Biotech. Bioeng. 38 (1991) 212–216

A1-Masry, W. A.: Influence of gas-separator and scale up on the hydrodynamics of external loop circulating bubble columns, Chemical Engineering Research and Design, 82(A3) (2004) 381–389

Al-Masry, W. A.: Effect of scale-up on average shear rates for aerated non-Newtonian liquids in external loop airlift reactors, Biotechnology and Bioengineering 62, No. 4 (1999) 494–498

Al-Masry, W. A.: Effects of antifoam and scale-up on operation of bioreactors, Chemical Engineering and Processing 38 (1999) 197–201

Al-Masry, W. A.: Effect of liquid volume in the gas-separator on the hydrodynamics of airlift reactors, J. Chem. Tech. Biotech. 74 (1999) 931–936

Al-Qodah, Z. and Al-Hassan, M.: Phase holdup and gas-to-liquid mass transfer coefficient in magneto stabilized G-L-S airlift fermenter, Chemical Engineering Journal 79 (2000) 41–52

Al-Qodah, Z. and Lafi, W.: Modelling of antibiotics production in magneto three-phase airlift fermenter, Biochemical Engineering Journal 7 (2001) 7–16

Al-Saghair, A., Al-Masry, A. and Ibrahim, A.: Hydrodynamics of three phase non-Newtonian systems circulating bubble columns, King Saud University, College of Engineering Research Centre, Final Research Report No. 7/420

Asenjo, J. A. and Merchuk, J. C.: Bioreactor system design, M. Dekker, New York (1995)

Astarita, G. and Apuzzo, G.: Motion of gas bubbles in non-Newtonian liquids, A.I.Ch.E. Journal Vol. 11, No. 5 (1965) 815–820

Ballica, R. and Ryu, D. D.Y.: Effects of rheological properties and mass transfer on plant cell bioreactor performance: Production of tropane alkaloids, Biotech. Bioeng. 42 (1993) 1181–1189

Becker, S., Sokolichin, A. and Eigenberger, G.: Gas-liquid flow in bubble columns and loop reactors: Part II. Comparison of detailed experiments and flow simulations, Chemical Engineering Science 49, No. 248 (1994) 5747–5762

Bello, R. A., Robinson, C. W. and Moo-Young, M.: Liquid circulation and mixing characteristics of airlift contactors, The Canadian Journal of Chemical Engineering 62 (1984) 573–577

Bello, R. A.: A characterization study of airlift contactors for application to fermentations, A thesis presented to the university of waterloo in partial fulfillment of the requirements for the degree of Doctor of Philosophy in Chemical Engineering (1981)

Bentifraouine, C., Xuereb, C. and Riba, J.: Effect of gas liquid separator and liquid height on the global hydrodynamic parameters of an external loop airlift contactor, Chemical Engineering Journal 66 (1997) 91–95

Benyahia, F., and Jones, L.: Scale effects on hydrodynamic and mass transfer characteristics of external loop airlift reactors, J. Chem. Tech. Biotech. 69 (3) (1997) 301–308

Bird, R. B., Stewart, W. E. and Lightfoot, E. N.: Transport phenomena (2nd ed.), John Wiley & Sons, Inc., USA (2007)

Bolton, G. T., Hooper, C. W., Mann, R. and Stitt, E. H.: Flow distribution and velocity measurement in a radial flow fixed bed reactor using electrical resistance tomography, Chemical Engineering Science 59 (2004) 1989–1997

Chavez-Parga, M. C., Gonzalez-Ortega, O., Negrete-Rodriguez, M. L. X., Medina-Torres, L. and Silva, E. M. E.: Hydrodynamics, mass transfer and rheological studies of gibberellic acid production in an airlift bioreactor, World J. Microbio. Biotech. 23 (2007) 615–623

Chetty, M.: On the estimation of effective shear rate in external loop airlift reactors: non-Newtonian fluids, Resources, Conservation and Recycling 18 (1996) 11–24

Chhabra, R. P. and Richardson J. F.: Non-Newtonian flow and applied rheology, Elsevier/Butterworth-Heinemann, London (2008)

Chhabra, R. P.: Bubbles, drops and particles in non-Newtonian fluids, CRC Taylor & Francis, Boca Raton, Florida (2007)

Chisti, M. and Moo-Young, M.: Improve the performance of airlift reactors, Chem. Eng. Prog 89 (6) (1993) 38–45

Chisti, M. and Moo-Young, M.: Hydrodynamics and oxygen transfer in pneumatic bioreactor devices, Biotech. Bioeng. 31 (1988) 487–494

Chisti, M. and Moo-Young, M.: Prediction of liquid circulation velocity in airlift reactors with biological media, J. Chem. Tech. Biotech. 42 (1988) 211-219

Chisti, M.: Airlift bioreactors, Elsevier Applied Science, New York (1989)

Choi, P. B.: Designing airlift loop fermenters, Chem. Eng. Prog. 86 (12) (1990) 32–37

Demming, S., Gautier, A., Legallais, C. and Ould-Dris, A.: Solid–liquid mass transfers in an Airlift Reactor incorporating alginate beads for the application as a bioartificial liver, Chemical Engineering and Processing 47 (2008) 2370–2378

Dhanasekharan, K. M., Sanyal, J., Jain, A. and Haidari, A.: A generalized approach to model oxygen transfer in bioreactors using population balances and computational fluid dynamics, Chemical Engineering Science 60 (2005) 213 – 218

Dhaouadi, H., Poncin, S., Hornut, J.M. and Wild, G.: Solid effects on hydrodynamics and heat transfer in an external loop airlift reactor, Chemical Engineering Science 61 (2006) 1300–1311

Dhaouadi, H., Poncin, S., Midoux, N. and Wild, G.: Gas–liquid mass transfer in an airlift reactor — analytical solution and experimental confirmation, Chemical Engineering and Processing 40 (2001) 129–133

Dhaouadi, H., Poncin, S., Hornut, J. M., Wild, G., Oinas, P. and Korpijarvi, J.: Mass transfer in an external-loop airlift reactor: experiments and modeling, Chemical Engineering Science, Vol. 52, Nos 21:22 (1997) 3909–3917

Douek, R. S., Livingston, A. G., Johansson, A. C. and Hewitt, G. F.: Hydrodynamics of an external-loop three-phase airlift (TPAL) reactor, Chemical Engineering Science, Vol. 49, No. 22 (1994) 3719–3737

Essadki, A. H., Bennajah, M., Gourich, B., Vial, Ch., Azzi, M. and Delmas, H.: Electrocoagulation/electroflotation in an external-loop airlift reactor—Application to the decolorization of textile dye wastewater: A case study, Chemical Engineering and Processing 47 (2008) 1211–1223

Fernandez, F. G. Acien, J. M. Fernandez Sevilla, J. A. Sanchez Perez, E. Molina Grima, Y. Chisti.: Airlift-driven external-loop tubular photobioreactors for outdoor production of microalgae: assessment of design and performance, Chemical Engineering Science 56 (2001) 2721–2732

Freitas, C., Fialova, M., Zahradnik, J. and Teixeira, J. A.: Hydrodynamics of a three-phase external-loop airlift bioreactor, Chemical Engineering Science 55 (2000) 4961–4972

Fuentes, M., Mussati, M. C., Scenna, N. J. and Aguirre, P. A.: Global modeling and simulation of a three-phase fluidized bed bioreactor, Computers and Chemical Engineering 33 (2009) 359–370

Garcia-Ochoa, F. and Gomez, E.: Theoretical prediction of gas–liquid mass transfer coefficient, specific area and holdup in sparged stirred tanks, Chemical Engineering Science 59 (2004) 2489–2501

Gavrilescu, M. and Tudose, R. Z.: Hydrodynamics of non-Newtonian liquids in external-loop airlift bioreactors Part 2: Study of liquid circulation velocity, Bioprocess Engineering 18 (1998) 83–89

Gavrilescu, M. and Tudose, R. Z.: Hydrodynamics of non-Newtonian liquids in external-loop airlift bioreactors Part 1: Study of the gas holdup, Bioprocess Engineering 18 (1998) 17–26

Gavrilescu, M. and Tudose, R. Z.: Mixing studies in external-loop airlift reactors, Chemical Engineering Journal 66 (1997) 97–104

Gumery, F., Ein-Mozaffari, F. and Dahman, Y.: Macromixing hydrodynamic study in draft-tube airlift reactors using electrical resistance tomography, Bioprocess Biosystem Engineering 34 (2011) 135–144

Gumery, F., Ein-Mozaffari, F. and Dahman, Y.: Characteristics of local flow dynamics and macro-mixing in airlift column reactors for reliable design and scale-up, International Journal of Chemical Reactor Engineering 7 (2009) Review R4

Guo, Y. X., Rather, M. N. and Ti, H. C.: Hydrodynamics and mass transfer studies in a novel external loop airlift reactor, Chemical Engineering Journal 67 (1997) 205–214

Han, S. J., Tan, R. B. H. and Loh, K. C.: Hydrodynamic behaviour in a new gas liquid solid inverse fluidization airlift bioreactor, Trans IChemE 78, Part C, (2000) 207–215

Holder, D. S.: Electrical Impedance Tomography: Methods, History and Applications (2005)

Horiuchi, J., Tabata, K., Kanno, T. and Kobayashi, M.: Continuous acetic acid production by a packed bed bioreactor employing charcoal pellets derived from waste mushroom medium; Journal of Bioscience and Bioengineering 89 (2) (2000) 126–130

Hosseini, S., Patel, D. K., Ein-Mozaffari, F., and Mehrvar, M.: Study of solid–liquid mixing in agitated tanks through electrical resistance tomography, Chemical Engineering Science 65 (2010) 1374–1384

Hristov, J.: External loop airlift with magnetically controlled liquid circulation, Powder Technology 149 (2005) 180–194

Hristov, J.: External-loop airlift magnetically stabilized bed – Minimum stabilization and fluidization conditions, China Particuology 3 (4) (2005) 197–203

Hu, W. M. S.: Characterization of hydrodynamic forces and interfacial phenomena in cell culture processes, Dissertation, Graduate School of The Ohio State University (2007)

Hwang, S. J. and Cheng, Y. L.: Gas holdup and liquid velocity in three phase internal loop Airlift reactor, Chemical Engineering Science 52 (1997) 3940–3960

Ishkintana L. K., Bennington, C. P. J. : Gas holdup in pulp fibre suspensions: Gas voidage profiles in a batch-operated sparged tower, Chemical Engineering Science 65 (2010) 2569–2578

Jin, H., Han, Y., Yang, S. and He, G.: Electrical resistance tomography coupled with differential pressure measurement to determine phase hold-ups in gas-liquid-solid outer loop bubble column, Flow Measurement and Instrumentation 21 (2010) 228–232

Jin, H., Yang, S., Wang, M., Williams, R. A.: Measurement of gas holdup profiles in a gas liquid cocurrent bubble column using electrical resistance tomography, Flow Measurement and Instrumentation 18 (2007) 191–196

Jin, H., Wang, M., Williams, R. A.: Measurement of gas holdup profiles in a gas liquid cocurrent bubble column using electrical resistance tomography, Chemical Engineering Journal 130 (2007) 179–185

Jin, H., Wang, M., Williams, R. A.: The effect of sparger geometry on gas bubble flow behaviors using electrical resistance tomography, Chinese Journal of Chemical Engineering 14(1) (2006) 127-131

Jin, B., Yu, Q., Yan, Q. X. and Leeuwen, J.: Characterization and improvement of oxygen transfer in pilot plant external air-lift bioreactor for mycelia biomass production, World Journal of Microbiology & Biotechnology 17 (2001) 265–272

Jin, B., Leeuwen, J., Doelle, H. W. and Yu, Q.: The influence of geometry on hydrodynamic and mass transfer characteristics in an external airlift reactor for the cultivation of filamentous fungi, World Journal of Microbiology & Biotechnology 15 (1999) 73–79

Kang, X., Wang, H., Wang, Y., Harvey, L. M. and McNeil, B.: Hydrodynamic characteristics and mixing behaviour of Sclerotium glucanicum culture fluids in an airlift reactor with an internal loop used for scleroglucan production, J. Ind. Microbio. Biotech., 27 (2001) 208–214

Kawase, Y. and Hashimoto, N.: Gas holdup and oxygen transfer in three-phase external-loop airlift bioreactors: Non-Newtonian fermentition broths, J. Chem. Tech. Biotech., 65 (1996) 325–334

Kawase, Y., Tsujimura, M. and Yamaguchi, T.: Gas holdup in external-loop airlift bioreactors, Bioprocess Engineering 12 (1995) 21-27

Kawase, Y., Omori, N. and Tsujimura, M.: Liquid-phase mixing in external-loop airlift bioreactors, Journal of Chemical Technology and Biotechnology, 61 (1994) 49–55

Kawase, Y.: Liquid circulation in external-loop airlift bioreactors, Biotech. & Bioeng., 35 (1990) 540–546

Kee, D. D. and Chhabra, R. P.: A photographic study of shapes of bubbles and coalescence in non-Newtonian polymer solutions, Rheologica Acta 27 (1988) 656–660

Kemblowski, Z., Przywarski, J. and Diab, A.: An average gas holdup and liquid circulation

velocity in airlift reactors with external loop, Chemical Engineering Science 48 (1993) 4023–4035

Kilonzo, P. M., Margaritis, A. and Bergougnou, M. A.: Hydrodynamics and mass transfer characteristics in an inverse internal loop airlift-driven fibrous-bed bioreactor, Chemical Engineering Journal 157 (2010) 146–160

Kilonzo P. M., Margaritis, A. and Bergougnou, M. A.: Hydrodynamic characteristics in an inverse internal-loop airlift-driven fibrous-bed bioreactor, Chemical Engineering Science 65 (2010) 692–707

Kilonzo, P. M., Margaritis, A., Bergougnou, M. A., Yu, J. and Qin, J.: Effects of geometrical design on hydrodynamic and mass transfer characteristics of a rectangular-column airlift bioreactor, Biochemical Engineering Journal 34 (2007) 279–288

Klein, J., Maia, J., Vicente, A. A., Domingues, L., Teixeira, J. A. and Jurascik, M.: Relationships between hydrodynamics and rheology of flocculating yeast suspensions in a high-cell-density airlift bioreactor, Biotechnology and Bioengineering 89 (4) (2005) 393–399

Lin, J., Han, M., Wang, T., Zhang, T., Wang, J. and Jin, Y.: Influence of the gas distributor on the local hydrodynamic behaviour of an external loop airlift reactor, Chemical Engineering Journal 102 (2004) 51–59

Liu, M., Zhang, T., Wang, T., Yu, W. and Wang, J.: Experimental study and modeling on liquid dispersion in external-loop airlift slurry reactors, Chemical Engineering Journal 139 (2008) 523–531

Liu, M., Zhang, T., Wang, T., Wang, J. and Jin, Y.: Flow behaviour and mass transfer in three-phase external-loop airlift reactors with large particles, China Particuology Vol. 4, Nos. 3–4 (2006) 178–182

Loh, K. and Ranganath, S.: External-loop fluidized bed airlift bioreactor (EFBAB) for the cometabolic biotransformation of 4-chlorophenol (4-cp) in the presence of phenol, Chemical Engineering Science 60 (2005) 6313–6319

Loh, K. and Liu, J.: External loop inversed fluidized bed airlift bioreactor (EIFBAB) for treating high strength phenolic wastewater, Chemical Engineering Science 56 (2001) 6171–6176

Mann, R., Stanley, S., Vlaev, D. and Wabo, E.: Augmented-reality visualization of fluid mixing in stirred chemical reactors using electrical resistance tomography, Journal of Electronic Imaging, 10(3) (2001) 620–629

Mann, R., Dickin, F., Wang, M., Dyakowski, T., Williams, R., Edwards, R., Forrest, A., Holden, P.: Application of electrical resistance tomography to interrogate mixing process at plant scale, Chemical Engineering Science, 52 (1997) 2087–2097

Meng, A. X., Hill, G. A. and Dalai, A. K.: Hydrodynamic characteristics in an external loop airlift bioreactor containing a spinning sparger and a packed bed, Ind. Eng. Chem. Res. 41 (2002) 2124–2128

Merchuk, J. C., Contreras, A., Garcia, F. and Molina, E.: Studies of mixing in a concentric tube airlift bioreactor with different spargers, Chemical Engineering Science 53 (4) (1998) 709–719

Merchuk, J. C., Ben-Zvi, S. (Yona) and Niranjan, K.: Why use bubble-column bioreactors,

Trends in biotechnology, 12 (1994) 501–511

Merchuk, J. C., Ladwa, N., Cameron, A., Bulmer, M. and Pickett, A.: Concentric-tube airlift reactors: Effects of geometric design on performance, AIChE Journal 40 (1994) 1105–1117

Mersmann, A.: Design and scale up of bubble and spray columns, German Chemical Engineering 1 (1978) 1–11

Mohanty, K., Das, D. and Biswas, M. N.: Treatment of phenolic wastewater in a novel multi-stage external loop airlift reactor using activated carbon, Separation and Purification Technology 58 (2008) 311–319

Mohanty, K., Das, D. and Biswas, M. N.: Mass transfer characteristics of a novel multi-stage external loop airlift reactor, Chemical Engineering Journal 133 (2007) 257–264

Mohanty, K., Das, D. and Biswas, M. N.: Hydrodynamics of a novel multi-stage external loop airlift reactor, Chemical Engineering Science 61 (2006) 4617–4624

Morrison, F. A.: Understanding rheology, Oxford University Press, USA (2001)

Nikakhtari, H. and Hill, G. A.: Hydrodynamic and oxygen mass transfer in an external loop airlift bioreactor with a packed bed, Biochemical Engineering Journal 27 (2005) 138–145

Nishikawa, M.: Communications to the editor; On the estimation of average shear rate in bubble columns, Biotech. Bioeng. 37 (1991) 691–692

Nishikawa, M., Kato, H. and Hashimoto, K.: Heat transfer in aerated tower filled with non-Newtonian liquid, Ind. Eng. Chem. Process Des. Dev. 16, No.1 (1977) 133–137

Pakzad, L., Ein-Mozaffari, F. and Chan, P.: Using electrical resistance tomography and computational fluid dynamics modeling to study the formation of cavern in the mixing of pseudoplastic fluids possessing yield stress, Chemical Engineering Science 63 (2008) 2508–2522

Pakzad, L.: Using electrical resistance tomography (ERT) and computational fluid dynamics to study the mixing of pseudoplastic fluids with a scaba 6SRGT impeller, A thesis presented to Ryerson university in partial fulfilment of the requirements for the degree of Master of Applied Science in the program of chemical engineering. Toronto, Ontario, Canada (2007)

Perez, J. A. S., Porcel, E. M. R., Lopez, J. L. C., Sevilla, J. M. F. and Chisti, Y.: Shear rate in stirred tank and bubble column bioreactors, Chemical Engineering Journal 124 (2006) 1–5

Popovic M., Kiefneer A. and Bajpai R.K.: Gas holdup and liquid circulation velocity in gas-liquid –solid airlift reactors, Canadian Journal of Chemical Engineering, 82 (2004) 1273–1274

Popovic, M. and Robinson C. W.: Mixing characteristics of external-loop airlifts: Non-newtonian systems 48 (1993) 1405–1413

Popovic, M. and Robinson C. W.: External-circulation-loop airlift bioreactors: Study of the liquid circulating velocity in highly viscous non-Newtonian liquids, Biotechnology and Bioengineering 32 (1988) 301–312

Prins, A. and Reit, K. V.: Proteins and surface effects in fermentation: antifoam and mass transfer, Trends in Biotechnology 5 issue 11(1987) 296–301

Randall, D. F. and Hill, G. A.: Hydrodynamic characteristics of a spinning sparger, external loop airlift bioreactor, The Canadian Journal of Chemical Engineering, 71 (1993) 419–425

Renzo D.F.: Liquid circulation in two and three phase external loop airlift reactors, Chem. Eng. Journal, 109 (2005) 49–55.

Roy, S. and Joshi, J. B.: CFD study of mixing characteristics of bubble column and external loop airlift reactor, Asia-Pac. J. Chem. Eng. 3 (2008) 97–105

Rubio F. C., Garcia, J. L., Molina, E. and Chisti, Y.: Steady-state axial profiles of dissolved oxygen in tall bubble column bioreactors, Chemical Engineering Science 54 (1999) 1711–1723

Ruff, K., Pilhofer, T. and Mersmann, A.: Ensuring flow through all the openings of perforated plates for fluid dispersion, Inter. Chemical Engineering 18 (1978) 395–401

Sarkar, S., Mohanty, K. and Meikap, B. C.: Hydrodynamic modeling of a novel multi-stage gas–liquid external loop airlift reactor, Chemical Engineering Journal 145 (2008) 69–77

Schugerl, K. and Bellgardt, K.-H.: Bioreaction Engineering: Modeling and Control, Springer, New York (2000)

Shimizu, K., Takada, S., Takahashi, T. and Kawase, Y.: Phenomenological simulation model for gas holdups and volumetric mass transfer coefficients in external-loop airlift reactors, Chemical Engineering Journal 84 (2001) 599–603

Sisak, C., Venyige, T., Martinov, M. and Vlaev, S. D.: Small-scale liquid mixing in a bioreactor column with xanthan-gum simulated filamentous media, Bioprocess Engineering 22 (2000) 253–256

Snape, J. B., Zahradnik, J., Fialova, M. and Thomas, N. H.: Liquid-phase properties and sparger design effects in an external loop airlift reactor, Chemical Engineering Science, Vol. 50, No. 20 (1995) 3175–3186

Tang, W. and Fan, L.: Steady state phenol degradation in a draft-tube, gas-liquid-solid fluidized-bed bioreactor, AIChE Journal, February Vol. 33, No. 2 (1987) 239–249

Tavares, C. R. G., Santanna, G. L. and Capdeville, B.: The effect of air superficial velocity on biofilm accumulation in a three-phase fluidized-bed reactor, Wat. Res. Vol. 29, No. 10 (1995) 2293–2298

Vial, C., Poncin, S., Wild, G. and Midoux, N.: Experimental and theoretical analysis of axial dispersion in the liquid phase in external-loop airlift reactors, Chemical Engineering Science 60 (2005) 5945–5954

Vial, C., Poncin, S., Wild, G. and Midoux, N.: Experimental and theoretical analysis of the hydrodynamics in the riser of an external loop airlift reactor, Chemical Engineering Science 57 (2002) 4745–4762

Wang, T., Wang, J. and Jin, Y.: Experimental study and CFD simulation of hydrodynamic behaviours in an external loop airlift slurry reactor, The Canadian Journal of Chemical Engineering 82 (2004) 1183–1190

Wen, J., Jia, X., Cheng, X. and Yang, P.: Characteristics of three-phase internal loop airlift bioreactors with complete gas recirculation for non-Newtonian fluids, Bioprocess Biosyst Eng 27 (2005) 193–205

Williams, R. A. and Beck, M. S.: Process tomography: principles, techniques and applications

(1995)

Xu, Z., Yu, J.: Hydrodynamics and mass transfer in a novel multi-airlifting membrane bioreactor, Chemical Engineering Science 63 (2008) 1941–1949

Yazdian, F., Shojaosadati, S. A., Nosrati, M., Hajiabbas, M. P. and Vasheghani-Farahani, E.: Investigation of gas properties, design, and operational parameters on hydrodynamic characteristics, mass transfer, and biomass production from natural gas in an external airlift loop bioreactor, Chemical Engineering Science 64 (2009) 2455–2465

Yuguo, Z., Zhao, W. and Xiaolong, C.: Citric acid production from the mash of dried sweet potato with its dregs by Aspergillus niger in an external-loop airlift bioreactor, Process Biochemistry 35 (1999) 237–242

Zhang, T., Tiefeng, W. and Jinfu, W.: Analysis and measurement of mass transfer in airlift loop reactors, Chinese J. Chem. Eng. 14(5) (2006) 604–610

Zhang, T., Zhao, B. and Wang, J.: Mathematical models for macro-scale mass transfer in airlift loop reactors, Chemical Engineering Journal 119 (2006) 19–26

Zhang, T., Wang, J., Wang, T., Lin, J. and Jin, Y.: Effect of internal on the hydrodynamics in external-loop airlift reactors, Chemical Engineering and Processing 44 (2005) 81–87

Zhao, Z. F.: Mixing time study in agitated multiple-lamp UV photoreactor using electrical resistance tomography, A thesis presented to Ryerson university in partial fulfillment of the requirements for the degree of Master of Applied Science in the program of chemical engineering, Toronto, Ontario, Canada (2007)

Zwietermg, M. H., Verlaan, P. and Krolikowski, A. K. M.: Optimal control of the dissolved oxygen concentration in an airlift-loop reactor, Computers chem. Eng. 16 (6) (1992) 563–572

APPENDICES

Appendix A: ERT Data for Mixing Time

Table 1. Mixing time for air-water system using cross shaped sparger configuration with liquid height = 1.63 m.

$U_{gr}\times10^2(m/s)$	1.087	1.633	2.284	2.938	3.264
$t_{m1}(s)$	29	24	21	18	16
$t_{m2}(s)$	30	24	21	18	17
$t_{m3}(s)$	30	24	20	18	16
mean	29.67	24	21.33	18	16.33
standard deviation	0.58	0	0.58	0	0.58

Table 2. Mixing time for air-water system using cross shaped sparger configuration with liquid height = 1.53 m.

$U_{gr}\times10^2(m/s)$	1.087	1.633	2.284	2.938	3.264
$t_{m1}(s)$	67	52	32	25	24
$t_{m2}(s)$	67	51	31	24	23
$t_{m3}(s)$	68	52	32	25	23
mean	67.33	51.67	31.67	24.67	23.33
standard deviation	0.58	0.58	0.58	0.58	0.58

Table 3. Mixing time for air-water system using circular shaped sparger configuration with liquid height = 1.63 m.

$U_{gr}\times10^2(m/s)$	1.087	1.633	2.284	2.938	3.264
$t_{m1}(s)$	35	30	25	20	18
$t_{m2}(s)$	35	31	26	21	17
$t_{m3}(s)$	35	31	26	20	18
mean	35	30.67	25.67	20.33	17.67
standard deviation	0	0.58	0.58	0.58	0.58

Table 4. Mixing time for air-water system using cross shaped sparger configuration and a perforated plate in the riser with liquid height = 1.63 m.

$U_{gr}\times10^2(m/s)$	1.087	1.633	2.284	2.938	3.264
$t_{m1}(s)$	110	85	78	72	67
$t_{m2}(s)$	110	86	77	72	68
$t_{m3}(s)$	110	85	78	72	68
mean	110	85.33	77.67	72	67.67
standard deviation	0	0.58	0.58	0	0.58

Table 5. Mixing time for air-water system using cross shaped sparger configuration and one packing in the riser with liquid height = 1.63 m.

$U_{gr}\times10^2$(m/s)	1.087	1.633	2.284	2.938	3.264
t_{m1}(s)	33	29	28	25	23
t_{m2}(s)	34	29	27	25	23
t_{m3}(s)	33	30	27	26	23
mean	33.33	29.33	27.33	25.33	23
standard deviation	0.58	0.58	0.58	0.58	0

Table 6. Mixing time for air-water system using cross shaped sparger configuration and a perforated plate between two packings with liquid height = 1.63 m.

$U_{gr}\times10^2$(m/s)	1.087	1.633	2.284	2.938	3.264
t_{m1}(s)	144	131	103	91	87
t_{m2}(s)	144	130	103	92	87
t_{m3}(s)	144	130	103	91	88
mean	144	130.33	103	91.33	87.33
standard deviation	0	0.58	0	0.58	0.58

Appendix B: ERT Data for Circulation Time

Table 7. Circulation time for air-water system using cross shaped sparger configuration in the riser for liquid height = 1.63 m.

$U_{gr}\times10^2(m/s)$	1.087	1.633	2.284	2.938	3.264
$t_{c1}(s)$	19	17	15	15	13
$t_{c2}(s)$	20	18	16	15	14
$t_{c3}(s)$	20	18	16	14	13
mean	19.67	17.67	15.67	14.33	13.33
Standard deviation	0.58	0.58	0.58	0.58	0.58

Table 8. Circulation time for air-water system using cross shaped sparger configuration in the riser for liquid height = 1.53 m.

$U_{gr}\times10^2(m/s)$	1.087	1.633	2.284	2.938	3.264
$t_{c1}(s)$	48	35	22	18	17
$t_{c2}(s)$	47	34	22	18	17
$t_{c3}(s)$	47	34	22	18	16
mean	47.33	34.33	22	18	16.67
Standard deviation	0.58	0.58	0	0	0.58

Table 9. Circulation time for air-water system using circular shaped sparger configuration in the riser for liquid height = 1.63 m.

$U_{gr}\times10^{2}(m/s)$	1.087	1.633	2.284	2.938	3.264
$t_{c1}(s)$	24	21	18	17	16
$t_{c2}(s)$	23	21	19	17	15
$t_{c3}(s)$	24	21	18	16	15
mean	23.67	21	18.33	16.67	15.33
Standard deviation	0.58	0	0.58	0.58	0.58

Table 10. Circulation time for air-water system using cross shaped sparger configuration and a perforated plate in the riser for liquid height = 1.63m.

$U_{gr}\times10^{2}(m/s)$	1.087	1.633	2.284	2.938	3.264
$t_{c1}(s)$	75	69	64	57	51
$t_{c2}(s)$	74	68	63	56	52
$t_{c3}(s)$	75	68	63	56	52
mean	74.67	68.33	63.33	56.33	51.67
Standard deviation	0.58	0.58	0.58	0.58	0.58

Table 11. Circulation time for air-water system using cross shaped sparger configuration and one packing in the riser for liquid height = 1.63 m.

$U_{gr}\times10^{2}(m/s)$	1.087	1.633	2.284	2.938	3.264
$t_{c1}(s)$	23	22	21	19	18
$t_{c2}(s)$	24	22	20	19	19
$t_{c3}(s)$	23	22	20	20	18
mean	23.33	22	20.33	19.33	18.33
Standard deviation	0.58	0	0.58	0.58	0.58

Table 12. Circulation time for air-water system using cross shaped sparger configuration and a perforated plate between two packings for liquid height = 1.63 m.

$U_{gr}\times10^{2}(m/s)$	1.087	1.633	2.284	2.938	3.264
$t_{c1}(s)$	108	94	79	72	65
$t_{c2}(s)$	108	94	79	72	66
$t_{c3}(s)$	108	95	80	71	65
mean	108	94.33	79.33	71.67	65.33
Standard deviation	0	0.58	0.58	0.58	0.58